ISSN 0972-9984 (Print)
ISSN 0973-7308 (Online)

# International Journal of Ecology & Development

## Special Issue: Digital Terrain Modelling


Volume 8 | No. F07 | Fall 2007

# International Journal of Ecology & Development

**ISSN 0972-9984 ( Print ); ISSN 0973-7308 (Online)**

# Editorial Board

# International Journal of Ecology & Development

ISSN 0972-9984 (Print); ISSN 0973-7308 (Online)


## Special Issue: Digital Terrain Modelling

## Guest Editor: I. V. Florinsky

## Contents


**Volume 8** **No. F07** **Fall 2007**

*International Journal of Ecology & Development*
*Fall 2007, Vol. 8, No. F07; Int. J. Ecol. Dev.*
*ISSN 0972-9984 ( Print ); ISSN 0973-7308 (Online)*


# Editorial

It is common knowledge that topography is a base of a landscape and one of the main factors in its development. Relief influences the migration and accumulation of substances moved by gravity along the land surface and in the soil, some climatic and meteorological characteristics, hydrological and soil processes, and properties of the vegetation cover. Resulting from the interaction of endogenous and exogenous geophysical processes of different spatial and temporal scales, topography carries information on both surface processes and geological features.

Digital terrain modelling is a system of quantitative methods to analyse and model topographic surface and relationships between relief and other landscape components. Digital terrain modelling had its origin in photogrammetry (Rosenberg, 1955; Spooner et al., 1957; Miller and Leflamme, 1958). In the last 50 years, great progress has been made in developing methods, algorithms, and software for digital terrain analysis, and in investigating relationships between topography and other environmental components. Nowadays digital terrain modelling is a scientific area based on ideas and approaches of geodesy, photogrammetry, geoinformatics, theory of signal and image processing, differential geometry, and other fields of science and technology. Digital terrain modelling is widely used to solve problems of geomorphology, geology, soil science, hydrology, glaciology, planetology, and other geosciences (Moore et al. 1991; Florinsky, 1998; Pike, 2002; Li et al., 2005).

This special issue presents a series of six papers dealing with various aspects of digital terrain modelling. Linnik et al. describe a study of regularities in the spatial distribution of the soil contamination by the Chernobyl-derived radiocaesium. Using techniques of *in situ* radiometry, geostatistics, generalised additive modelling, and digital terrain modelling, these authors clarifies a complicated spatial structure of $^{137}Cs$ patterns in geochemically connected parts of the landscape. A feature of this investigation is its detailed scale: the radiometric survey was carried out with the resolution down to two meters. This work tangibly amplifies our knowledge about the behaviour of this critical pollutant in landscapes.

Conventional soil mapping includes delineation of soil patterns marked by some degree of homogeneity. In this process, a pedologist tries to consider an integral influence of soil formation factors including topography. This is a rather subjective procedure wherein a professional experience and intuition play an important part. Recently, several schemes of digital soil mapping have been proposed. Some of them include elements of digital terrain modelling. A question arises: what is the best combination of quantitative topographic attributes suited for digital soil mapping? Buivydaite and Mozgeris present a comprehensive comparison of a conventional detailed soil map with maps of twenty three topographic attributes as well as maps of land surface segmentation based on three different approaches. They found that landscape segmentation, based on a fundamental theory of the topographic surface in the gravity, gave the best fit to the soil map.

Most of works dealing with relationships between topography and soil properties in agricultural landscapes has been conducted in Canada, USA, and Australia on fields tilled over up to 100-150 years without dramatic modifications of the land surface and soil cover. This may be one of the reasons why high correlations have been systematically observed for the system 'topography-soil' in agrolandscapes. A question arises: how much would a strong, long-term agricultural load reduce the natural topographic control of soil properties? This issue is discussed by Samsonova et al. Using *in situ* measurements of soil electrical resistivity, geostatistics, and digital terrain modelling, they demonstrate that the absence of relationships between soil and topographic attributes may indicate a serious disturbance of the soil cover.

Florinsky describes basic principles of applying the digital terrain analysis (specifically, maps of relative accumulation zones) to solve three practical tasks: exploration of alluvial placers, prediction of landsliding on reservoir shores, and prediction of soil degradation and contamination along gas and oil pipelines.

There are several publicly available, free-of-cost digital elevation models (DEMs) with near-global coverage: GTOPO30, GLOBO, ETOPO2, and SRTM-based data. However, quality of these DEMs leaves something to be desired. There are two main problems with SRTM-derived DEMs: voids and inclusions of non-topographic components (i.e., trees and anthropogenic objects). Elsner and Bonnici demonstrate

that the conventional filling of voids in SRTM-based DEMs by interpolation does not resolve the problem, at least for desert regions.

Notice that GTOPO30, the 30 arc-seconds gridded global DEM, which is routinely used to fill voids in SRTM data, is a rather noisy DEM. Golyandina et al. use a portion of GTOPO30 to exemplify the effectiveness of the two-dimensional singular spectrum analysis for denoising, generalisation, and decomposition DEMs into components of different scales. This method opens the way to utilise noisy DEMs for derivation of secondary topographic variables (e.g., land surface curvatures).

Digital terrain modelling is one of the most dynamically developing branches of geosciences. It is impossible to discuss all current methodologies and applications of digital terrain analysis within the frames of the spatial issue, which represents 'instant image' of a rapidly moving research field.

## REFERENCES

Florinsky, I.V., 1998, *Combined Analysis of Digital Terrain Models and Remotely Sensed Data in Landscape Investigations*, Progress in Physical Geography, 22, 33-60.

Li, Z., Zhu, Q., and Gold, C., 2005, *Digital Terrain Modeling: Principles and Methodology*. CRC Press, New York.

Miller, C.L., and Leflamme, R.A., 1958, *The Digital Terrain Model – Theory and Application*, Photogrammetric Engineering, 24, 433-442.

Moore, I.D., Grayson, R.B., and Ladson, A.R., 1991, *Digital Terrain Modelling: A Review of Hydrological, Geomorphological and Biological Applications*, Hydrological Processes, 5, 3-30.

Pike, R.J., 2002, *A Bibliography of Terrain Modeling (Geomorphometry), the Quantitative Representation of Topography - Supplement 4.0*. U.S. Geological Survey Open-File Report 02-465.

Rosenberg, P., 1955, *Information Theory and Electronic Photogrammetry*, Photogrammetric Engineering, 21, 543-555.

Spooner, C.S. Jr., Dossi, S.W., and Misulia, M.G., 1957, *Let's Go over the Hill – Potential Benefits of Profile Scanning the Stereo-Model*, Photogrammetric Engineering, 23, 909-920.

**I. V. Florinsky**

*Institute of Mathematical Problems of Biology*
*Russian Academy of Sciences*
*Pushchino, Moscow Region, 142290, Russia*
e-mail: iflor@mail.ru

*International Journal of Ecology & Development*
*Fall 2007, Vol. 8, No. F07; Int. J. Ecol. Dev.*
*ISSN 0972-9984 ( Print ); ISSN 0973-7308 (Online)*


# Spatial Variability and Topographic Factors of $^{137}$Cs Soil Contamination at a Field Scale

**V.G. Linnik [1], A.A. Saveliev [2], A.P. Govorun [3], O.M. Ivanitsky [1], A.V. Sokolov [1]**

[1] Vernadsky Institute of Geochemistry and Analytical Chemistry
Russian Academy of Sciences
Kosygin Street 19, Moscow, 117975, Russia
e-mail: linnik@geokhi.ru

[2] Faculty of Ecology, Kazan State University
18 Kremlevskaja street, Kazan, 420008, Russia

[3] RECOM Ltd, Russian Research Centre 'Kurchatov Institute'
Kurchatov Sq. 1, 123182, Moscow, Russia

Received 1 November 2006; accepted 15 March 2007

## ABSTRACT

*The spatial variability of $^{137}$Cs contamination was evaluated at a field scale, at three study sites marked by different landscape positions. Two of them are situated in a forest, and one – in a meadow. The sites are located 170 km away from the Chernobyl Nuclear Power Plant. The objectives of the research were (a) to characterise variability of $^{137}$Cs contamination across the sites, and (b) to determine and describe any relation of $^{137}$Cs contamination with topography. Soil radioactive contamination was measured using in situ radiometric technique. Field radiometry data were analysed using classical statistics and geostatistics. To describe local geometry of the sites, Laplacian models were derived from digital elevation models. A generalised additive model was used to model the dependence of $^{137}$Cs spatial distribution on the relief features. For hydromorphic areas of the sites, the variogram analysis showed that the $^{137}$Cs spatial distribution consists in patchy patterns with the typical size from meters to tens of meters. For watershed areas, the $^{137}$Cs spatial distribution was random and did not form any patterns. The $^{137}$Cs distribution is depend crucially on the local topography in hydromorphic conditions. Laplacian is the most informative index for the process of the $^{137}$Cs lateral migration while elevation is of subsidiary importance.*

**Keywords:** Field Radiometry, Radionuclide, Geostatistics, $^{137}$Cs, Spatial Variation, Generalized Additive Model, Digital Elevation Model, Laplacian.

**Mathematics Subject Classification:** 62P12, 62H99, 86A32.

**JEL Classification:** Q19, Q50.

## INTRODUCTION

The accident at the Chernobyl Nuclear Power Plant has contaminated vast areas in the Bryansk, Tula, Kaluga, and Orel Regions of Russia. This territory, including large agricultural and forested areas, is one of the most $^{137}$Cs-contaminated terrains in Russia (Fig. 1a). Owing to a wide variety of factors, radioactive contamination of landscapes due to the Chernobyl accident appears rather complicated. Some geostatistical methods were used to study the structure of the radioactively contaminated areas. Kanevsky (1994) and Kanevsky et al. (1997) published the first application of geostatistics to measure the Chernobyl-derived radiocaesium. These studies were based on the mean values of $^{137}$Cs contamination of settlements in the Bryansk Region and corresponded to maps of radioactive contamination at the scales of 1 : 50,000 - 1 :200,000. Similar investigations were also done for Western Europe (Dubois and de Cort, 2001; Dubois and Bossew, 2003; Dubois et al., 2003). In these studies, geostatistic methods were used to draw maps of radioactive contamination and to assess their reliability. However, detailed field studies of the spatial distribution of artificial radionuclides and the role of landscape factors (e.g. topography and soil type) in forming their structure were not performed. To optimise soil sampling for the tasks of radioecological monitoring, a large-scale investigation was carried out on experimental sites within the Chernobyl exclusion zone extending 30 km from the plant (Khomutinin et al., 2001). However, the impact of topography on the character of the $^{137}$Cs spatial distribution was not considered.

The possible impact of topography on $^{137}$Cs lateral mobility is connected with the well known fact: $^{137}$Cs is well absorbed by soil (Siegel and Bryan, 2003). Then $^{137}$Cs may be moved from positive microrelief forms to negative ones together with small soil particles by water flows according to peculiarities of microtopography.

It is essential to investigate the role of topographic factors in forming of contamination patterns of radionuclides. This is because environmental modelling and assessment of radioactively contaminated territories need spatial models of distribution and behaviour of radionuclides relating to landscape formation processes. In soil science and ecology, there is a trend to use quantitative relationships between relief and soil characteristics to predict soil properties (Rawls

et al., 1991; Moore et al., 1993; Florinsky et al., 2002) and digital soil mapping (Behrens and Scholten, 2006). These approaches are based on the use of topographic attributes, such as slope, aspect, profile and plan curvatures (Evans, 1980; McKenzie and Ryan, 1999), derived from digital elevation models (DEMs). DEMs are also employed to compute combined terrain attributes (e.g. wetness index, sediment transport index), which can be also used in soil-landscape modelling (Thompson et al., 1997, McKenzie et al., 1999). A detailed review of methods for description of relief parameters can be found elsewhere (Florinsky, 1998).

Recently, generalized additive models (GAM) (Hastie and Tibshirani, 1990) have been widely used in ecological applications (Miller and Franklin, 2002; Oksanen and Minchin, 2002; de Frutos et al., 2007). GAM allows one to eliminate a systematic component (a spatial trend) of the variability, explained by the individual inputs of spatially distributed predictors, as well as to estimate the significance of each predictor assuming non-linear form of the dependence.

The object of this work was to examine the spatial variation of $^{137}$Cs contamination at a field scale using geostatistics, GAM, and digital terrain modelling. This would contribute to better understanding of the soil radioactive contamination variability.

## STUDY SITES

The study area is situated in the western part of the Bryansk Region, Russia, southwestward the Town of Novozybkov, near the Village of Barky (Fig. 1b). There are the Polessie landscapes including soddy-podzolic, sandy and loamy sand soils, with minor areas of gleyed soils there (Vorobiev et al., 1993). The area is about 170 km away from the Chernobyl Nuclear Power Plant. The radioactive condensed fallout is currently represented by $^{137}$Cs (Fig. 1a).

The research was conducted at the Barky cross-section including three study sites located at different elevation levels of a fluvioglacial plain (Fig. 1c). Sites B1 and B2 were selected in a forest, and a site B4 – in a meadow. For the sites B1, B2, and B4, elevation ranges were 152.68–154.68 m, 160.74–162.8 m, and 139.93–142.85 m, with areas of 0.57, 0.98, and 0.95 ha, correspondingly.

The site B1 is located in the bottom part of a gentle slope with the southern aspect. Gleyed soils dominate there; the plant cover consists of fir and aspen trees, and blueberry. The site B2 is located at a flat watershed covered by a pine forest. There are soddy-podzolic soils there. The site B4 includes parts of a terrace and a flood plain of Kamenka Stream. Meadow gleyed and peaty soils dominate on the flood plain, while meadow and sod-podzolic sandy soils are observed on the terrace.

## MATERIALS AND METHODS

### Topographic Survey

An optical theodolite was used for topographic survey of three sites. Elevations were measured at 563, 821, and 498 points at the sites B1, B2, and B4, correspondingly. Measurement accuracy was 1 cm. All the trees of diameter 10 cm and more are marked at topographic plans at the scale of 1 : 200.

### Radiometric Survey

$^{137}$Cs soil contamination was measured using *in situ* radiometric technique and laboratory-based spectrometric techniques. A field radiometric technique was carried out by a CORAD, a collimated radiometer (Chesnokov et al., 1997, 1999; Fogh et al., 2000). Standard deviation for a CORAD survey results is 22.6% (Martynenko et al., 2003). Direct measurements using a spectrometric survey with a radiometer are effective. They provide the data representativeness that cannot be obtained with soil sampling. Moreover, the field radiometric method is indispensable to obtain large datasets in studies of $^{137}$Cs spatio-temporal patterns, and to explore the dependence of spatial distribution of radionuclides on topography.

Data on radioactive contamination of the sites were obtained by radiometric surveys in 1992-1993. The surveys were done to organise a radioecological monitoring (Linnik, 1994; Govorun and Linnik, 1995) and to verify the CORAD radiometer (Martynenko et al., 2003). At the sites B1 and B2, CORAD measurements were carried out as a regular grid with a grid size of 10 m (Fig. 2). The number of measurements ranged from 78 to 126 for the site B1 and B4, correspondingly.

To analyse the $^{137}$Cs spatial distribution with resolution of 2 m, a detailed radiometric survey was also conducted within the site B1 at two contrasting plots B1-1 and B1-2 with sizes of 10x10 m (Fig. 2). The plot B1-1 is located in the hydromorphic part of the site with a rather complicated relief including small hummock and a downturn. The plot B1-2 is located within a relatively flat area.

Soil samples were also collected at five points of each site (four points at the site corners, and a point at the site centre). The samples were analysed by conventional laboratory spectrometric techniques. Co-ordinates of soil sampling points are other than those of the CORAD survey points. To consider the complex topography of the site B4, five samples were collected at both the flood plain and the terrace.

**Digital Terrain Modelling**

The multilevel B-splines (Wolberg, 1997; Saveliev et al., 2005) were used to construct DEMs of the sites using results of the topographic survey. Spline interpolation parameters were chosen to provide a sufficient accuracy for detailed DEMs ('leave-one-out' cross-validation standard deviation of 0.018 m), such as a DEM grid size of 0.1 m (Fig. 3b). The initial spline control grid of 10x10 knots, 6 levels of hierarchy was used. The DEMs have a representative scale of 0.5 m that allowed us to restore relief details. Generalised DEMs with a grid size of 0.25 m (Fig. 3c) were constructed to characterise relief elements with a typical size of several meters. We used the initial spline control grid of 2x2 knots and 5 levels of hierarchy.

We examined the relationship between $^{137}$Cs contamination ($G$, mcCi/m$^2$) and local topography described by two attributes, such as elevation and Laplacian:

$$\nabla(\nabla f) = \Delta f = \left( \frac{\partial^2}{\partial x^2} + \frac{\partial^2}{\partial y^2} \right) f(x, y). \quad (1)$$

Laplacian is a close approximation of mean curvature, so it may be used to describe the rate of convexity/concavity of a surface (Jost, 2002). In the grid approximation of Laplacian, the recharge cells (net flow into the cells) are positive, and discharge cells (net flow out of the cell) are negative, if the local flow rate is proportional to the local gradient. Negative values of Laplacian correspond to convex zones of the land surface where overland and intrasoil flows tend to dissipate, while positive ones refer

to concave zones where flows tend to accumulate.

Digital models of Laplacian were calculated for the DEMs and for points of CORAD measurements at the plots B1-1 and B1-2 without geodetic measurements at each points of the CORAD survey. To shorten the range of Laplacian values *l*, they were transformed into values *l'* using a logarithm and preserving the continuity at zero:

$$l' = \begin{cases} \ln(1+l), l \geq 0 \\ -\ln(1-l), l < 0 \end{cases}. \quad (2)$$

For the generalised DEMs, the range of Laplacian values is considerably narrower, so an additional log-transformation of the values was not conducted.

**Generalized Additive Models (GAM)**

If there is a clear non-linear relationship between a response variable and explanatory variables, there is an option to apply smoothing methods like GAM. In these methods, smoothing curves are used to model the relationship between the response variable and explanatory variables. The curve for each covariate is estimated as a nonparametric function in an iterative manner using the scatterplot smoothers. Such a smoother may be regarded as a moving average, where the window size defines a smoothness of a result. Another way is to use a spline with a 'wiggliness' (curvature) penalty added to the fit error. The penalty weight defines a smoothness level (Hastie and Tibshirani, 1990; Schimek, 2000).

GAM is a model with a predictor given by a sum of smoothers. GAM with two covariates can be exemplified by

$$G(x_1, x_2) = a_0 + s_1(x_1, \Theta_1) + s_2(x_2, \Theta_2) + \varepsilon, \quad (3)$$

where *G* is a response variable, intercept $a_0$ is a constant, $s_1(\ldots)$ and $s_2(\ldots)$ are smooth functions of covariates $x_1$ and $x_2$, and $\varepsilon$ is a normally distributed error. Parameters $\Theta_1$ and $\Theta_2$ define the smoothness of the functions. The use of arbitrary complex functions (e.g. high degree polynomials) can result in overfitting estimates of $s_1$ and $s_2$. Therefore, the penalised likelihood maximisation is used to fit the model in which the measure of the model fit (a negative log likelihood) is modified by the addition of smoothness penalty, penalising its 'wiggliness'.

The GAM penalised likelihood maximisation problem is solved by penalised Iteratively Reweighted Least Squares (Wood, 2006). At each iteration, a penalised weighted least squares problem is solved, and the smoothing parameters of the problem are estimated by generalised cross validation until both model parameter estimates and smoothing parameter estimates converge.

**Geostatistical Analysis**

We used geostatistics to analyse the spatial variability of $^{137}$Cs soil contamination. The spatial structure of $^{137}$Cs contamination was characterised by sample variograms $\gamma(h)$ calculated from the experimental data using an equation (Isaaks and Srivastava, 1989; Cressie, 1993):

$$\gamma(h) = \frac{1}{2n}\sum_{i=1}^{n}[Z(x_i + h) - Z(x_i)]^2 , \quad (4)$$

where $x_i$ and $x_i + h$ are sampling locations separated by a vector $h$, $Z(x_i)$ and $Z(x_i + h)$ are measured values of the variable $Z$ ($^{137}$Cs contamination) at the corresponding locations, and $n$ is the number of points measured by CORAD.

To estimate the possible anisotropy of $^{137}$Cs spatial patterns, we calculated experimental variograms for the four directions of the separating vector $h$: 0°, 45°, 90°, and 135°. According to the well known 'rule-of-thumb', semi-variance should not be calculated for separation distances greater than about 50% or 66% of the width or length of a study site. For the sites B1 and B2, the area length is about 100 m, so we used the maximal distance 67 m. For the plot B1-1 and B1-2, the maximal distance of 9.5 m was used due to the regularity of locations. This choice of maximal distances were also supported by distance histograms.

The linear and GAM models were used to consider the systematic dependence of $^{137}$Cs contamination on covariates (co-ordinates and relief variables). The modelled values were subtracted from $^{137}$Cs measured ones before the variogram calculation.

We used the following blueprint of the model analysis. First, we fitted a linear model to the data and estimated the significance of the covariates. (GAM can be fitted if all the covariates are insignificant in the linear model.) The variogram analysis was then applied either to the residuals from the fitted model (if covariates are significant) or

vice versa to $^{137}$Cs values. To model the $^{137}$Cs spatial distribution (the dependent variable *G*), we used the following covariates (predictors): Laplacian value (*Laplace*), elevation (*H*), and *X* and *Y* co-ordinates. We used elevations either from field measurements (*H*) or derived from a detailed DEM ($H_{mba1}$) or a generalised DEM ($H_{mba2}$). Laplacian values derived from detailed and generalised DEMs were denoted as $Laplace_1$ (Fig. 3B) and $Laplace_2$ (Fig. 3c) correspondingly.

## RESULTS AND DISCUSSION

Statistical characteristics for $^{137}$Cs soil contamination are given in Table 1. The maximum variability of $^{137}$Cs deposits, 24.5%, was found at the site B1.

For the site B1, data were fitted by a linear model $G_1$:

$$G_1 = a_0 + a_1 Laplace_1 + a_2 H + a_3 X + a_4 Y . \quad (5)$$

This demonstrates that all the covariates used are insignificant. Hence, the $^{137}$Cs spatial distribution (Fig. 3a), measured by the radiometric survey on a regular grid with the grid size of 10 m, does not depend on selected topographic parameters (Laplacian and elevation) and planimetric co-ordinates within the site B1.

Geostatistical analysis demonstrated (Fig. 4) that the variogram values for the intermediate lags (at the distance of 25-30 m) are significantly higher than the $^{137}$Cs variance ($\sigma^2$ = 39.7) at 5% confidence level for each direction (permutation test with 5000 permutations was used). The same is applicable to the distance about 45 m. This gives some evidence of a negative correlation, or, to be more exact, a 'chess board' effect. It can be caused by patches marked by a high level of $^{137}$Cs contamination with a typical size of about 25 m alternating with patches marked by a low level of $^{137}$Cs contamination.

To analyse a detailed model of the $^{137}$Cs spatial distribution at the plots B1-1 and B1-2, we replaced measured values of elevation in the model $G_1$ (Eq. 5) with its interpolated values:

$$G_2 = a_0 + a_1 Laplace_1 + a_2 H_{mba1} + a_3 X + a_4 Y . \quad (6)$$

This linear model did not also reveal a significance of covariates. The same result was obtained for the generalised DEMs.

For the plot B1-1, the variogram analysis revealed the following properties of the $^{137}$Cs spatial distribution (Fig. 5a). The variogram behaviour depends on direction: its value is minimal in 0°-direction for all lags, that is, the $^{137}$Cs variability in 0°-direction is lower than in 90°- and 135°-directions. Most likely, this is because 0°-direction is collinear with the general direction of the local water flow. In other words, the land surface profile is rather smooth in 0°-direction, whereas it is wavy, with more expressed convex and concave forms, in the perpendicular direction. The land surface resembles a washboard with grooves striking in 0°-direction. So, not elevation but the groove orientation (and thus the direction of the local water flow) influences the pattern isotropy of the $^{137}$Cs spatial distribution. At the plot B1-1, patterns with a typical size of 5 m were also revealed which coincide with small pits.

For the plot B1-2, application of the linear model (Eq. 6) showed that all parameters are insignificant. This means that the $^{137}$Cs distribution is not related to the variables used in the model. The variogram analysis did not demonstrate a spatial correlation for all the four directions at the plot B1-2 (Fig. 5b). Hence, the character of the $^{137}$Cs spatial distribution may be considered as random, at least for large lags.

For the plot B1-1, a non-linear GAM model $G_3$

$$G_3 = a_0 + s(Laplace_1) + s(H_{mba1}) \quad (7)$$

showed a significance of elevation ($H_{mba1}$) and a weak significance of the land surface curvature ($Laplace_1$). These factors explained 30% of the $^{137}$Cs total variance. For the generalised DEM, there was a significant dependence on the land surface curvature ($Laplace_2$): a model $G_4$ explained about 25% of the $^{137}$Cs variance:

$$G_4 = a_0 + s(Laplace_2). \quad (8)$$

An influence of planimetric co-ordinates, that is, a spatial trend was not detected for both cases (Eqs. 7 and 8), as confirmed by variograms (Fig. 5). Thus, we can accept the independence of $G$ values on co-ordinates, elevation, and the land surface curvature in the framework of the linear model $G_2$ (Eq. 6).

In the model $G_4$ (Eq. 8), the $^{137}$Cs quadratic dependence on $Laplace_2$ indicates that the spatial distribution of $^{137}$Cs contamination has a complex structure, resulting from

alternation of small hummocks and pits at different elevation levels (153.5-153.9 m). $^{137}$Cs contamination, increasing in both concave and convex zones of the land surface, reaches minimum at flat areas (Fig. 6).

For the watershed site B2, all parameters were insignificant within the framework of the linear model $G_1$ (Eq. 5). A variogram, calculated in four directions, demonstrated that there was no spatial correlation with any direction or distance (Fig. 7a). So, the $^{137}$Cs spatial distribution may be considered as a 'white noise' at the site B2. Only $H_{mba1}$ is significant for the non-linear model $G_3$ (Eq. 7) with elevation and Laplacian as covariates. The variance explained was 8.9%, and the mean value (intercept) is 30.4. The dependence of $^{137}$Cs on elevation is presented on Figure 7b.

For the site B4, an analysis of the $^{137}$Cs omnidirectional variogram (Fig. 8a) reveals a spatial structure at lags exceeding 40 m, which approximately corresponds to the site division into the flood plain and terrace. However, a marked anisotropy of the $^{137}$Cs distribution in different directions was not observed (Fig. 8b). Separate variograms showed that contamination patterns are rather smooth at the terrace and more random at the flood plane.

To find potential areas of the $^{137}$Cs washing-out and accumulation within the site B4 (Fig. 9a), a Laplacian digital model was derived from the DEM in the valley of Kamenka Stream (Fig. 9b). We attempted to consider a principal difference in the geomorphic structure of the site B4 (the flood plain versus the terrace) governing different mechanisms of the $^{137}$Cs redistribution. At the terrace, a lateral washing-out of radionuclides was observed because of the difference in elevation. At the flood plain, flooding and lateral washing-out processes occur. The site was divided into four portions. According to Laplacian values, concave and convex zones were chosen on the terrace and on the flood plain. $^{137}$Cs washing-out areas (*Laplace* < 0) were found predominantly in the upper part of the terrace, whereas $^{137}$Cs accumulation areas (*Laplace* > 0) occur in the lower part of the footslope.

It was found that the $^{137}$Cs mean contamination at the terrace is 29.93 mcCi/m$^2$, while at the flood plain – 30.88 mcCi/m$^2$ (Table 2, Fig. 9a), with the mean value of 30.35 for the entire site B4 (Table 1). Laplacian mean values at the terrace and flood

plain correspond to the convex areas (*Laplace* < 0), with the washing-out potential of -0.00137 at the terrace against -0.00087 at the flood plain (viz. 1.57 times higher). Solving a balance equation, we can estimate that 0.475 mcCi/$m^2$ (viz. about 1.6 % of the $^{137}$Cs total activity) were washed out from the terrace of the site B4 from 1986 to 1992. Flooding processes, which were not discussed in this study, might be also significant for the contribution of the $^{137}$Cs deposits to the flood plain.

The most intensive lateral migration of $^{137}$Cs in landscapes has occurred during 3-4 years after the Chernobyl accident of 1986. In the year 2000, intensity of the $^{137}$Cs washing-out has decreased almost in 100 times in comparison with an initial level (Zhukova et al., 2002). Therefore, measurements of 1992-1993 years, used in this study, characterises the period of the maximal rate of the $^{137}$Cs lateral migration.

## CONCLUSIONS

The maximum spatial variability of $^{137}$Cs deposits, 24.5%, was observed in hydromorphic conditions of the forested site B1. At the site B1, the $^{137}$Cs spatial distribution consists in patch patterns with the size of about 5 m within the hydromorphic part of the site, and of about 30-40 m within the forested part of the site. In automorphic conditions (the plot B1-2 and the site B2), the $^{137}$Cs spatial distribution is random and does not form patterns. At the site B4, the $^{137}$Cs spatial distribution is governed by geomorphic structures: the flood plain and the terrace. The washing-out potential of the terrace exceeds that of the flood plain. This is reflected in increasing of the $^{137}$Cs contamination rate by 1.6 % at the flood plain as compared with the terrace. The $^{137}$Cs distribution is depend crucially on the local topography in hydromorphic conditions. Laplacian is the most informative index for the process of the $^{137}$Cs lateral migration while elevation is of subsidiary importance.

## REFERENCES

Behrens, T., and Scholten, T., 2006, *Digital Soil Mapping in Germany – A Review*, Journal of Plant Nutrition and Soil Science, 169, 434-443.

Chesnokov, A.V., Fedin, V.I., Govorun, A.P., Ivanov, O.P., Liksonov, V.I., Potapov, V.N., Smirnov, S.V., Scherbak, S.B., and Urutskoev, L.I., 1997, *Collimated Detector Technique for Measuring a $^{137}$Cs Deposit in Soil Under a Clean Protected Layer*, Applied Radiation Isotopes, 48, 1265-1272.

Chesnokov, A.V., Govorun, A.P., Fedin, V.I., Ivanov, O.P., Liksonov, V.I., Potapov, V.N., Scherbak, S.B., Smirnov, S.V. and Urutskoev, L.I., 1999, *Method and Device to Measure $^{137}$Cs Soil Contamination In-Situ*, Nuclear Instruments and Methods, A 420, 336-344.

Cressie, N., 1993, *Statistics for Spatial Data*, John Wiley, New York.

De Frutos, A., Pedro, P., Olea, P.P., and Ruben, V., 2007, *Analyzing and Modelling Spatial Distribution of Summering Lesser Kestrel: The role of Spatial Autocorrelation*, Ecological Modeling, 200, 33-44.

Dubois, G., and Bossew, P., 2003, *Chernobyl $^{137}$Cs Deposition in Austria: Analysis of the Spatial Correlation of the Deposition Levels*, Journal of Environmental Radioactivity, 65, 29-45.

Dubois, G. and de Cort, M., 2001, *Mapping $^{137}$Cs: Data Validation Methods and Data Interpretation*, Journal of Environmental Radioactivity, 53, 271-289.

Dubois, G., Malczewski, J., and de Cort, M., (Eds.), 2003, *Mapping Radioactivity in the Environment*, Office for Official Publications of the European Communities, Luxembourg.

Evans, I.S., 1980, *An Integrated System of Terrain Analysis and Slope Mapping*, Zeitschrift für Geomorphologie, Suppl. 36, 274-295.

Florinsky, I.V., 1998, *Combined Analysis of Digital Terrain Models and Remotely Sensed Data in Landscape Investigations*, Progress in Physical Geography, 22, 33-60.

Florinsky, I.V., Eilers, R.G., Manning, G., and Fuller, L.G., 2002, *Prediction of Soil Properties by Digital Terrain Modelling*, Environmental Modelling and Software, 17, 295-311.

Fogh, C.L., Andersson, K.G., and Roed, J., 2000, *In Situ Performance of the CORAD Device Measuring Contamination Levels and Penetration Ratio of $^{137}$Cs*, Nuclear Instruments and Methods in Physics Research, B 160, 408-414.

Govorun, A.P., Linnik, V.G., 1995, *Use of Field Radiometry for Studying the Migration of Radionuclides in Various Landscapes in Bryansk Region*, in Abstracts, All-Russian Conference on Radioecological, Medical, and Socio-economic Consequences of the Chernobyl Accident. Rehabilitation of Territories and Population, May 21-25, Golitsyno, Russia. Tveruniversalbank, Moscow (in Russian).

Hastie, T., and Tibshirani, R., 1990, *Generalized Additive Models*, Chapman and Hall/CRC, London.

Isaaks, E.H., and Srivastava, R.M., 1989, *An Introduction to Applied Geostatistics*, Oxford University Press, Oxford.

Jost, J., 2002, *Riemannian Geometry and Geometric Analysis*, Springer, Berlin.

Kanevsky, M., 1994, *Chernobyl Fallout: Stochastic Simulations of the Spatial Variability and Probabilistic Mapping*, Nuclear Safety Institute, Moscow.

Kanevsky, M., Demyanov, V. and Maignan, M., 1997, *Spatial Estimations and Simulations of Environmental Data by Using Geostatistics and Artificial Neural Networks*. in Pavlovsky-Glahn, V. (Ed.), Proceedings of the 3rd Annual Conference of the International Association for Mathematical Geology, IAMG'97. CIMNE, Barcelona.

Khomutinin, Ju.V., Kashparov, V.A., and Zhebrovskaya, E.I., 2001, *Optimisation of Selection and Measurements of the Samples in a Course of the Radioecological Monitoring*, Vipol, Kiev (in Russian).

Linnik, V.G., 1994, *Assessment and Prediction of a Radioecological Situation Using GIS-Technology: A Case of Restoration of Radionuclide Contaminated Territory of Bryansk Region*. in Proceedings

SPECTRUM'94: Nuclear and Hazardous Waste Management International Topical Meeting, Vol. 3. August 14-18, Atlanta, USA.

Martynenko, V.P., Linnik, V.G., Govorun, A.P., and Potapov, V.N., 2003, *Comparison of the Results of Field Radiometry and Sampling in the Investigation of $^{137}$Cs Soil Content in the Bryansk Region*, Atomic Energy, 95, 727-733.

McKenzie, N.J., and Ryan, P.J., 1999, *Spatial Prediction of Soil Properties Using Environmental Correlation*, Geoderma, 89, 67-94.

Miller, J., and Franklin, J., 2002, *Modeling the Distribution of Four Vegetation Alliances Using Generalized Linear Models and Classification Trees with Spatial Dependence*, Ecological Modelling, 157, 227- 247.

Moore, I.D., Gessler, P.E., Nielsen, G.A., and Peterson, G.A., 1993, *Soil Attribute Prediction Using Terrain Analysis*, Soil Science Society of America Journal, 57, 443-452.

Oksanen, J., and Minchin, P.R., 2002, *Continuum Theory Revisited: What Shape are Species Responses Along Ecological Gradients?* Ecological Modelling, 157, 119-129.

Rawls, W.J., Gish, T.J., and Brakensiek, D.L., 1991, *Estimating Soil Water Retention from Soil Physical Properties and Characteristics,* Advances in Soil Science, 16, 213-234.

Saveliev, A.A., Romanov, A.V., and Mukharamova, S.S., 2005, *Automated Mapping Using Multilevel B-Splines*, Applied GIS, 1, 17-01-17-19.

Schimek, M. (Ed.), 2000, *Smoothing and Regression: Approaches, Computation and Application*. Wiley, New York.

Siegel, M.D., and Bryan, C.R., 2003, *Environmental Geochemistry of Radioactive Contamination*, in Holland, H.D., and Turekian, K.K. (Eds.), Treatise on Geochemistry, Vol. 9. Elsevier, Amsterdam.

Thompson, J.A., Bell, J.C., and Butler, C.A., 1997, *Quantitative Soil-Landscape Modeling for Estimating the Areal Extent of Hydromorphic Soils*, Soil Science Society of America Journal, 61, 971-980.

Vorobiev, G.T., Guchanov, D.E., Kurganov, A.A., Markina, Z.N., Novikov, A.A., and Svetov, V.A., 1993, *Caesium-137 in Soils and Crops in Bryansk, Kaluga, Orel, and Tula Regions in 1986-1992*. Grani, Bryansk (in Russian).

Wood, S.N., 2006, *Generalized Additive Models: An Introduction*. Chapman and Hall/CRC, London.

Wolberg, G., 1997, *Nonuniform Image Reconstruction Using Multilevel Surface Interpolation*, International Conference on Image Processing, 1, 906-916.

Zhukova, O.M., Shiryaeva, N.M., Myshkina, N.K., Denisova, V.V., and Skurat, V.V., 2002, *Prediction of Migration of Radionuclides in the Iput River Basin*, Journal of Engineering Physics and Thermophysics, 75, 256-267.

Table 1. Descriptive statistics of the $^{137}Cs$ (mcCi/m$^2$) distribution in soils at the sites B1, B2, and B4.

| Study site | B1 | | B2 | | B4 | |
|---|---|---|---|---|---|---|
| Year of measurement | 1993 | | 1993 | | 1992 | |
| | CR | S | CR | S | CR | S |
| Number | 78 | 5 | 121 | 5 | 126 | 10 |
| Mean | 25.7 | 28.78 | 30.35 | 20.55 | 30.35 | 33.67 |
| Median | 25.2 | 26.04 | 29.44 | 21.32 | 30.2 | 35.46 |
| Minimum | 12.5 | 16.12 | 19.46 | 12.4 | 22.0 | 16.72 |
| Maximum | 46.1 | 41.47 | 40.62 | 29.21 | 44.1 | 53.35 |
| Standard deviation | 6.3 | 11.61 | 4.32 | 6.11 | 3.46 | 10.75 |
| Variance | 24.5 | 40.3 | 14.2 | 29.7 | 11.4 | 31.9 |
| Skewness | 0.44 | | 0.22 | | 0.48 | |
| Kurtosis | 0.5 | | -0.18 | | 1.53 | |

CR – CORAD measurements;

S – laboratory spectrometric measurements of soil samples.

Table 2. Means of $^{137}Cs$ (mcCi/m$^2$) and Laplacian values for the flood plain and the terrace of the site B4.

| Terrain type | Flood plain (elevation > 141.5 m) | Terrace (elevation < 141.5 m) |
|---|---|---|
| $^{137}Cs$ | 29.93 | 30.88 |
| *Laplace* | -0.00137 | -0.00087 |

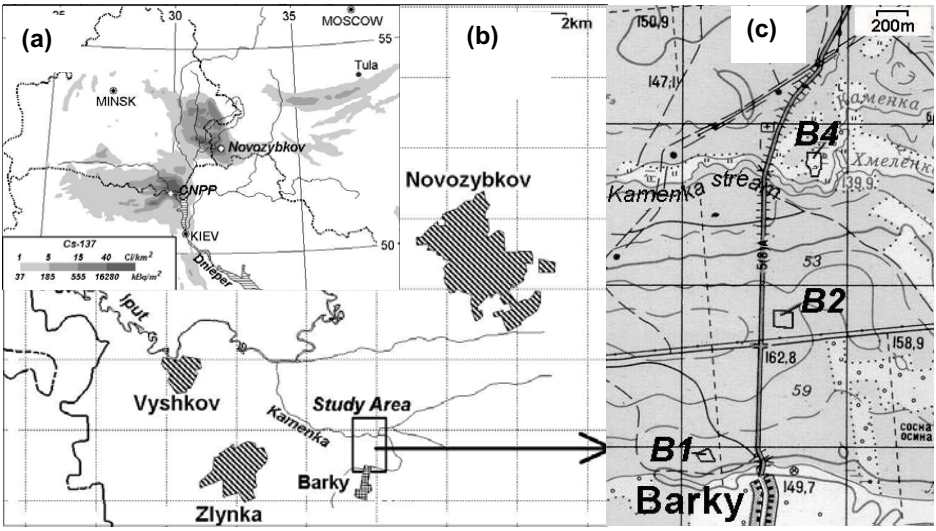


Fig. 1. Geographical location of the study area: (a) map of $^{137}Cs$ soil deposition in Ukraine, Belarus and in the west of the Russian Federation due to the Chernobyl accident; (b) Western part of the Bryansk Region, the Novozybkov study area (between 52°25'31"-52°27'20" N and 31°49'50"-31°51'45" E); (c) the Barky cross-section, the study sites B1, B2, and B4.

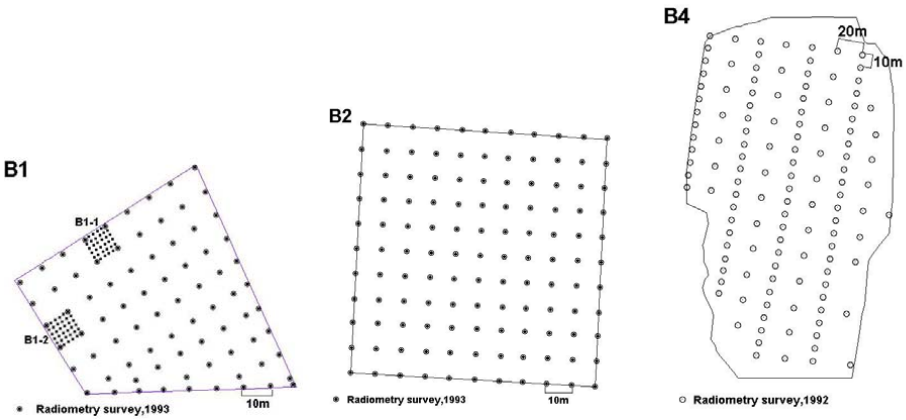


Fig. 2. Grid design of the radiometric survey at the sites B1, B2, and B4.

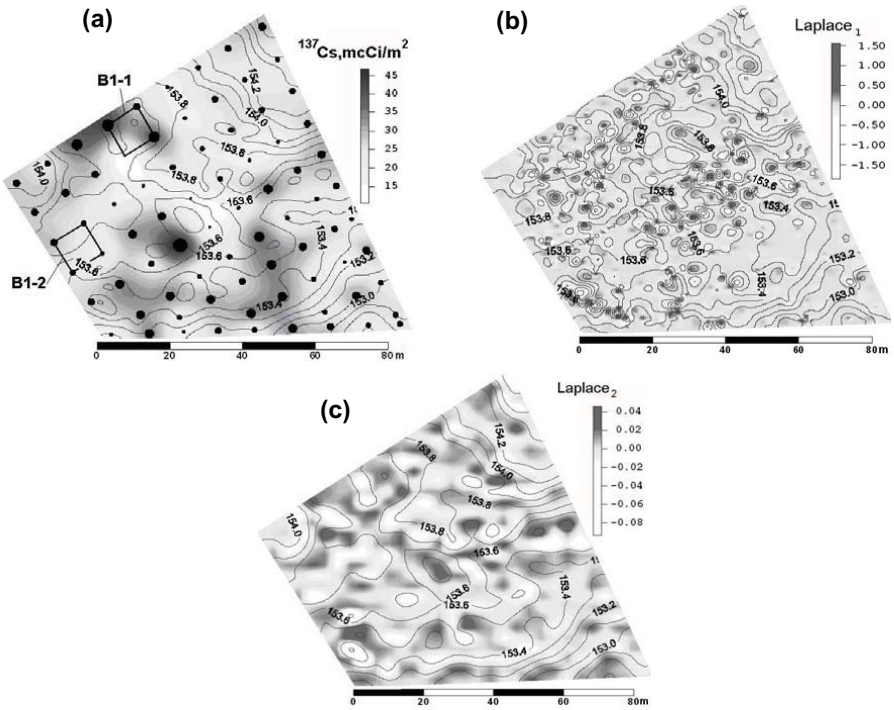


Fig. 3. Site B1: $^{137}$Cs contamination (a); elevation (contours) and Laplacian (greyscale) indicating the rate of convexity/concavity (white/dark grey) for the detailed (b) and generalised (c) DEMs.

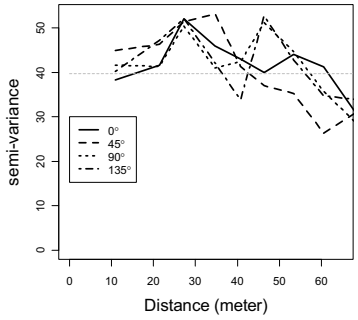


Fig. 4. Site B1: $^{137}$Cs experimental variogram for four directions with ±22.5$^o$ angle tolerance. Maximum distance is 67 m, 9 bins for each direction, average number of pairs for each bin is 70, RMSE = 19, minimum is 20.

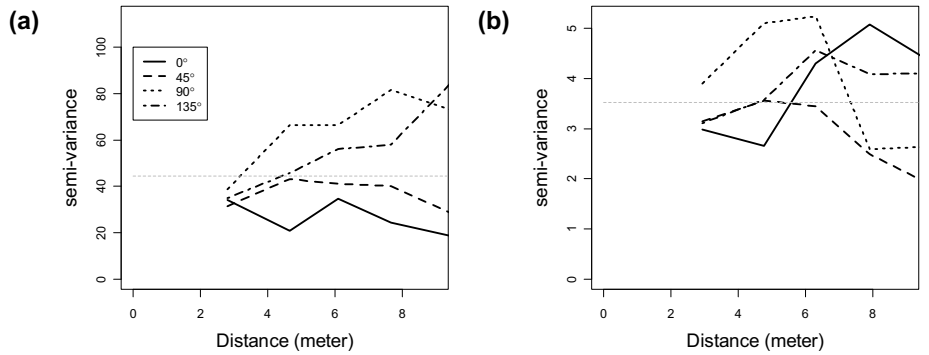


Fig. 5. $^{137}$Cs variogram models for four directions with ±22.5$^{o}$ angle tolerance; maximum distance is 9.5 m, 5 bins for each direction, average number of pairs for each site bin is 31, RMSE = 6, minimum is 20: (a) plot B1-1, (b) plot B1-2.

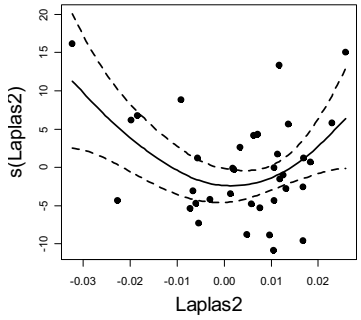


Fig. 6. Plot B1-1: dependence of $^{137}$Cs on Laplacian.

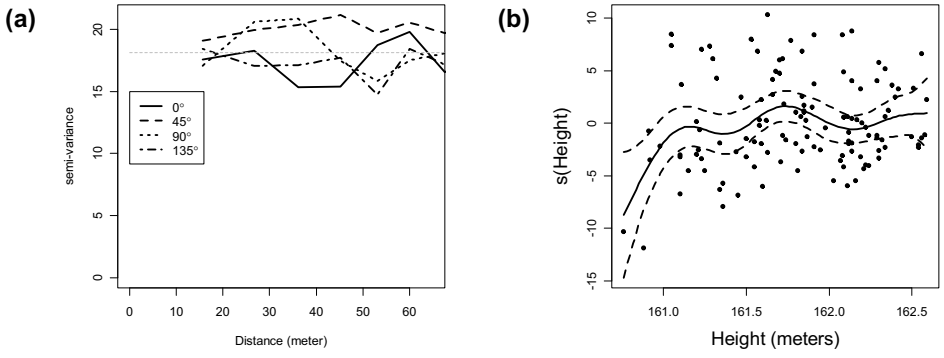


Fig. 7. Site B2: (a) $^{137}$Cs variogram model for four directions with ±22.5$^{o}$ angle tolerance; (b) dependence of $^{137}$Cs on elevation.

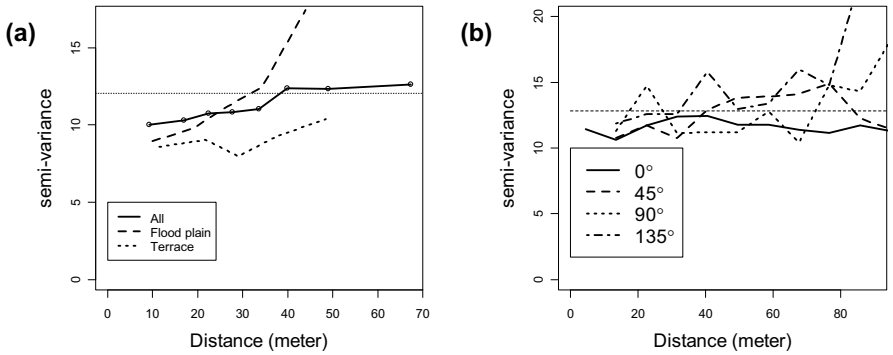


Fig. 8. Site B4: (a) $^{137}$Cs omnidirectional variogram; (b) $^{137}$Cs variogram model for four directions with ±22.5$^{o}$ angle tolerance.

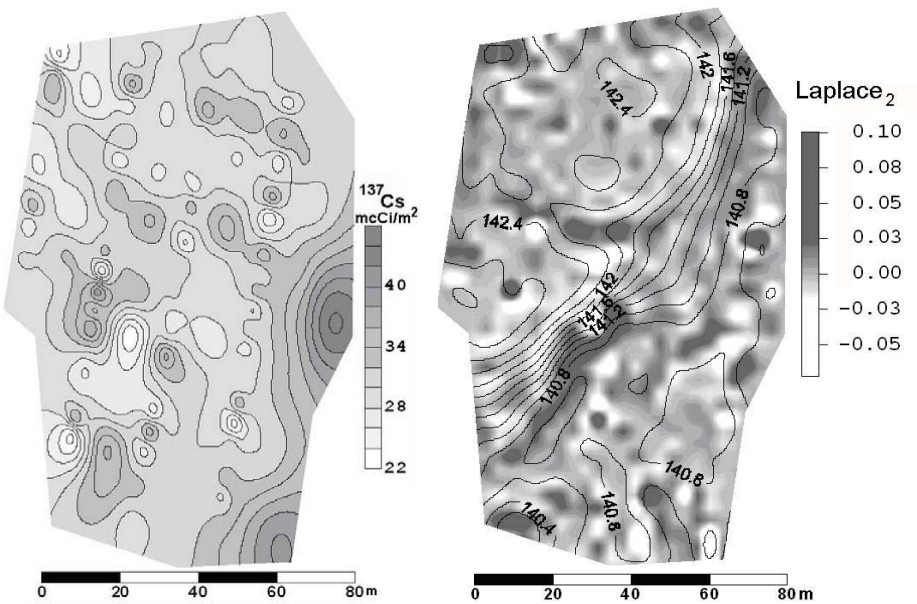


**(a)** **(b)**

Fig. 9. Site B4: (a) $^{137}$Cs contamination; (b) elevation (contours) and Laplacian for the generalised DEM (greyscale) indicating the convexity/concavity rate (white/dark grey, correspondingly).

*International Journal of Ecology & Development*
*Fall 2007, Vol. 8, No. F07; Int. J. Ecol. Dev.*
*ISSN 0972-9984 ( Print ); ISSN 0973-7308 (Online)*


# Comparison of Automated Landform Classification and Soil Mapping Units at a Farm Level

**Vanda Valerija Buivydaite [1], Gintautas Mozgeris [2]**

[1] Department of Soil Science & Agrochemistry, Agronomic Faculty
Lithuanian University of Agriculture
Studentu St. 11, LT–53361 Akademija, Kaunas R., Lithuania
e-mail: Vanda.Buivydaite@lzuu.lt

[2] GIS Education and Research Centre, Institute of Environment
Lithuanian University of Agriculture
Studentu St. 13, LT–53361 Akademija, Kaunas R., Lithuania

Received 7 December 2006; accepted 23 April 2007

## ABSTRACT

*More than twenty morphometric attributes derived from digital elevation models (DEMs) were correlated with soil mapping units available from conventional soil maps at a scale of 1 : 2,000. The following topographic attributes were involved into the analysis: slope steepness, slope aspect, elevation, horizontal curvature, vertical curvature, mean curvature, surface insolation, maximal curvature, minimal curvature, catchment area, depression depths, dispersal area, hill heights, gradient factor, difference curvature, horizontal and vertical excess curvatures, rotor, unsphericity, total Gaussian curvature, total accumulation curvature, total ring curvature, and topographic index. A DEM with a grid size of 30 m was best suited to describe the relationships between soil units and terrain variables. Soil typological units and their classes correlated stronger with the landform types derived using the Shary landform classification (the contingency coefficients were over 0.6) rather than the Troeh and Gauss landform classifications. Mean and horizontal curvatures, elevation, slope, gradient factor, and topographic index were best correlated with the soil typological units of the soil classification system of Lithuania, which is based on the international soil classification.*

**Keywords:** Soil Map, Digital Elevation Model, Morphometric Variable, Landform Type.
**Mathematics Subject Classification:** 86A30, 62P12, 62H30, 62H99.
**JEL Classification:** Q19, Q50.

## INTRODUCTION

Achievements in soil cartography and Geographic Information Systems (GIS) allow one to develop soil map models based on reproducible pedogeomorphological

approaches. Quantitative description of landforms can be used to produce soil maps of a new generation in a wide range of scales: from large scales (1 : 2,000) to meso-scales (1 : 10,000) and to small scales (1 : 1,000,000) (Wilson and Gallant, 2000). Most of the hydrological, geomorphological, and ecological researches of the past century has been conducted at the global and micro-scales. The meso- and large scales have received less attention. However, various environmental problems, such as accelerated soil erosion and non-point-source pollution, require changes in management strategies at these scales (Moore and Hutchinson, 1991). The influence of land surface morphology on catchment hydrology and surface insolation are the most important factors operating at a large scale. Numerous studies have shown that variations in elevation, slope, aspect, and local topographic horizon can cause substantial differences in the spatial and temporal distributions of the light, heat, water, and mineral nutrients required by photosynthesising plants, affecting, in turn, the distribution and abundance of flora and fauna (Wilson and Gallant, 2000). During the past decade, the popularity of works on these tasks has increased due to availability of high-resolution digital elevation data and computerised tools of terrain analysis (Shary, 1995; Burrough and McDonnell, 1998; Wilson and Burrough, 1999; Florinsky et al., 2002; Shary et al., 2002; MacMillan et al., 2003; McBratney et al., 2003; Smith et al., 2006).

In Lithuania, investigations of relief were launched more than two centuries ago, and were mainly focused on structural geomorphology, glacier accumulative formations, such as glaciofluvial, glaciolacustrine, fluvial, eolian, littoral, organogenic, and limnic relief (Česnulevičius, 1999). Compilation of GIS-based morphoisographic maps of the land surface of Lithuania has been initiated in 1997 for the systematisation of soil cover structures at scales of 1 : 25,000 and 1 : 1,000,000 (Buivydaite, 2003; Mozgeris and Buivydaite, 2004). This was the first attempt to use morphometric investigations in the context of soil survey applications in Lithuania.

The main objective of this paper is to compare three systems of landform classification, and soil mapping units at a farm level. We discuss the usability of this sort of landform classification for soil survey. More than twenty morphometric attributes, derived from DEMs, have been correlated with the soil mapping units from conventional soil maps at the scale of 1 : 2,000.

## MATERIALS AND METHODS

The Experimental Station of the Lithuanian University of Agriculture (Kaunas Region, Lithuania) was chosen as a test polygon. The study area occupied 75.3 ha. Detailed soil (Fig. 1a) and topographic (Fig. 2a) maps are available for this area at the scale of 1:2,000. The maps were scanned, geo-referenced, and integrated in a GIS database. The initial sources for DEMs were contours with a contours interval of 0.25 m. DEMs were generated using a standard module of ArcInfo software based on the method by Hutchinson (1993). The method includes a drainage enforcement algorithm for removing spurious sinks or pits in the fitted elevation grid, and an algorithm calculating ridge and stream lines with points of maximum local curvature of contours (Weibel and Heller, 1991). For the study area, five DEMs with different resolution were generated using cell sizes of 5, 10, 20, 30, and 40 m.

The DEM derivatives were computed for each cell on the elevation grid using 3×3 moving window. We computed the following morphometric variables: slope steepness (Fig. 3a), gradient factor, slope aspect, surface insolation, mean curvature (Fig. 3b), horizontal curvature (Fig. 3c), vertical curvature, maximal curvature, minimal curvature, difference curvature, horizontal and vertical excess curvatures, rotor, unsphericity, total Gaussian curvature, total accumulation curvature, total ring curvature, catchment area, dispersal area, depression depths, and hill heights. These morphometric attributes are essential to model specific aspects of overland and intrasoil gravity-driven transport of substances, and thus to study and model regularities in spatial distribution of soil properties. Definitions, formula, and detailed interpretations of these variables can be found elsewhere (Shary et al., 2002). In addition, we computed the topographic index (Fig. 3d), indicating the amount of the water flowing towards a certain location, and the local slope, which is a measure of the drainage from a place (Moore et al., 1993; Angelstam et al., 2003). Morphometric attributes were derived from DEMs using Analytical GIS Eco 1.05 (Shary et al., 2002) and ArcInfo 9.2 (© ESRI Inc., 1982-2006).

Three landform classification systems have been evaluated:

1. The classification system by Troeh (1964), which is based on field-specific

forms and can be described in surface runoff terms. The system includes four landform types defined by signs of vertical and horizontal curvatures (Fig. 1b).

2. The classification system suggested by Gauss (Shary et al., 2002). The system includes four landform types defined by total Gaussian curvature and mean curvature (Fig. 1c).
3. The classification system presented by Shary (1995), which is a generalisation of the two classifications indicated above. The system includes twelve landform types defined by horizontal, vertical, mean, and difference curvatures (Fig. 1d).

A network of about 300 sampling points was generated to extract and analyse the values from all GIS coverages developed. Sampling points corresponded to the cell centre for grids with the cell size of 20 m and coarser. The network of sampling points was used in subsequent analyses for all variants of DEM grid sizes.

Contingency tables and Pearson's contingency coefficient (Pcc) was used to describe the correlation between two qualitative variables:

$$Pcc = \frac{c}{\max c}, \tag{1}$$

where

$$c = \sqrt{\frac{\chi^2}{totfrq + \chi^2}}, \tag{2}$$

$$\max c = \sqrt{\frac{\max cls - 1}{\max cls}}, \tag{3}$$

$$\chi^2 = \sum \frac{(o_i - e_i)^2}{e_i}, \tag{4}$$

$o_i$ is an observed cell frequency in a contingency table, $e_i$ is the cell frequency according to variable independence, $totfrq$ is the total number of observations, and $\max cls$ is the maximum number of classes.

The correlation between a qualitative variable and one or more quantitative variables was studied by performing a variance analysis and calculating the total, within and between sums of squares, correlation coefficients, and degree of determination for

each qualitative/quantitative variable pair. Pearson's correlation coefficient was used to describe the correlation between two ore more quantitative variables.

## RESULTS

Definitions of soils in the study area are based on the soil typological units (Sdv99nr) of the soil classification system of Lithuania (LTDK-99) correlated with the international soil classification (FAO, 1998; Buivydaite et al., 2001). For more in-depth statistical analysis, the soils were grouped (a) by the soil type category; and (b) within the soil type, by soil subtype, soil genera, soil species, and soil variety categories. In the study area, Luvisols and Cambisols are prevailing soil typological units. Within a soil type category, soils were grouped into classes:

- According to the depth of carbonates and hydromorphism (natural drainage): calcaric hypergleyic (Sdv1nr), calcaric hypogleyic (Sdv2nr), and eutric hypogleyic (Sdv3nr).
- According to the texture of the topsoil Ap horizon (Ts1apnr), subsurface B horizon (Ts1bnr), subsoil C horizon (Ts1cnr), subsoil 2C horizon (Ts12cnr), and soil texture group (Textgr).

The strongest relationship between landform types and soil typological units (Sdv99nr), soil classes (Sdv1nr, Sdv2nr, and Sdv3nr), soil texture (Ts1apnr, Ts1bnr, Ts1cnr, and Ts12cnr), soil texture groups (Textgr), and cell sizes was detected for the Shary classification system (Table 1). Contingency coefficient varies depending on the soil typological unit used but is never less than 0.30.

Soil classes – calcaric hypergleyic, calcaric hypogleyic, and eutric hypogleyic subgroups – best correlated with the landform types of the Shary classification system. Contingency coefficients (Table 2) are highest for DEMs with grid sizes of 30-40 m.

The study has been mainly focused on the correlation analysis of soil attributes and morphometric variables. Mean curvature (Fig. 3b), horizontal curvature (Fig. 3c), elevation, slope (Fig. 3a), gradient factor, and topographic index (Fig. 3d) have the strongest correlation with the soil typological unit (Table 3).

There is the same trend for correlation coefficients: they reach the maximum value for the DEM grid size of 30 m or larger. Landform types according to the Shary classification system (Fig. 1d) can be considered as some kind of generalisation of numerous morphometric variables. Landform types may be grouped as follows:

- C-depressions with positive and negative difference curvature;
- C-saddles mean-concave, convergent-decelerating, with positive difference curvature; C-saddles mean-concave, convergent-accelerating, with positive difference curvature; C-saddles mean-concave, convergent-decelerating, with negative difference curvature; C-saddles mean-concave, divergent-decelerating, with negative difference curvature;
- C-saddles mean-convex, convergent-accelerating, with positive difference curvature; C-saddles mean-convex, divergent-accelerating, with positive difference curvature; C-saddles mean-convex, divergent-decelerating, with negative difference curvature; C-saddles mean-convex, divergent-accelerating, with negative difference curvature;
- C-hills with positive and negative difference curvature.

This grouping of landform types allows one to test the major soil and land surface attributes in cell-by-cell cartographic modelling as it is used to study various phenomena other than soils.

## DISCUSSION

The cell size strongly affects the original DEM and the features of derived variables (Evans and Cox, 1999; Smith at al., 2006). The correlation coefficients between cell values, generated with different DEM grid sizes (Table 4), are very high and practically not changing for elevation grids if the cell size increases.

Contrarily, the correlation between slope values decreases with the increase in difference of the DEM grid size. The slope and other DEM derivatives are computed within 3×3 moving window. Variables, such as slope, are assumed to have constant value within a cell. However, this is not true when elevations vary over short distances. The standard deviations of elevation values from the DEMs within a

moving window, with a size corresponding to that used for calculation of slope, were calculated for each variant of original DEM grid size (Fig. 2).

Visually, there is no difference in DEM values when different grid sizes are used to generate the elevation model, but the variance of cell values, used for slope computation, increases with increased original DEM grid size. t and $\chi^2$ tests confirm that there is no statistical difference between means and distributions of DEM values extracted at sampling points from grids with different cell size. This is the opposite finding if dealing with focal standard deviations of DEM values. Only neighbouring variants of original DEM grid size (e.g., 5 and 10, 10 and 20 m) do not result in statistically significant differences in distributions of corresponding sampling point values. Therefore, the cell size is considered as one of the factors potentially influencing the observed relationships.

Increase of contingency coefficients was found for morphometric variables derived with relatively larger cell sizes: 30 and 40 m. Larger cell sizes are not used because DEMs are getting too coarse. The effect of the source DEM grid size on the morphometric variables by itself is beyond the scope of our investigation. Therefore, we consider the DEM grid size of 30 m is the best to describe the relationships between soils and terrain attributes under conditions of the study.

The possibilities to apply quantitative methods of land surface analyses for soil survey raise many conceptual and methodological issues. The results obtained demonstrate that terrain attributes could be utilised to describe key soil patterns at a large scale in other areas marked by similar conditions. Further work is needed to establish whether terrain attributes, expressed in the form of landform types and morphometric variables, can be introduced into cartographic modelling of various biophysical systems.

In the future, the approach described could be tested and used for detail systematisation of the soil cover structure not only of Lithuania. New generation of morphopedological maps could be used not only as a basis for thematic maps of soil-topographic associations, but also for ecological maps of other types.

## CONCLUSIONS

The DEM grid size of 30 m is the most appropriate to describe relationships between soil and terrain attributes under local conditions of this study. The soil typological units and classes are best correlated with the landforms types of the Shary classification system rather than the Troeh and Gauss systems. Contingency coefficients between the soil typological units of the Lithuanian soil classification system and the Shary landform types are higher than 0.6 if other conditions are optimal. Soil classes according to the depth of carbonates and hydromorphism are best correlated with the landform types of the Shary classification system: the contingency coefficient is 0.48 if other conditions are optimal. The soil typological units are best correlated with mean and horizontal curvatures, elevation, slope, gradient factor, and topographic index.

## REFERENCES

Angelstam, P., Mikusinski, G., Eriksson, J.A., Jaxgård, P., Kellner, O., Koffman, A., Ranneby, B., Roberge, J.-M., Rosengren, M., Rystedt, S., and Seibert, J., 2003, *Gap Analysis and Planning of Habitat Networks for the Maintenance of Boreal Forest Biodiversity*, Final report to Mistra/RESE. Department of Natural Sciences, Centre for Landscape Ecology, Örebro University, Örebro.

Buivydaite, V.V., 2003, *Scientific Fundamentals of Lithuanian Soil Cover Structure Systematisation: Basic Maps*, Vagos, Lithuanian University of Agriculture Research Papers, 59, 29-36 (in Lithuanian, with English summary).

Buivydaite, V.V., Juodis, J., Motuzas, A., and Vaičys, M., 2001, *Lietuvos Dirvožemių Klasifikacijos*, in Eidukevičienė, M., and Vasiliauskienė, V., (Eds.), Lietuvos Dirvožemiai. Lietuvos Mokslo, Vilnius (in Lithuanian, with English abstract).

Burrough, P.A., and McDonnell, R.A., 1998, *Principles of Geographical Information Systems*, Oxford University Press, Oxford.

Česnulevičius, A., 1999, *Lietuvos Reljefas: Morfografiniai ir Morfometriniai Aspektai*, Geografijos institutas, Vilnius (in Lithuanian, with English summary).

Evans, I.S., and Cox, N.J., 1999, *Relations between Land Surface Properties: Altitude, Slope and Curvature*, in Hergarten, S., and Neugebauer, H.J. (Eds.), Process Modeling and Landform Evolution. Springer, Berlin.

FAO, 1998, *World Reference Base for Soil Resources*, Food and Agriculture Organization of the United Nations, International Soil Reference and Information Centre, International Society of Soil Science, Rome.

Florinsky, I.V., Eilers, R.G., Manning, G., and Fuller, L.G., 2002, *Prediction of Soil Properties by Digital Terrain Modeling*, Environmental Modeling and Software, 17, 295-311.

Hutchinson, M.F., 1993, *Development of a Continent-Wide DEM with Applications to Terrain and Climate Analysis*, in Goodchild, M.F., Parks, B.O., and Steyaert, L.T. (Eds.), Environmental Modeling with GIS. Oxford University Press, New York.

MacMillan, R.A., Martin, T.C., Earle, T.J., and McNabb, D.H., 2003, *Automated Analysis and Classification of Landforms Using High-Resolution Digital Elevation Data: Applications and Issues*, Canadian Journal of Remote Sensing, 29, 592-606.

McBratney, A.B., Mendonça Santos, M.L., and Minasny, B., 2003, *On Digital Soil Mapping*, Geoderma, 117, 3-52.

Moore, I.D., and Hutchinson, M.F., 1991, *Spatial Extension of Hydrologic Process Modeling*, in Proceedings of the International Hydrology and Water Resources Symposium, Perth, 2-4 Oct. 1991. Institute of Engineers of Australia, Perth.

Moore, I.D., Lewis, A., and Gallant, J.C., 1993, *Terrain Attributes: Estimation Methods and Scale Effects*, in Jakeman, A.J., Beck, M.B., and McAleer, M.J. (Eds.), Modelling Change in Environmental Systems. Wiley, New York.

Mozgeris, G., and Buivydaite, V.V., 2004, *On Possibilities of Quantitative Land Surface Analyses Methods is Soil Survey*, Vagos, Lithuanian University of Agriculture Research Papers, 62, 31-43.

Shary, P.A., 1995, *Land Surface in Gravity Points Classification by Complete System of Curvatures*, Mathematical Geology, 27, 373-390.

Shary, P.A., Sharaya, L.S., and Mitusov, A.V., 2002, *Fundamental Quantitative Methods of Land Surface Analysis*, Geoderma, 107, 1-32.

Smith, M.P., Zhu, A-X., Burt, J.E., and Stiles, C., 2006, *The Effects of DEM Resolution and Neighborhood Size on Digital Soil Survey*, Geoderma, 137, 58-69.

Troeh, F.R., 1964, *Landform Parameters Correlated to Soil Drainage*, Soil Science Society of America Proceedings, 28, 808-812.

Weibel, R., and Heller, M., 1991, *Digital Terrain Modelling*, in Maguire, D.J., Goodchild, M.F., and Rhind, D. (Eds.), Geographical Information Systems: Principles and Applications, Vol. 1. Longman, Harlow.

Wilson, J.P., and Burrough, P.A., 1999, *Dynamic Modeling, Geostatistics, and Fuzzy Classification: New Sneakers for a New Geography*, Annals of the Association of American Geography, 89, 736-746.

Wilson, J.P., and Gallant, J.C., 2000, *Digital Terrain Analysis*, in Wilson, J.P., and Gallant, J.C. (Eds.), Terrain Analysis: Principles and Applications. Wiley, New York.

Table 1. Contingency coefficients between the soil typological units (Sdv99nr), their classes according to the depth of carbonates and hydromorphism (Sdv1nr, Sdv2nr, Sdv3nr), soil texture (Ts1apnr, Ts1bnr, Ts1cnr, Ts12cnr), and soil texture groups (Textgr), and grid sizes for the different landform classification systems.

| Soil typological units and classes | Landform classification system | | | | | | | | | | | | | | |
|---|---|---|---|---|---|---|---|---|---|---|---|---|---|---|---|
| | Troeh | | | | | Gauss | | | | | Shary | | | | |
| | Grid size, m | | | | | Grid size, m | | | | | Grid size, m | | | | |
| | 5[a] | 10[b] | 20[c] | 30[d] | 40[e] | 5 | 10 | 20 | 30 | 40 | 5 | 10 | 20 | 30 | 40 |
| Sdv99nr | 0.41 | 0.38 | 0.40 | 0.51 | 0.47 | 0.41 | 0.41 | 0.42 | 0.50 | 0.50 | 0.60 | 0.51 | 0.53 | 0.64 | 0.62 |
| Sdv1nr | 0.35 | 0.30 | 0.28 | 0.39 | 0.37 | 0.33 | 0.33 | 0.30 | 0.47 | 0.42 | 0.49 | 0.44 | 0.37 | 0.56 | 0.49 |
| Sdv2nr | 0.28 | 0.25 | 0.27 | 0.38 | 0.40 | 0.29 | 0.33 | 0.29 | 0.44 | 0.41 | 0.38 | 0.41 | 0.39 | 0.52 | 0.51 |
| Sdv3nr | 0.24 | 0.19 | 0.20 | 0.32 | 0.2 | 0.23 | 0.15 | 0.20 | 0.27 | 0.23 | 0.44 | 0.32 | 0.31 | 0.50 | 0.41 |
| Ts1apnr | 0.16 | 0.21 | 0.14 | 0.20 | 0.16 | 0.23 | 0.22 | 0.24 | 0.17 | 0.22 | 0.30 | 0.34 | 0.35 | 0.32 | 0.33 |
| Ts1bnr | 0.29 | 0.30 | 0.25 | 0.35 | 0.35 | 0.28 | 0.38 | 0.27 | 0.30 | 0.32 | 0.43 | 0.48 | 0.39 | 0.50 | 0.49 |
| Ts1cnr | 0.24 | 0.23 | 0.22 | 0.31 | 0.30 | 0.28 | 0.29 | 0.22 | 0.31 | 0.29 | 0.38 | 0.45 | 0.40 | 0.48 | 0.46 |
| Ts12cnr | 0.24 | 0.28 | 0.25 | 0.33 | 0.33 | 0.27 | 0.31 | 0.26 | 0.29 | 0.32 | 0.38 | 0.45 | 0.39 | 0.48 | 0.48 |
| Textgr | 0.31 | 0.35 | 0.33 | 0.41 | 0.35 | 0.37 | 0.42 | 0.34 | 0.41 | 0.39 | 0.51 | 0.54 | 0.46 | 0.58 | 0.56 |

[a] based on 298 samples

[b] based on 283 samples

[c] based on 307 samples

[d] based on 303 samples

[e] based on 308 samples

Table 2. Contingency coefficients between landform types of different landform classification systems and soil classes (based on the depth of carbonates and hydromorphism) for different DEM grid sizes.

| Classification system | Grid size, m | | | | |
|---|---|---|---|---|---|
| | 5 | 10 | 20 | 30 | 40 |
| Troeh | 0.22 | 0.23 | 0.25 | 0.38 | 0.35 |
| Gauss | 0.25 | 0.27 | 0.27 | 0.39 | 0.34 |
| Shary | 0.36 | 0.37 | 0.36 | 0.48 | 0.50 |

Table 3. Correlation coefficients between the soil typological units and morphometric variables.

| Morphometric variable | Grid size, m | | | | |
|---|---|---|---|---|---|
| | 5 | 10 | 20 | 30 | 40 |
| Elevation | 0.31 | 0.30 | 0.37 | 0.38 | 0.34 |
| Slope steepness | 0.30 | 0.23 | 0.19 | 0.39 | 0.41 |
| Gradient factor | 0.30 | 0.23 | 0.20 | 0.39 | 0.42 |
| Surface insolation | 0.24 | 0.35 | 0.32 | 0.42 | 0.37 |
| Horizontal curvature | 0.27 | 0.28 | 0.34 | 0.39 | 0.35 |
| Vertical curvature | 0.29 | 0.24 | 0.22 | 0.35 | 0.28 |
| Mean curvature | 0.26 | 0.31 | 0.35 | 0.44 | 0.40 |
| Maximal curvature | 0.27 | 0.29 | 0.29 | 0.34 | 0.38 |
| Minimal curvature | 0.28 | 0.28 | 0.29 | 0.29 | 0.31 |
| Difference curvature | 0.18 | 0.14 | 0.23 | 0.33 | 0.20 |
| Horizontal excess curvature | 0.13 | 0.20 | 0.21 | 0.26 | 0.22 |
| Vertical excess curvature | 0.16 | 0.15 | 0.23 | 0.34 | 0.19 |
| Unsphericity | 0.13 | 0.20 | 0.24 | 0.32 | 0.25 |
| Total Gaussian curvature | 0.16 | 0.18 | 0.19 | 0.13 | 0.19 |
| Total accumulation curvature | 0.18 | 0.17 | 0.15 | 0.18 | 0.20 |
| Total ring curvature | 0.15 | 0.21 | 0.23 | 0.23 | 0.17 |
| Rotor | 0.17 | 0.22 | 0.26 | 0.20 | 0.34 |
| Catchment area | 0.30 | 0.30 | 0.29 | 0.28 | 0.26 |
| Dispersal area | 0.12 | 0.14 | 0.19 | 0.26 | 0.22 |
| Depression depth | 0.23 | 0.13 | 0.26 | 0.11 | 0.24 |
| Hill height | 0.18 | 0.37 | 0.13 | 0.26 | 0.16 |
| Topographic index | 0.35 | 0.28 | 0.41 | 0.38 | 0.40 |

Table 4. Correlation coefficients between elevation and slope steepness generated with different grid sizes.

| Grid size, m | 5 | 10 | 20 | 30 |
|---|---|---|---|---|
| | | Elevation | | |
| 5 | | 0.98 | 0.95 | 0.93 |
| 10 | 0.90 | | 0.97 | 0.94 |
| 20 | 0.68 | 0.819 | | 0.95 |
| 30 | 0.48 | 0.61 | 0.79 | |
| | | Slope steepness | | |

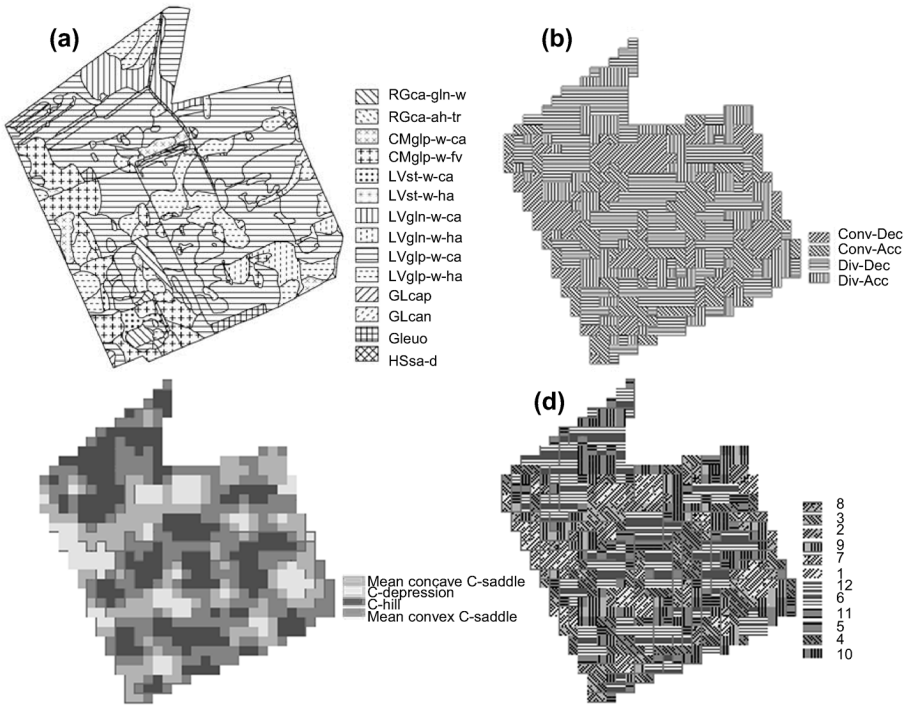


Fig. 1. The study area: (a) soils: RGca-gln-w – Endohypgleyi-Calcaric Regosols, RGca-ah-tr – Anthropi-Calcaric Regosols (Terric), CMglp-w-cap – Epicalcari-Epihypogleyic Cambisols, CMglp-w-fv – Fluvi-Epihypogleyic Cambisols, LVst-w-ca – Calcari-Hypostagnic Luvisols, LVst-w-ha – Hapli-Hypostagnic Luvisols, LVgln-w-ca – Calcari-Endohypogleyic Luvisols, LVgln-w-ha – Hapli-Endohypogleyic Luvisols, LVglp-w-ca – Calcari-Epihypogleyic Luvisols, LVglp-w-ha – Hapli-Epihypogleyic Luvisols, GLcap – Epicalcaric Gleysols, GLcan – Endocalcaric Gleysols, GLeuo – Orthieutric Gleysols, HSsa-d – Bathi-Saprihistic Histosols; (b) landforms classified by the Troeh system for the grid size of 30 m: Conv-Dec – convergent-decelerating, Conv-Acc – convergent-accelerating, Div-Dec – divergent-decelerating, and Div-Acc – divergent-accelerating; (c) landforms classified by the Gauss system for the grid size of 30 m; and (d) landforms classified by the Shary system for the grid size of 30 m: 1 – C-depressions with positive difference curvature; 2 – C-saddles mean-concave, convergent-decelerating, with positive difference curvature; 3 – C-saddles mean-concave, convergent-accelerating, with positive difference curvature; 4 – C-saddles mean-convex, convergent-accelerating, with positive difference curvature; 5 – C-saddles mean-convex, divergent-accelerating, with positive difference curvature; 6 – C-hills with positive difference curvature; 7 – C-depressions with negative difference curvature; 8 – C-saddles mean-concave, convergent-decelerating, with negative difference curvature; 9 – C-saddles mean-concave, divergent-decelerating, with negative difference curvature; 10 – C-saddles mean-convex, divergent-decelerating, with negative difference curvature; 11 – C-saddles mean-convex, divergent-accelerating, with negative difference curvature; 12 – C-hills with negative difference curvature.

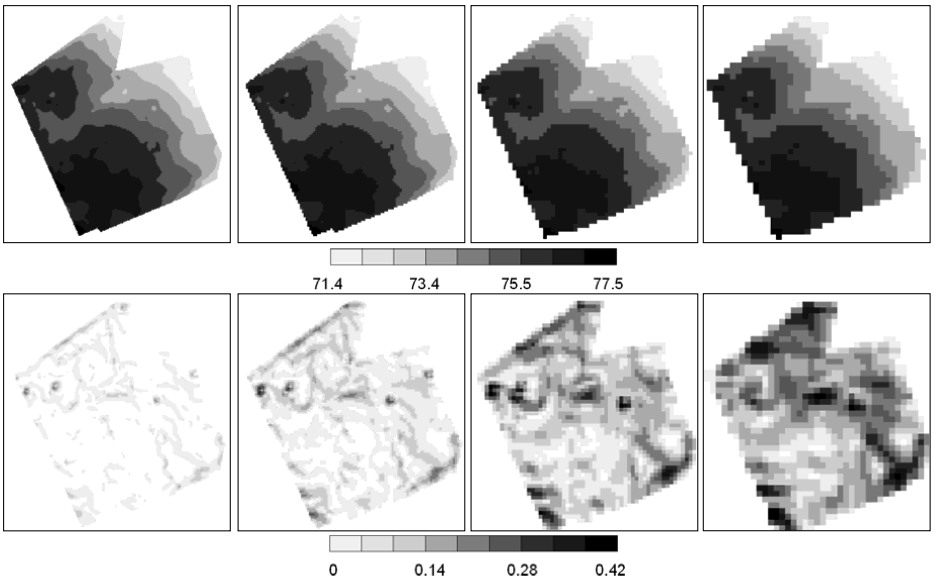


Fig. 2. The study area, maps of elevation, m, (upper) and focal standard deviations of the DEM (lower) for grid sizes of (a) 5 m, (b) 10 m, (c) 20 m, and (d) 30 m.

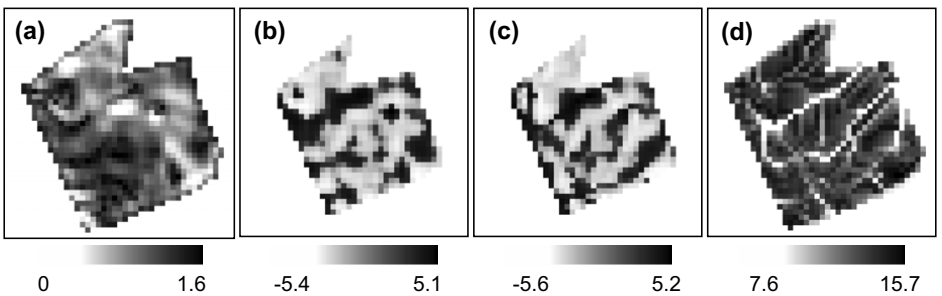


Fig. 3. Maps of some morphometric variables of the study site for the grid size of 30 m: (a) slope steepness, °; (b) mean curvature, $m^{-1}$; (c) horizontal curvature, $m^{-1}$; and (d) topographic index, logarithmic scale.

*International Journal of Ecology & Development*
*Fall 2007, Vol. 8, No. F07; Int. J. Ecol. Dev.*
*ISSN 0972-9984 ( Print ); ISSN 0973-7308 (Online)*


# A Study of Disturbed Soil Cover using Soil Electrical Resistivity and Topographic Data

**V. P. Samsonova [1], A. I. Pozdnyakov, J. L. Meshalkina [2]**

Faculty of Soil Science
Moscow State University
Leninskie Gory, Moscow, 119992, Russia

[1] e-mail: vkbun@mail.ru

[2] e-mail: meshalky@ru.ru

Received 5 December 2006; accepted 16 May 2007

## ABSTRACT

*The soil maps are overwhelmingly created using topographic data as secondary information. Under the condition of anthropogenic pressure on territories, connections 'topography-soils' may be weakened. The research was focused on the terrain of Bryansk Opolje, one of the ancient agricultural areas in Russia. The soil cover disturbance is seen in a number of places because of continuous cultivation, erosion, and reclamation. The main types of soils are grey forest soils and grey forest soils with the second humus horizons. The traditional soil mapping has been performed on the 16-hectare field. The electrical resistivity has been measured at nodes of the sampling grid with the grid size of 25 m. The additional measurements were done using four transects with a 5 m distance crossing various landscape positions. A topographic map at the scale of 1 : 5,000 was digitised to produce a digital elevation model (DEM). Slope steepness, slope aspect, profile curvature, tangential curvature, and Laplacian were derived from the DEM. Electrical resistivity was closely linked with soil classification areas, which was proved by the one-way ANOVA. For the entire field, none of the topographic attributes was totally connected with either soil distributions or electrical resistivity. At the same time, connections between terrain attributes and electrical resistivity are clearly expressed for some parts of the study area. In the case of reclaimed territories, where connections between relief and soils may be disturbed to a considerable degree, electrophysical methods may be informative for the soil mapping purposes.*

**Keywords:** Electrical Resistivity, Spatial Variability, Soil Properties, Topography, Precision Agriculture, Digital Elevation Model.

**Mathematics Subject Classification:** 62P12, 86A25, 86A32.

**JEL Classification:** Q19, Q50.

## INTRODUCTION

The proliferation of precision agriculture technologies, that take into account a variety of growth conditions for crops, contributes to the relevance of large-scale soil

mapping of arable lands. The relation of topographic attributes with soil properties has been used in soil mapping practically from the moment of the origin of soil science. On undisturbed areas where interaction between components of a biogeocoenosis has been forming for centuries, connections between soils and relief can be explicitly traced. Under the condition of anthropogenic load on territories, such as agricultural use, reclamations, etc., connections may be weakened or even be missing. Therefore, the study of possibilities of other bases for mapping is necessary for such type of objects.

The soils and specific soil properties mapping, primarily for agrochemical and soil data, requires much time and labour effort to dig profiles, select and analyse soil probes. The use of relevant information, on the one hand, such as digital terrain models and, on the other hand, easily defined, cheap, and interpreted parameters, such as electrical resistivity (ER) along with basic soil attributes enables one to solve the assigned tasks more efficiently.

Over the last decades, there has been a distribution of digital terrain models that open new opportunities for explaining spatial variability of specific soil properties (Chistov and Florinsky, 1997), and may become a component of digital soil mapping models (McBratney et al., 2003). Thus, for example, Manning et al. (2001) come to the conclusion that spatial distributions of the most agronomically relevant attributes (soil moisture and nitrate) were expressed at a landscape scale broader than that at which soil series occurred within the site.

Geophysical methods, such as ER measurement, enable one to define areas of electrically contrasting soils, which have distinct properties and, therefore, should be used in agriculture in different ways (Pozdnyakova and Zhang, 1999; Tabbagh et al., 2000; Corwin and Lesch, 2003; Simbahan and Dobermann, 2006). ER is a composite soil attribute, which is generally related to soil texture, stones, salts, and organic matter content as well as to the arrangement of the genetic soil horizons. This is the complex of the factors directly influencing yield of the most of crops. The advantage of ER measurements is that it can be measured directly in the field without actual collecting of soil samples and analysing them in the laboratory. Thus, application of ER techniques to determine soil attributes can tremendously decrease time and labour required to delineate management zones within the fields.

The *opoljes*, the unique landscape complexes of the Central Russia, may serve an explicit example of the territory that has been under the influence of agricultural activities for a long time. Dark-grey (forest) soils (or Phaeozems Albic (FAO, 1998), or Greyzems Haplic (FAO-UNESCO, 1988), or Humus Gleysols (FAO-UNESCO, 1974)) of Bryansk Opolje were formed on loessial loam and calcareous loesses underlaid by carbonaceous rocks. These terrains represent undulating plain with closed depressions, the genesis of which is explained by some scientists by the karst (Milkov, 1964), others consider it as palaeo-cryogenic development (Velichko et al., 1996; Alifanov et al., 2006). The soil cover of these terrains is heterogeneous with a large number of bushy hollows filled with hydromorphic soils. Their diameter is measured by several tens of metres and the depth is 0.4-2.5 m. The number of hollows may count to 5-10 per $km^2$ (Alifanov et al., 2006). A clear dependency between soils and topography is registered on undisturbed areas: grey forest soils often variously eroded are widespread on uplands, while gleyed soils and forest soils with the second humus horizons occur in depressions. Under agricultural use, the terrain is often more or less reclaimed. The radical reclamation may consist of backfilling hollows, levelling, and some other modifications of the relief.

The objective of this study was to study possibilities to use digital terrain attributes and ER measurements for soil mapping of Bryansk Opolje anthropogenic terrains.

## STUDY SITE

The study was conducted on one of production fields of the Bryansk State Agricultural Academy in early June 2006 (Fig. 1a). The size of the study area is 370 by 320 m. The study area is situated on a gentle slope (about 1 degree). However, there are closed depressions with the depth up to 2 m and the diameter of 40-50 m there. This causes a strong spatial heterogeneity of the study area.

There was reclamation of the territory in the middle 1970s resulted in considerable soil disturbance in a number of places. Trees were removed from boggy hollows and the land was reclaimed. Middle part of the soil profile was levelled, and then the mixture of the upper soil layers was uniformly distributed over the terrain.

The field was tilled in fall 2005, and its pre-sowing cultivation was done in May 2006.

The field was under oats in 2005, and under buckwheat in 2006.

## MATERIALS AND METHODS

### Soil Survey

Soil survey was carried out to describe the soil cover of the study area. Sixty-four soil profiles were described. The four main profiles are dug in accordance with basic landscape positions (Fig. 1b).

### ER Survey

ER was measured by the device Landmapper$^{TM}$ ERM-01 (Fig. 2). Landmapper$^{TM}$ ERM-01 measures apparent specific ER (or electrical conductivity) of soils and similar structures for the fast non-invasive mapping and monitoring of agricultural fields as well as construction and remediation sites. In a typical setting, a four-electrode probe is placed on the surface and an ER value is read from the digital display. The device measures ER in a surface layer of the depth from 2 cm down to 5 m, which is set by varying the size of a four-electrode probe. Measurements are based on well-known four-electrode principle, which allows one to avoid influence of electrode contact potential on measured electrical conductivity or resistivity of the media and obtain accurate readings. The field tests were performed in USA, Russia, and Canada in collaboration with Advanced Soil and Water Systems, Inc., Canada (Pozdnyakov and Pozdnyakova, 2002).

The measurements were taken in June and September 2006 under similar weather conditions. Since soil moisture in arable layer was within the range of 18-22%, moisture variability was not supposed to affect dramatically ER values. In digging profiles, ER was measured by AMNB linear four-electrode probe with distance between electrodes of AB = 150 cm and MN = 50 cm. Due to this parameters, the depth of survey reached up to 50 cm, that is, mostly A horizon and in a number of cases A+B horizons or A+C horizons were covered (Pozdnyakov, 2001).

ER measurements was carried out using almost parallel transects with the distance between sampling points about 25 m. The measurements were done with five replications in all sampling points. Four sampling transects of different length with 5 m distance between sampling points were added to consider some topographic

features. Totally, ER was measured at 515 points (Fig. 1c). Sampling points, soil profiles, and points of ER measurements were georeferenced by Garmin Legend Cx GPS navigator. Figure 3a shows spatial distribution of ER within the field.

**Digital Terrain Modelling**

An irregular digital elevation model (DEM) of the study area was produced by digitising a topographic map, scale of 1 : 5,000. Within the area, the basic elevation component may be approximated by a linear function of the Cartesian co-ordinates:

$$Z = 0.0080\ X - 0.0076\ Y + 1.3208 \quad (1)$$

with $R^2 = 0.58$; the residuals have distinct spatial structure. To describe variogram of this structure, the anisotropy spherical model (Goovaerts, 1999) was used with the following parameters: nugget c0 = 0.1, sill c1 = 0.33, a = 120, anisotropy angle of 40°, and anisotropy ratio of 2. A square-gridded DEM with a grid size of 4 m was interpolated using the trend described and ordinary kriging for residuals (Fig. 3b).

Digital models of five topographic attributes were derived from the square-gridded DEM, such as slope steepness, slope aspect, profile curvature (or vertical curvature) (Fig. 3c), tangential curvature (or horizontal curvature), and Laplacian (Fig. 3d). Slope steepness controls the velocity of overland and intrasoil runoff. Slope steepness and aspect together influence the thermal regime of slopes. Profile curvature is the measure of relative deceleration of flows. Tangential curvature is the measure of flow convergence. Laplacian approximates mean curvature, which represents flow convergence and relative deceleration with equal weights. Negative values of curvatures relate to convex landforms, while positive ones relate to concave landforms. Definitions, formula, and detailed interpretations of the variables can be found elsewhere (Shary, 2006). Digital terrain modelling was carried out with Surfer Version 8.00 (© 1993-2002, Golden Software, Inc.).

**Statistical Analysis**

Descriptive statistics was supplemented with quartiles. One-way ANOVA was calculated using soil classes as a factor. To estimate relationships between ER and relief, Spearman correlations were calculated between ER and slope steepness, profile curvature, tangential curvature, and Laplacian. Slope aspect is a circular

variable, so we calculated Spearman correlations between ER and sine and cosine of slope aspect (King et al., 1999). We determined correlations for the entire study area as well as for selected subareas 50 by 50 m in the central part of the study area (Fig. 3). The central part was chosen to exclude all kind of border effects. Statistica 6.1 (© 1984-2004, StatSoft, Inc.) was used for data analysis.

## RESULTS

### Soil Cover

Because of the land improvement, the soil cover of the area consists of combinations of several soil types and subtypes (Shishov et al., 2004). They are dark agrozems, argillo-illuvial agrozems, and agro- dark grey typical soils with the second humus horizon. Dark agrozems are located on the highest landscape positions, while the arable dark humus horizon occurs immediately on the C horizon represented by carbonate loess. The most widespread soil type is argillo-illuvial agrozems whose profile retains the B horizon. The signs of illuvial process in the B horizon are expressed not so strongly because of its light texture and height silt content in soil-forming rocks. Agro- dark grey typical soils were conserved on the borders of the field and in some spots. Agro- dark grey soils with the second humus horizon could be found in former depressions. The second humus horizon is the most dark-coloured in the profile with crumbled and pulvered structure. Large structural aggregates explicitly tend to be flaggy. In accordance with the given classification, we have conditionally divided the soil cover of the study area into 4 classes considering what horizon is under a plough layer: class 1 – the second humus layer, class 2 – AUe or AEl, class 3 – the B horizon, class 4 – the C horizon. The modern arable layer makes 22-24 cm. Thus, the depth of humus part of profile can be considered a characteristic that forms separate classes (Fig. 4a).

### Relationships between Topography and Soil Cover

Figure 4b demonstrates that there is no evident relationship between elevation and soil classification areas. Moreover, transects within the field show that any of the mentioned soil classes may be found on similar landscape positions (Fig. 5).

### ER

In the course of this study, ER values varied from 36 up to 127 Ωm. The analytical error calculated for repeated measurements in sampling points had constituted 0.46 Ωm that corresponds to the variance of 0.21 $(\Omega m)^2$.

Parallel measurements in rows and inter-rows spacing of sowings enabled us to assess the variance linked with the ER variation on small distances. It was estimated at 28.8 $(\Omega m)^2$ that is essentially higher than the variance of repeated measurements in separate points with the same position of the electrode probe. However, the total variance of ER on the whole study area exceeded this value by more than 10 times (Table 1). Therefore, the heterogeneity of the soil cover makes the main contribution to the ER variability.

The one-way ANOVA has shown that ER average values for all classes of soils, except for the 3$^{rd}$ and 4$^{th}$, are definitely different with the significance level of p = 0,001 (Fig. 6). ER connection with soil classes is conditioned by its dependency on soil profile, and, first of all, on the diversity of physical and chemical properties.

### ER and Terrain Attributes

Correlation coefficients of terrain attributes and ER are close to zero that can be regarded as indication of missing connections between these parameters (Table 2). However, the division of the field into subareas with sizes of 50 by 50 m (Fig. 3) has revealed that correlation coefficients differ significantly from zero for some subareas (Table 2, Fig. 7). In particular, subareas, where correlation coefficients between landsurface curvatures and Laplacian and ER values are negative, correspond to undisturbed (natural) conditions. In these cases, high ER values relate to depressions, where soils with the second humus horizon are spread. The positive correlation coefficients and the absence of dependency indicate disturbed subareas.

## DISCUSSION AND CONCLUSIONS

The connection between soil classification areas and terrain attributes, which is typical for undisturbed territories, is practically missing on the study area that had been subject to strong impact of land reclamation.

For the study area, the prediction of soil properties based on such general soil-forming factors as topography appears rather difficult. The prediction mistakes may be caused by various, often not much predictable, connections between secondary variables and variables of interest rather than by insufficient information on secondary variables. Such connections may be essentially local (mosaic), which is characteristic only for a part (generally not very large) of the study area. Carroll and Oliver (2005) received similar results.

It is likely that the absence of connections between topographic attributes and organic matter status of arable soils (Simbahan et al., 2006) also depends on mosaic structure of the soil cover. It is worth a mention that mosaic structure of arable soil cover is widespread enough, but too many profiles are needed to clearly reveal it.

The plough layer of arable grey forest soils is low-contrast in terms of common soil fertility properties, such as organic matter content, nutrients, structure, etc. The study demonstrated that under these conditions ER spatial variability is primarily associated with properties of the underlying subplough layer. This result opens opportunities to delineate areas with more thick humus horizon. This may be used to assess the soil organic matter content at areas located in similar landscapes.

In this study, relations between terrain attributes and ER were not observed for the entire study area. Generally, this may be related to three factors. First, the absence of relationships may be a natural phenomenon. Second, the connections may be revealed only locally, that was shown at Table 2. Third, it may be related to the fact that the grid size used for interpolations does not correspond to natural patterns. Florinsky and Kuryakova (2000) have shown, that the relations between terrain attributes and soils properties are not revealed on all grid sizes, but only on that ones, which match to typical sizes of a landform controlling the spatial distribution of the soil property in the landscape.

In the case of low variability of soil properties of the plough layer and high contrast of plough and subplough layers of the soil profile, ER along with terrain attributes is an indispensable indirect tool to indicate disturbances of natural interconnections in the landscape.

## ACKNOWLEDGMENTS

The study was executed with financial support of the RFBR grant 05-04-48573.

## REFERENCES

Alifanov, V.M., Gugalinskaya, L.A., Ivannikova, L.A., and Ovchinnikov, A.Yu., 2006, *Soil Polygenesis in the Northeast Part of Vladimir Opolie*, Eurasian Soil Science, 39, 31-39.

Carroll, Z.L., and Oliver, M.A., 2005, *Exploring the Spatial Relations Between Soil Physical Properties and Apparent Electrical Conductivity*, Geoderma, 128, 354-374.

Chistov, S.V., and Florinsky, I.V., 1997, *Environmental Cartography*. Russian Ecological Federal Information Agency, Moscow (in Russian, with English abstract).

Corwin, D.L., and Lesch, S.M., 2003, *Application of Soil Electrical Conductivity to Precision Agriculture: Theory, Principles and Guidelines*, Agronomy Journal, 95, 455-471.

FAO, 1998, *World Reference Base for Soil Resources*, Food and Agriculture Organization of the United Nations, International Soil Reference and Information Centre, International Society of Soil Science, Rome.

FAO-UNESCO, 1974, *FAO-UNESCO Soil Map of the World, Vol. 1, Legend*. UNESCO, Paris.

FAO-UNESCO, 1988, *FAO-UNESCO Soil Map of the World, Revised Legend*. FAO, Rome.

Florinsky, I.V., and Kuryakova, G.A., 2000, *Determination of Grid Size for Digital Terrain Modelling in Landscape Investigations - Exemplified by Soil Moisture Distribution at a Micro-Scale*, International Journal of Geographical Information Science, 14, 815-832.

Goovaerts, P., 1999, *Geostatistics in Soil Science: State-of-the-Art and Perspectives*, Geoderma, 89, 1-45.

King, D., Bourennane, H., Isambert, M., and Macaire, J.J., 1999, *Relationship of the Presence of a Non-Calcareous Clay-Loam Horizon to DEM Attributes in a Gently Sloping Area*, Geoderma, 89, 95-111.

Manning, G., Fuller, L.G., Eilers, R.G., and Florinsky, I., 2001, *Soil Moisture and Nutrient Variation within an Undulating Manitoba Landscape*, Canadian Journal of Soil Science, 81: 449-458.

McBratney, A.B., Mendonça Santos, M.L., and Minasny, B., 2003, *On Digital Soil Mapping*, Geoderma, 117, 3-52.

Milkov, F.N., 1964, *About the Nature of Opoljes of Russian Plain*, Voprosy Regionalnogo Landshaftovedenia i Geomorphologii SSSR, 8, 20-27 (in Russian).

Pozdnyakov, A.I., 2001, *Field Electrophysics of Soils*. Nauka, Moscow (in Russian).

Pozdnyakov, A.I., and Pozdnyakova, L.A., 2002, *Electrical Fields and Soil Properties*, in Transactions of the 17th World Congress of Soil Science, 14-21 August 2002, Bangkok, Thailand, Symposium 53. ISSS, Bangkok (CD ROM).

Pozdnyakova, L., and Zhang, R., 1999, *Geostatistical Analyses of Soil Salinity in a Large Field*, Precision Agriculture, 1, 153-165.

Shary, P.A., 2006, *Variables of Geomorphometry: The Current State-of-Art*, in Liu, X., and Wang, Y. (Eds.), Full Papers, Proceedings of International Symposium on Terrain Analysis and Digital Terrain

Modelling (TADTM 2006), 23-25 Nov. 2006, Nanjing, China. Nanjing Normal University, Nanjing (CD-ROM).

Shishov, L.L., Tonkonogov, V.D., Levedeva, I.I., and Gerasimova, M.I., 2004, *Soils Classification and Diagnostics of Russi*a. Dokuchaev Soil Science Institute, Moscow (in Russian).

Simbahan, G.C., and Dobermann, A., 2006, *Sampling Optimization Based on Secondary Information and Its Utilization in Soil Carbon Mapping*, Geoderma, 133, 345-362.

Simbahan, G.C., Dobermann A., Goovaerts P., Ping J., and Haddix, M.L. 2006, *Fine-Resolution Mapping of Soil Organic Carbon Based on Multivariate Secondary Data*, Geoderma, 132, 471-489.

Tabbagh, A., Dabas, M., Hesse, A., and Panissod, C. 2000, *Soil Resistivity: A Non-Invasive Tool to Map Soil Structure Horizonation*, Geoderma, 97, 393-404.

Velichko, A.A., Morosova, T.D., Nechaev, V.P., and Porogeniakova, O.M., 1996, *Palaeocryogenesis, Soil Cover, and Farming*. Nauka, Moscow (in Russian).

Table 1. Descriptive statistics of ER (Ωm).

| Valid N | Mean | Median | Min | Max | Lower quartile | Upper quartile | Std. Dev. | CV, % |
|---|---|---|---|---|---|---|---|---|
| 515 | 67.8 | 63.6 | 36.0 | 127.0 | 52.8 | 82.5 | 19.5 | 28.9 |

Table 2. Coefficients of Spearman rank correlation between ER and terrain attributes for the entire study area, and their minimal and maximal values for subareas 50 by 50 m (Fig. 7).

| | Sample size | Slope steepness | Sin (Slope a*spect*) | Profile curvature | Tangential curvature | Laplacian |
|---|---|---|---|---|---|---|
| Entire area | 2300 | 0.160 | 0.043 | 0.007 | 0.068 | 0.057 |
| Min | 144 | -0.523 | -0.589 | -0.268 | -0.276 | -0.441 |
| Max | 144 | 0.418 | 0.552 | 0.564 | 0.508 | 0.735 |

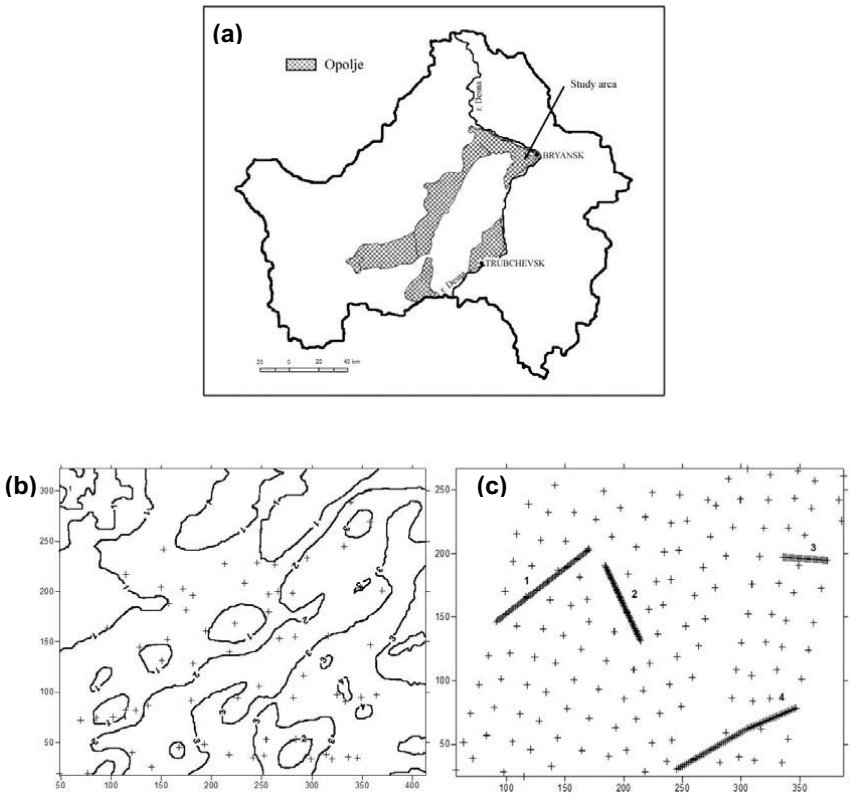


Fig. 1. Geographic location of the study area within Bryansk Region, Russia (a), points of digging profiles on the contour map of related elevations (b), and points of ER measurements (c).

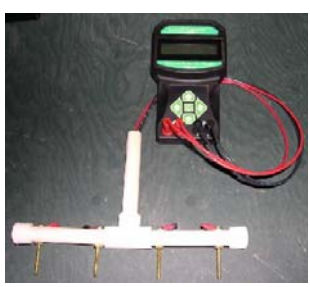

Fig. 2. Landmapper$^{TM}$ ERM-01.

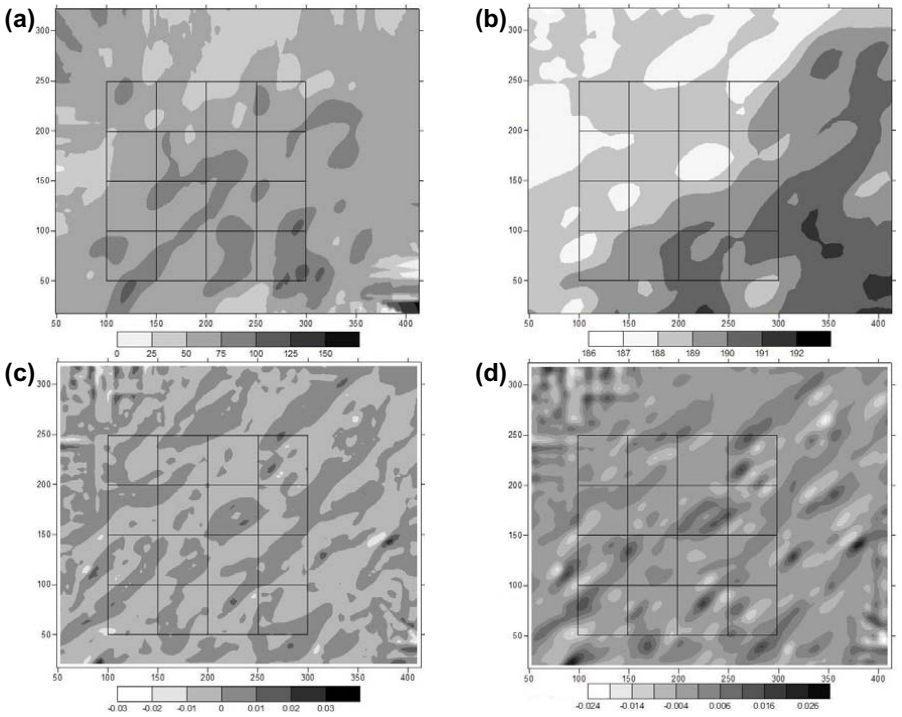


Fig. 3. Maps of the study area: (a) ER, Ωm; (b) related elevations, m; (c) profile curvature, $m^{-1}$; and (d) Laplacian, $m^{-1}$; subareas 50 by 50 m are indicated.

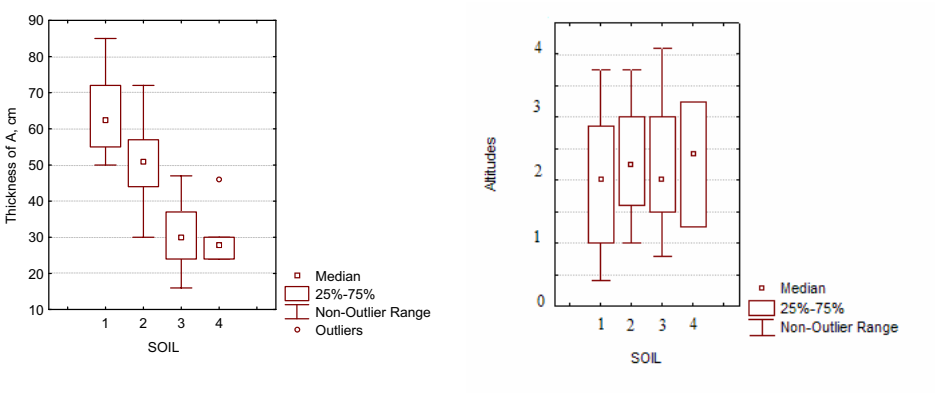


(a) (b)

Fig. 4. Correspondence of soil classes and the thickness of the humus horizon (a) and elevations (b). The horizon under a plough layer: 1 class – the second humus horizon, 2 class – AUe or AEl, 3 class – the B horizon, 4 class – the C horizon.

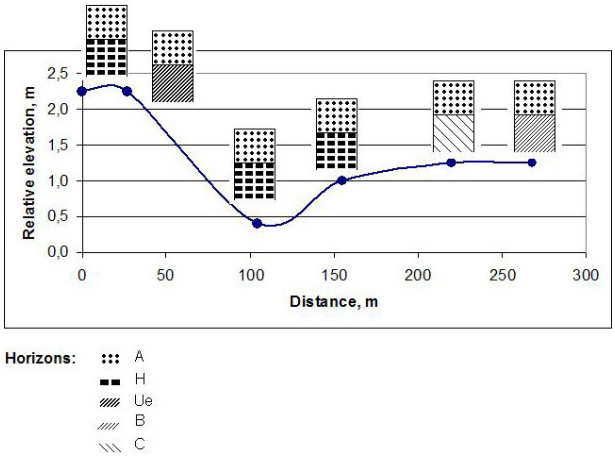


Fig. 5. Soil profiles at different landscape positions.

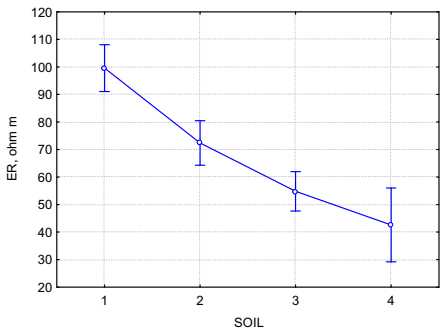


Fig. 6. Means and confidence intervals of ER (Ωm) for different soil classes.

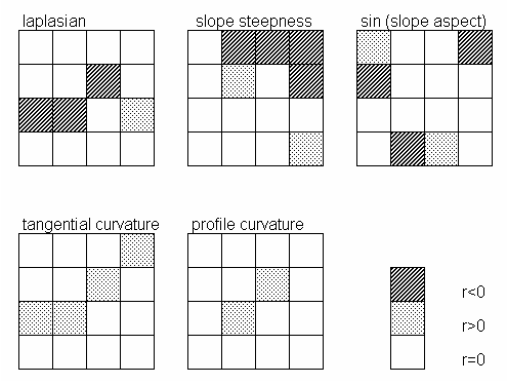


Fig. 7. Mosaic-like distribution of signs of rank correlation coefficients of ER with terrain attributes within separated subareas 50 by 50 m.

*International Journal of Ecology & Development*
*Fall 2007, Vol. 8, No. F07; Int. J. Ecol. Dev.*
*ISSN 0972-9984 ( Print ); ISSN 0973-7308 (Online)*


# Solving Three Problems of Exploration and Engineering Geology by Digital Terrain Analysis

**I.V. Florinsky**

Institute of Mathematical Problems of Biology
Russian Academy of Sciences
Pushchino, Moscow Region, 142290, Russia

e-mail: iflor@mail.ru

Received 10 December 2006; accepted 15 April 2007

## ABSTRACT

*In the smooth-surface approximation, local accumulation of a flow is controlled by relative deceleration and convergence. Flow deceleration is determined by vertical curvature of the land surface, while flow convergence is controlled by horizontal curvature. There is a concurrent action of flow convergence and relative deceleration at areas marked by negative values of both of these curvatures. These areas are said to be relative accumulation zones. We describe basic principles of applying maps of relative accumulation zones to solve three problems of exploration and engineering geology: (1) exploration of alluvial placers; (2) prediction of landsliding on reservoir shores; and (3) prediction of soil degradation and contamination along pipelines. The deposition of placer minerals is most likely to occur in relative accumulation zones with slope steepness below 3°, all other factors being equal. The activation of slope instability is most probably to occur in relative accumulation zones with slope steepness beyond 15°, which are adjacent to, upslope the reservoir water level. Soil degradation (waterlogging and salinisation) may be observed in relative accumulation zones adjacent to, upslope a pipeline. After the pipeline failure, one can use a map of specific catchment area to determine paths of lateral migration of petroleum in the landscape. Petroleum products are most likely to concentrate in relative accumulation zones situated along a flow line originating at a pipeline hole. To refine the prediction, one should analyse accumulation zone maps together with geological, geophysical, geochemical, soil, plant, and remotely sensed data as well as with models of other topographic variables.*

**Keywords:** Digital Terrain Model, Accumulation, Placer, Reservoir, Landslide, Pipeline, Soil, Degradation, Contamination.

**Mathematics Subject Classification:** 62H99, 62P12, 86A05, 86A60, 86A30.

**JEL Classification:** Q19, Q50.

## INTRODUCTION

There is a concept of relative accumulation zones in geomorphometry and digital terrain modelling. In the smooth-surface approximation, the velocity of a gravity-driven flow varies in proportion to the slope factor (sin *G*). *G*, slope steepness, is an

angle between a tangent and horizontal planes at a given point on the land surface. The local accumulation of a flow is controlled by two mechanisms, relative deceleration and convergence. Relative deceleration of a flow is determined by vertical curvature ($k_v$). $k_v$ is the curvature of a normal section including the gravity acceleration vector at a given point. A flow tends to accelerate when $k_v > 0$, and to decelerate when $k_v < 0$. Convergence of a flow is controlled by horizontal curvature ($k_h$). $k_h$ is the curvature of a normal section, which is perpendicular to the normal section with $k_v$. A flow diverges when $k_h > 0$, and converges when $k_h < 0$. Digital models of $G$, $k_v$, and $k_h$ are derived from digital elevation models (DEMs). Details and formula can be found elsewhere (Shary et al., 2002).

There is a concurrent action of convergence and relative deceleration of flows within areas characterised by both $k_h < 0$ and $k_v < 0$. These areas are said to be relative accumulation zones. If divergence and relative acceleration of flows act simultaneously ($k_h > 0$ and $k_v > 0$), these areas are referred to as relative dissipation zones. Areas with other combinations of $k_h$ and $k_v$ signs are lumped together as transit zones. It should be noted that we consider zones of *relative* accumulation rather than dead-end depressions. A flow may pass through a great quantity of relative accumulation zones before entering into a dead-end depression. Models of $k_v$ and $k_h$ are used to derive maps of relative accumulation zones.

Maps of relative accumulation zones represent areas where geometrical peculiarities of the relief provide conditions for the local accumulation of gravity-driven substances, such as water (meteoric water, soil moisture), dissolved and suspended substances (salts, clay and organic particles, etc.), and other liquids (e.g., petroleum products). Maps of relative accumulation zones are used to solve various practical and fundamental problems of geosciences: prediction of slope instability (Lanyon and Hall, 1983), studies of lateral migration of artificial radionuclides in landscapes (Gurov and Kertsman, 1991), studies and modelling of soil properties at a field scale (Pennock et al., 1987; Florinsky et al., 2002; Shary, 2005), predictive soil mapping at small scales (Florinsky et al., 2000; Florinsky and Eilers, 2002), and studies of forest ecosystems (Shary, 2005). Relative accumulation zones may coincide with intersections of lineaments, faults, and fracture zones (Florinsky, 1993), and thus they constitute areas of contact and interaction of overland lateral flows and

ascending and descending flows of groundwater and fluids (Florinsky, 2000). Maps of relative accumulation zones are usually used together with geological, geochemical, soil, plant, and remotely sensed data as well as with digital models of other topographic variables (e.g., slope gradient, catchment area).

In this paper, we describe basic principles of applying maps of relative accumulation zones to solve three problems of exploration and engineering geology: (a) exploration of alluvial placers; (b) prediction of landsliding on reservoir shores; and (c) prediction of soil degradation and contamination along pipelines.

## EXPLORATION OF ALLUVIAL PLACERS

Placers are important sources of valuable minerals (Edwards and Atkinson, 1986). Alluvial placers are formed by chemical and physical weathering of primary deposits, subsequent transportation of mineral grains and crystals by water, and their deposition in valleys and channels (Bilibin, 1956; Macdonald, 1983; Shilo, 1985). Alluvial placers, constituting strip-like sand and gravel deposits located along valleys, range in length from 3 to 6 km, and in width from 10 and 100 m (Bilibin, 1956).

Relief influences formation of alluvial placers. The deposition of placer minerals usually occurs in areas where topographic characteristics offer deceleration of water currents and concentration of suspended particles (Bilibin, 1956; Macdonald, 1983). To find these sites, geologists commonly use a visual analysis of topographic maps (Muzylev, 1954). In terms of geomorphometry, desired areas correspond to relative accumulation zones marked by low values of sin *G*. Some methods of digital terrain analysis (e.g., derivating maps of flow line direction and catchment area) are utilised to model the formation of alluvial placers (McFarlane, 2000). However, up to now, maps of relative accumulation zones have not been used to search placer deposits.

To exemplify a basic principle of the implementation of relative accumulation zone maps, we consider a low-mountain area. The area size is about 4 by 4 km. A square-gridded DEM of the study area has a mesh size of 10 m (Fig. 1a). There is a primary deposit of some placer mineral in sources of two valleys, in the southeastern corner of the study area. A type of the mineral is not critical. The primary deposit is a source of placers in the two valleys. What is wanted is the location of placers.

To reduce a high-frequency noise, we applied three iterations of smoothing to the DEM using 5×5 kernel with squared inverse distance weights. Digital models of slope factor (Fig. 1b), horizontal curvature (Fig. 1c), and vertical curvature (Fig. 1d) were derived from the smoothed DEM by the method of Evans (1980). Models have a resolution of 10 m. A map of relative accumulation, transit, and dissipation zones (Fig. 1e) was obtained using $k_v$ и $k_h$ models.

It is known that the distribution of placer productivity along a valley depends on a stream gradient, all other factors being equal. For example, in the Lena Gold Placer Region (Siberia, Russia), up to 93% of the metal are located within areas marked by $G < 3°$ (Shilo, 1985). In the following analysis, we will utilise this threshold. It corresponds to $\sin G \approx 0.05$. The slope factor map (Fig. 1b) demonstrates that areas of $\sin G \leq 0.05$ are long and narrow strips located along thalwegs and water divides. Hereafter, we will consider only two valleys rising in the area of the primary deposit. In these valleys, let us to delineate sites of $\sin G \leq 0.05$ located within relative accumulation zones (Fig. 1e), which are situated downslope the primary deposit. As a result, we can obtain a map of sites where local geometry of the relief creates good conditions to form placers (Fig. 1f).

The prospective areas range in length from 100 to 150 m, and in width from 10 to 30 m (Fig. 1f). The areas form chains with a total length of about 4 km beginning from the primary deposit. To refine the map obtained, one should consider a density value of a particular mineral, its mineral resistance to chemical and mechanical erosion, and a settling rate, a function of specific gravity of a mineral, grain size and shape, and some other factors (Macdonald, 1983). These parameters may influence a threshold value of $\sin G$, and a distance that grains and crystals are moved from the primary deposit, that is, a total length of a chain of prospective areas. To adjust the map obtained, one may use results of geological, geomorphological, geochemical, and geophysical ground surveys as well as remotely sensed data.

In placer exploration, conventional visual analysis of topographic maps is rather subjective. Its results depend on the experience and intuition of a geologist. This leads to missing of prospective areas. Application of maps of relative accumulation

zones can assist to plan prospecting grids and to reduce a cost of exploration. The principle described can be also used to reveal a modern alluvial placer formed due to erosion of a palaeo-placer rather than a primary deposit. Besides, the principle may be applied to search placers of ancient valleys uplifted by vertical tectonic movements and currently located on water divides. This may be favoured by the ability of digital terrain modelling to discover previously unknown, relict drainage networks (Almeida Filho et al., 2005).

## PREDICTION OF LANDSLIDING ON RESERVOIR SHORES

It is well known that the filling of a reservoir and fluctuation of the reservoir water level amplify slope instability renewing old landslides and provoking new slope movement. Slope instability on reservoir shores is triggered by (a) water erosion of footslopes; (b) saturation of slope sediments due to the rise of groundwater; (c) weathering of sediments because of their periodical moistening and drying caused by the water level fluctuation; and (d) increase of the groundwater hydrodynamic pressure during rapid changes of the reservoir water level (Minervina and Khositashvili, 1974; Záruba and Mencl, 1982; Finarov, 1986). The life of a reservoir may be shortened because of bank collapsing and adding to the rapid silting of the reservoir. Slope failures endanger the operation of the control structures of hydroelectric schemes and make difficult water management. Sometimes, landsliding on reservoir shores leads to catastrophic damages (Kiersch, 1964).

Topography is one of the main factors of landslide formation, and one of the landslide indicators (Emelyanova, 1972; Záruba and Mencl, 1982). Therefore, digital terrain modelling is widely used in techniques to recognise, analyse, and assess slope instability risk (Guzzetti et al., 1999; Montgomery et al., 2000; Fernandes et al., 2004). These methods are based on integrating data of geomorphometry (slope gradient, aspect, and shape), geology (spatial distribution of ‘critical’ sediments), meteorology (precipitation amounts), and hydrology (groundwater regime). A slope is commonly recognised as instable if its steepness is more than 15° (Emelyanova, 1972). Landslides usually occur in relative accumulation zones, all other factors being equal (Lanyon and Hall, 1983). This is because convex-convex form of slopes provides sufficient moistening of soils and sediments there. There are various engineering, geomorphic, and mathematical methods to reveal, evaluate, and predict

landsliding on reservoir shores (Minervina and Khositashvili, 1974; Finarov, 1986). Maps of relative accumulation zones have not been used for this purpose.

To exemplify a basic principle of application of maps of relative accumulation zones, we consider a mountainous area with a large depression. The area size is about 4 by 4 km. A square-gridded DEM of the study area has a mesh size of 10 m (Fig. 2a). A reservoir is under construction in the depression. After reservoir filling, the maximal water level will be 1343 m. It is desired to find potentially instable sites on the depression slopes, which may be activated by the reservoir filling and operation.

To reduce a high-frequency noise, we applied three iterations of smoothing to the DEM using 3×3 kernel with linear inverse distance weights. Digital models of slope steepness (Fig. 2b), horizontal curvature (Fig. 2c), and vertical curvature (Fig. 2d) were derived from the smoothed DEM by the method of Evans (1980). Models have a resolution of 10 m. A map of relative accumulation zones (Fig. 2e) was obtained using $k_v$ и $k_h$ models.

Areas marked by $G > 15°$ are typical for the western and northeastern slopes of the depression as well as for ridges in the southeastern corner of the study area (Fig. 2b). However, there is a terrace about 500 m wide between the reservoir and the northeastern and northwestern slopes, and one of the southeastern ridges. Therefore, it is unlikely that landsliding on these slopes may be connected with the reservoir operation. We can also eliminate a slope in the northwestern corner of the study area from the further consideration: the slope belongs to an adjacent catchment. Hereafter, our main concern is the southwestern slope of the depression and the scarp along the northeastern reservoir shore marked by the narrow and long stripe of values $G > 15°$ (Fig. 2b).

Let us delineate areas marked by $G > 15°$ within relative accumulation zones, which are (a) adjacent to, upslope the maximal water level (1343 m), and (b) situated on the southwestern slope. Relying on the map obtained (Fig. 2f), we can conclude that the southwestern slope of the depression is characterised by the highest landslide hazard. This is because many potentially instable sites are located there one above the other. This configuration may lead to the ‘domino effect’, when a movement of

the masses in one site may trigger movements throughout the slope. On other reservoir shores, areas of potential slope instability are, more or less, evenly distributed along the terrace scarp. To adjust the map obtained and to range revealed areas according to the instability level, one can use data on soils, sediments, plant cover, and groundwater.

## PREDICTION OF SOIL DEGRADATION AND CONTAMINATION ALONG PIPELINES

Petroleum and gas pipelines have an adverse effect on soils. First, in a pipeline installation, an area of the disturbed soil cover may range from 400 to 1000 ha per 100 km of a pipeline route (Geltser and Geltser, 1994). As a result, technogenic soils are formed. They are marked by degraded physical, chemical, and biological properties (Naeth et al., 1988; Burgess and Harry, 1990; Geltser and Geltser, 1994). Second, pipeline damage may lead to an outflow of oil and petroleum products. Their flowing and concentration in local depressions result in soil contamination and destruction of the plant cover, while the further infiltration leads to groundwater deterioration (Eiceman et al. 1985; Couillard, 1986). Third, a pipeline can play a role of a geochemical barrier. Underground and elevated pipeline sections are usually constructed to pass gullies, intermittent and ephemeral streams. Nevertheless, pipeline elements can retard overland and intrasoil lateral flows of water and solved or suspended substances drained by natural channels (Crampton, 1988; Naeth et al., 1988; Burgess and Harry, 1990). This can lead to changes in water and salt regimes, waterlogging, and salinisation of lands on adjacent territories. These processes may influence a pipeline insulation and cause corrosive failures, in addition to the general degradation of a landscape.

Environmental monitoring of pipeline corridors is usually carried out using remotely sensed data (Jadkowski et al., 1994; Um and Wright, 1996; Gauthier et al., 2001). Some approaches of digital terrain modelling, such as derivation of slope steepness and curvatures, are used in pipeline routing (Feldman et al., 1995; Rylsky, 2004). Up to now, maps of relative accumulation zones have not been used to predict soil degradation and contamination along pipelines.

To exemplify a basic principle of application of maps of relative accumulation zones,

we consider a terrain with a gentle topography. The area size is about 600 by 500 m. A square-gridded DEM of the area has a mesh size of 1.5 m (Fig. 3a). A petroleum pipeline crosses the area. Assume that there is a single failure of the pipeline. The challenge is to predict a migration way of petroleum flowing from the hole, and areas of petroleum concentration. In addition, there is a need to find sites where soil degradation is feasible due to action of the pipeline as a barrier for natural flows.

To reduce a high-frequency noise, we applied three iterations of smoothing to the DEM using 3×3 kernel with linear inverse distance weights. A digital model of specific catchment area (Fig. 3b) was derived from the smoothed DEM by the method of Martz and de Jong (1988). Models of horizontal curvature (Fig. 3c) and vertical curvature (Fig. 3d) were derived from the smoothed DEM by the method of Evans (1980). Models have a resolution of 1.5 m. A map of relative accumulation zones (Fig. 3e) was produced using $k_v$ и $k_h$ models.

A thalweg network is delineated on the map of catchment area (Fig. 3b). This map can be used to determine paths of lateral migration of petroleum (Fig. 3f). Petroleum will concentrate in accumulation zones situated along a flow line originating at the point of the pipeline hole (Fig. 3f). The migration distance of petroleum depends on several factors, such as the volume of petroleum leaking out the pipeline, velocity of this leakage, velocity of the petroleum flow on the land surface, properties of the soil and vegetation covers, etc. This information should be used to refine the map obtained, and to estimate the dynamics of soil contamination.

Soil degradation (waterlogging and salinisation) may occur in relative accumulation zones adjacent to, upslope the pipeline (Fig. 3f). Indeed, local geometry of the relief forms natural conditions for increased moistening of the soil profile and salt concentration in relative accumulation zones (Pennock et al., 1987; Florinsky, 2000; Florinsky et al., 2000; Florinsky et al., 2002). Constructive elements of a pipeline, situated adjacent to, downslope a relative accumulation zone, may form a barrier for overland and intrasoil flows intensifying natural processes of moistening or salinisation. Salinisation may prevail in relative accumulation zones if soils and/or groundwaters contain water-soluble salts. Arid and semiarid climatic conditions can favour soil salinisation. Waterlogging is more probable if the environment is free of

water-soluble salts. To estimate dynamics, manifestation, and direction of soil degradation, one should use data on physical and chemical properties of soils as well as regime and chemical content of groundwaters.

## COMMENTS

Maps of relative accumulation zones cannot replace existed geological methods. The principles described can serve as additional computerised tool.

Appropriate resolution of a DEM is determined by typical sizes of the object under study. In the search of placers and instable slopes, the typical size is the minimal width of a placer or landslide in the given natural conditions. For each particular study, this parameter may be considered as constant if the study is carried out within a territory with homogeneous topography. In the pipeline monitoring, different portions of a pipeline may require DEMs with different resolution. This is because relief type and typical sizes of landforms can alter along the pipeline route.

All calculations and mapping were done with LandLord 4.0 (Florinsky et al., 1995).

## ACKNOWLEDGMENTS

The author is grateful to Robert Eilers (Manitoba Land Resource Unit, Agriculture and Agri-Food Canada, Winnipeg, Canada) for discussing ideas of this paper.

## REFERENCES

Almeida Filho, R., de Miranda, F.P., and Beisl, C.H., 2005, *Evidência de Uma Mega Captura Fluvial no Rio Negro (Amazônia) Revelada em Modelo de Elevação Digital da SRTM*, in Anais XII Simpósio Brasileiro de Sensoriamento Remoto, Goiânia, 16-21 abril 2005, INPE.

Bilibin, Yu.A., 1956, *Principles of Geology of Placers. 3rd ed*. Soviet Academic Press, Moscow (in Russian).

Burgess, M.M., and Harry, D.G., 1990, *Norman Wells Pipeline Permafrost and Terrain Monitoring: Geothermal and Geomorphic Observations, 1984-1987*, Canadian Geotechnical Journal, 27, 233-244.

Couillard, D., 1986, *Consequences Associated with a Crude Petroleum Leak from a Pipeline*, Journal of Environmental Management, 23, 247-257.

Crampton, C., 1988, *Terrain Evaluation and Pipeline Construction in the Canadian North*, The Musk-Ox, 36, 19-28.

Edwards, R., and Atkinson, K., 1986, *Ore Deposit Geology and Its Influence on Mineral Exploration*. Chapman and Hall, London.

Eiceman, G.A., Gardea, J.L., Nan, N.Y., and Sprester, F.R., 1985, *Distribution of Hydrocarbons in Soil through Contamination from a Leaking Natural Gas Pipeline*, International Journal of Environmental Analytical Chemistry, 23, 21-35.

Emelyanova, E.P., 1972, *Main Regularities of Landsliding Processes*. Nedra, Moscow (in Russian).

Evans, I.S., 1980, *An Integrated System of Terrain Analysis and Slope Mapping*, Zeitschrift für Geomorphologie, Suppl. 36, 274-295.

Feldman, S.C., Pelletier, R.E., Walser, E., Smoot, J.C., and Ahl, D., 1995, *A Prototype for Pipeline Routing Using Remotely Sensed Data and Geographic Information System Analysis*, Remote Sensing of Environment, 53, 123-131.

Fernandes, N.F., Guimarães, R.F., Gomes, R.A.T., Vieira, B.C., Montgomery, D.R., and Greenberg, H., 2004, *Topographic Controls of Landslides in Rio de Janeiro: Field Evidence and Modeling*, Catena, 55, 163-181.

Finarov, D.P., 1986, *Geomorphological Analysis and Prediction of Changes in Reservoir Shores and Bottoms*. Nauka, Leningrad (in Russian).

Florinsky, I.V., 1993, *Analysing Digital Elevation Models to Reveal Linear Structures of the Land Surface*. Ph.D. Thesis. Institute of Soil Science and Photosynthesis, Pushchino (unpublished, in Russian).

Florinsky, I.V., 2000, *Relationships between Topographically Expressed Zones of Flow Accumulation and Sites of Fault Intersection: Analysis by Means of Digital Terrain Modelling*, Environmental Modelling and Software, 15, 87-100.

Florinsky, I.V., and Eilers, R.G., 2002, *Prediction of the Soil Carbon Content at Micro-, Meso- and Macroscales by Digital Terrain Modelling*, in Transactions of the 17th World Congress of Soil Science, 14-21 August 2002, Bangkok, Thailand, Symposium 52. ISSS, Bangkok (CD ROM).

Florinsky, I.V., Eilers, R.G., and Lelyk, G.W., 2000, *Prediction of Soil Salinity Risk by Digital Terrain Modelling in the Canadian Prairies*, Canadian Journal of Soil Science, 80, 455-463.

Florinsky, I.V., Eilers, R.G., Manning, G., and Fuller, L.G., 2002, *Prediction of Soil Properties by Digital Terrain Modelling*, Environmental Modelling and Software, 17, 295-311.

Florinsky, I.V., Grokhlina, T.I., and Mikhailova, N.L., 1995, *LANDLORD 2.0: The Software for Analysis and Mapping of Geometrical Characteristics of Relief*, Geodezia i Cartografia, 5, 46-51 (in Russian).

Gauthier, R.P., Maloley, M., and Fung, K.B., 2001, *Land-Cover Anomaly Detection along Pipeline Rights-of-Way*, Photogrammetric Engineering and Remote Sensing, 67, 1377-1391.

Geltser, Y.G., and Geltser, V.Y., 1994, *Changes in Arable Sod Podzolic Soil Cenoses Associated with Pipeline Construction*, Eurasian Soil Science, 26, 37-47.

Gurov, V.N., and Kertsman, V.M., 1991, *Topography as a Factor for Possible Movement of Radionuclides*, in Khitrov, L.M. (Ed.), Geochemical Migration Ways of Artificial Radionuclides in Biosphere, Proceedings of the 5th Conference, Pushchino, Dec. 1991. Vernadsky Institute of Geochemistry and Analytical Chemistry, Moscow (in Russian).

Guzzetti, F., Carrara, A., Cardinali, M., and Reichenbach, P., 1999, *Landslide Hazard Evaluation: A Review of Current Techniques and Their Application in a Multi-Scale Study, Central Italy*, Geomorphology, 31, 181-216.

Jadkowski, M.A., Convery, P., Birk, R.J., and Kuo, S., 1994, *Aerial Image Databases for Pipeline Rights-of-Way Management*, Photogrammetric Engineering and Remote Sensing, 60, 347-355.

Kiersch, G.A., 1964, *Vaiont Reservoir Disaster*, Civil Engineering, 34, 32-39.

Lanyon, L.E., and Hall, G.F., 1983, *Land Surface Morphology: 2. Predicting Potential Landscape Instability in Eastern Ohio*, Soil Science, 136, 382-386.

Macdonald, E.H., 1983, *Alluvial Mining. The Geology, Technology, and Economics of Placers*. Chapman and Hall, London.

Martz, L.W., and de Jong, E., 1988, *CATCH: A Fortran Program for Measuring Catchment Area from Digital Elevation Models*, Computers and Geosciences, 14, 627-640.

McFarlane, C., 2000, *A GIS-Based Placer Gold Potential Assessment for the Bighole River Basin, Southwest Montana*, in GIS Hydro 2000, Geographic Information Systems in Water Resources. Center for Research in Water Resources, University of Texas at Austin, Austin http://www.crwr.utexas.edu/gis/gishydro00/Class/trmproj/McFarlane/termproject.htm.

Minervina, E.E., and Khositashvili, G.R., 1974, *Changes in Shores of Mountain Reservoirs: Methods and Examples of Prediction*. Energia, Moscow (in Russian).

Montgomery, D.R., Schmidt, K.M., Greenberg, H.M., and Dietrich, W.E., 2000, *Forest Clearing and Regional Landsliding*, Geology, 28, 311-314.

Muzylev, S.A. (Ed.), 1954, *A Guide to Methods of Geological Survey and Exploration*. Gosgeoltekhizdat, Moscow (in Russian).

Naeth, M.A., Chanasyk, D.S., McGill, W.B., Bailey, A.W., and Hardin, R.T., 1988, *Changes in Soil-Water Regime after Pipeline Construction in Solonetzic Mixed Prairie Rangeland*, Canadian Journal of Soil Science, 68, 603-610.

Pennock, D.J., Zebarth, B.J., and de Jong, E., 1987, *Landform Classification and Soil Distribution in Hummocky Terrain, Saskatchewan, Canada*, Geoderma, 40, 297-315.

Rylsky, I.A., 2004, *Optimisation of Pipeline Routing Using GIS Techniques*, Vestnik Moscovskogo Universiteta, Geography Series, 4, 34-40 (in Russian, with English abstract).

Shary, P.A., 2005, *Estimating Interrelations between Topography, Soil, and Plants with New Approaches of Geomorphometry (Exemplified by an Agrolandscape and a Forest Ecosystem in the Southern Moscow Region)*, Ph.D. Thesis. Institute of Physical, Chemical, and Biological Problems of Soil Science, Pushchino (unpublished, in Russian).

Shary, P.A., Sharaya, L.S., and Mitusov, A.V., 2002, *Fundamental Quantitative Methods of Land Surface Analysis*, Geoderma, 107, 1-32.

Shilo, N.A., 1985, *Principles of Placer Geology. 2nd rev. ed*. Nauka, Moscow (in Russian).

Um, J.-S., and Wright, R., 1996, *Pipeline Construction and Reinstatement Monitoring: Current Practice, Limitations and the Value of Airborne Videography*, The Science of the Total Environment, 186, 221-230.

Záruba, Q., and Mencl, V., 1982, *Landslides and Their Control. 2nd rev. ed*. Elsevier, Amsterdam.

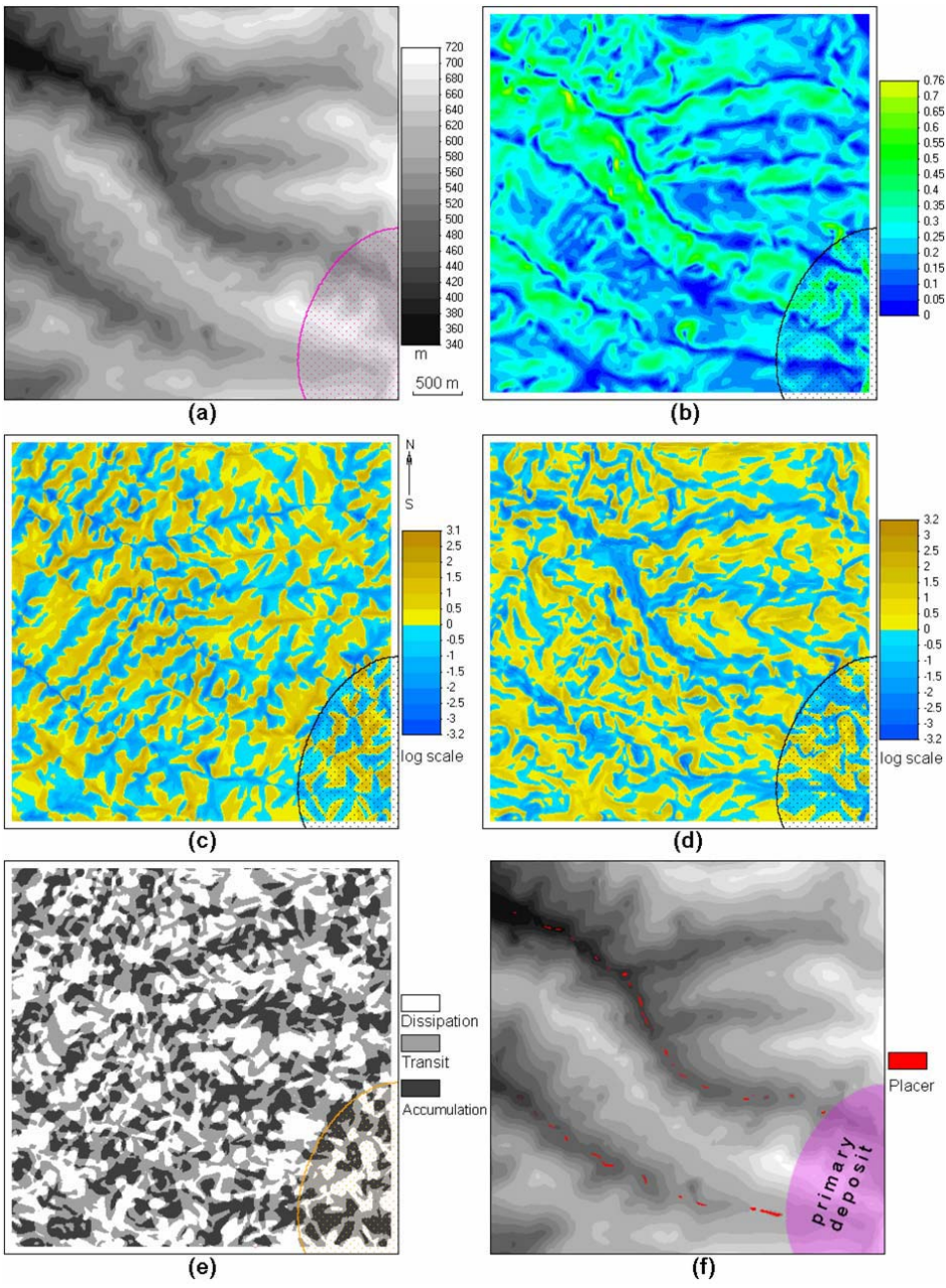


Fig. 1. Exploration of alluvial placers: (a) elevation, (b) slope factor, (c) horizontal curvature, (d) vertical curvature, (e) relative accumulation, transit, and dissipation zones, and (f) the most prospective areas. The primary deposit is hatched.

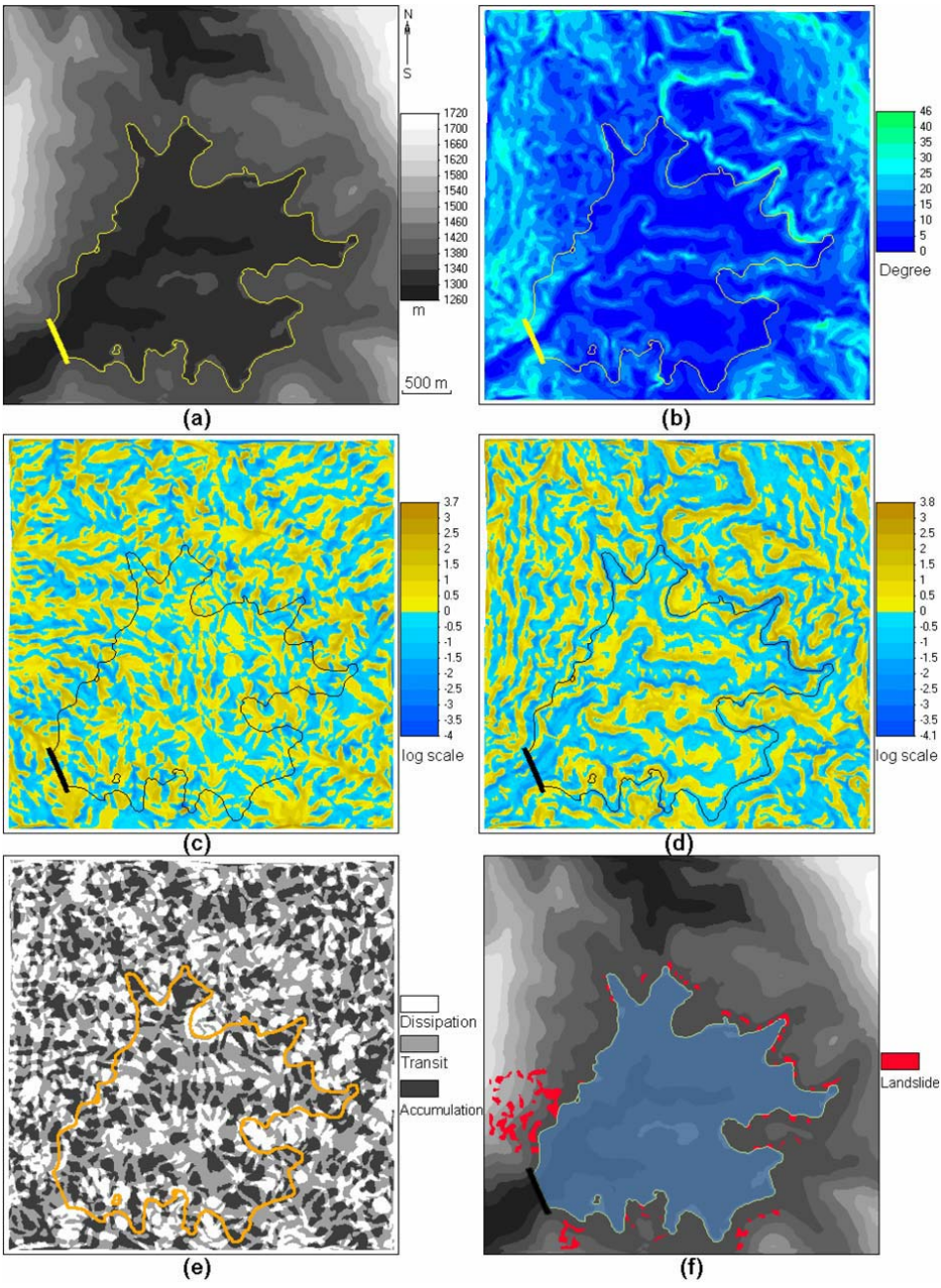


Fig. 2. Prediction of slope instability on reservoir shores: (a) elevation, (b) slope steepness, (c) horizontal curvature, (d) vertical curvature, (e) relative accumulation, transit, and dissipation zones, and (f) areas of possible slope instability. The dam and the maximal water level (1343 m) are delineated.

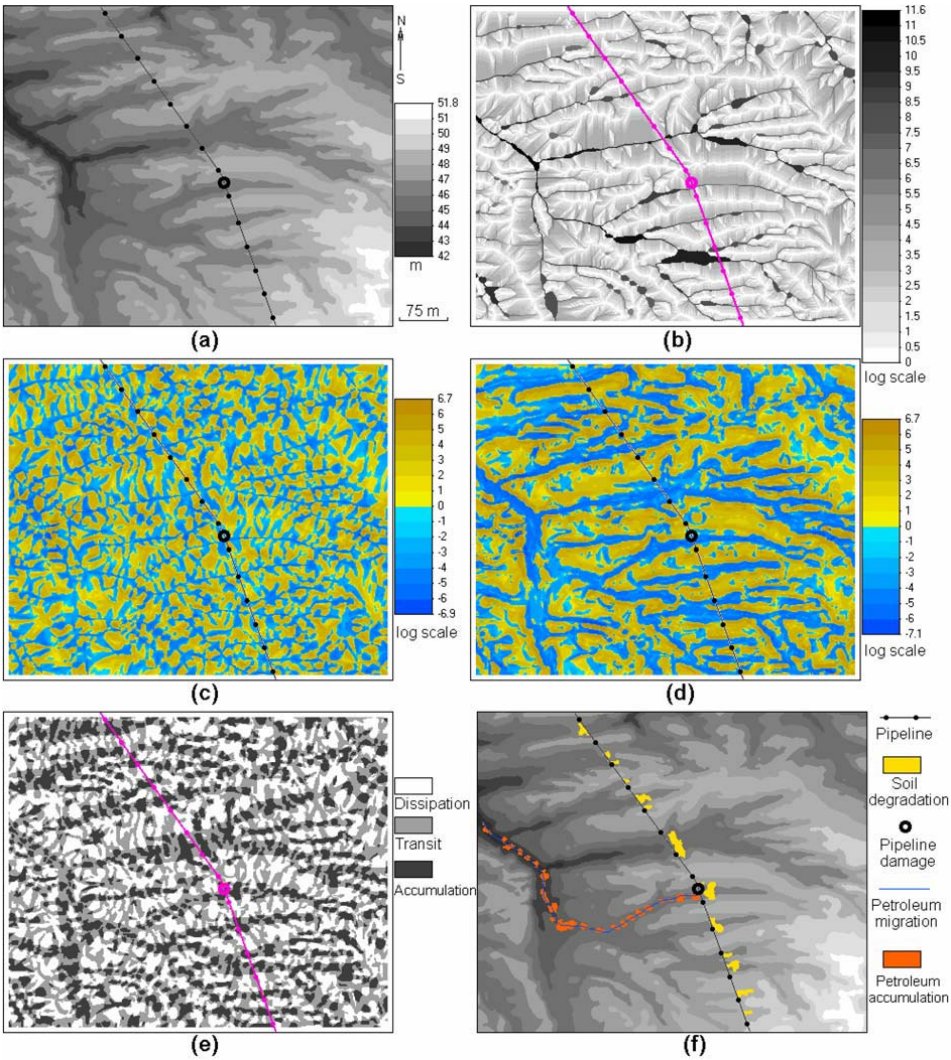


Fig. 3. Prediction of soil degradation and contamination along the pipeline: (a) elevation, (b) specific catchment area, (c) horizontal curvature, (d) vertical curvature, (e) relative accumulation, transit, and dissipation zones, and (f) areas of possible degradation and contamination of soil cover.

*International Journal of Ecology & Development*
*Fall 2007, Vol. 8, No. F07; Int. J. Ecol. Dev.*
*ISSN 0972-9984 ( Print ); ISSN 0973-7308 (Online)*


# Vertical Accuracy of Shuttle Radar Topography Mission (SRTM) Elevation and Void-Filled Data in the Libyan Desert

**Paul Elsner [1], Michael Bonnici [2]**

School of Geography

Birkbeck College, University of London

Malet Street, London WC1E 7HX, UK

[1] e-mail: p.elsner@bbk.ac.uk

[2] e-mail: mike.bonnici@gmail.com

Received 21 January 2007; accepted 5 May 2007

## ABSTRACT

*Elevation data produced by NASA's Shuttle Radar Topography Mission (SRTM) is currently the most detailed publicly available, free-of-cost, near-global digital elevation model (DEM). While generally very successful in collecting complete and accurate elevation data, the mission C-band Radar had limitations over specific landscapes, including sand deserts. This paper presents the results of a validation study using data from ground surveys in the Libyan Sahara. It tests (a) the accuracy of finished Level 2 SRTM DEM data; and (b) the performance of an interpolation procedure that is routinely applied to fill SRTM data voids on a global scale. The results show that SRTM data consistently meets its own accuracy specifications, with a root mean square error (RMSE) of 1.3 to 5.2 m. Interpolated void-filled data achieved lower accuracy, with RMSE of approximately 7 m for an area of smaller dunes, and RMSE of 14 m within an extensive field of strongly undulating dunes with heights of more than 100 m, meaning that the accuracy specification of SRTM data in this area is not met. It is concluded that void-filling by interpolation in areas of extensive dune fields does not reproduce the representative topography of such a landscape, and spatially higher resolved elevation data is needed to achieve this via interpolation*.

**Keywords:** Shuttle Radar Topography Mission, SRTM, Digital Elevation Model, Sahara, Validation, Accuracy Assessment.

**Mathematics Subject Classification:** 65G99, 62H35, 86A30, 65D05.

**JEL Classification:** Q19, Q50.

## INTRODUCTION

Digital elevation models (DEMs) belong to the most fundamental data sets in environmental science. The availability of DEMs with high quality and resolution is

central to a wide range of ecological models (Tappeiner et al., 1998; Krysanova et al., 1999; Van Niel and Austin, 2006).

The currently most detailed, near-global data set was acquired by the Shuttle Radar Topography Mission (SRTM) using C-band radar interferometry. All land masses between 60º N and 56º S were imaged at least once, representing about 80% of the Earth's land mass (Farr and Kobrick, 2000). The spatial resolution of the publicly available SRTM data is 1-arc-second (about 30 m at the Equator) for the United States area, and 3-arc-seconds (about 90 m at the Equator) for non-U.S. areas. The accuracy specifications for finished SRTM data follow requirements of the U.S. National Imagery and Mapping Agency (NIMA). The absolute vertical error is 16 m (90% linear error, LE90), the absolute horizontal error is 20 m (90% circular error), and the relative vertical error is 10 m (LE90) (Rodriguez et al., 2005, 2006).

Goncalves and Fernandes (2005) analysed the completeness of the global SRTM Level 2 data set and found that more than 15% of tiles have 1% of the surface area as voids, and more than 5% percent of tiles have voids of around 5%. Particularly large voids occur in mountainous regions where geometric artefacts are the result of foreshortening, layover, and radar shadow (Dowding et al., 2004). Also affected are dry sand deserts where insufficient signal response is caused by a low complex dielectric constant (CDC) of the reflecting surface. Individual tiles from the Himalaya and the Sahara have data voids of more than 10%.

A number of approaches have been developed to fill data voids in SRTM. For a comprehensive review see Gamache (2004). The only void-free SRTM data set with global coverage is that offered by the Consortium for Spatial Information of the Consultative Group for International Agriculture Research (CGIAR-CSI). CGIAR-CSI filled the voids by contouring existing SRTM Level 2 data and supplementing it with point data from auxiliary sources (CGIAR-CSI, 2006). In the case of Africa, the auxiliary data stem from the GTOPO30 DEM (U.S. Geological Survey, 1996). Contours and points are then interpolated and the resulting data is used to fill the voids in the original SRTM data. The interpolation is based on the algorithm of Hutchinson (1989) which applies a spline function with drainage enforcement to produce a hydrologically sound surface.

Ecological models can be very sensitive to errors in elevation data and it is hence important to have a clear understanding of DEM accuracy (Van Niel and Austin, 2006). A number of validation studies have been undertaken for original SRTM data and found that finished Level 2 SRTM data generally exceeds the given accuracy specifications (Smith and Sandwell, 2003; Falorni et al., 2005; Rodriguez et al., 2005, 2006; Hofton et al., 2006). Jarvis et al. (2004) assessed the accuracy of the void-filling algorithm applied by CGIAR-CSI for a mountainous region in Colombia and report acceptable agreement with elevation from a reference data source but less satisfactory correlation of derivatives like slope and aspect.

Little information is currently available on the accuracy of the CGIAR-CSI void filling procedure in desert areas where large SRTM data voids exists. This study shall address this issue. The aim and objective of the presented study is to assess both the accuracy of SRTM data and the accuracy of the CGIAR-CSI void-filling procedure in an arid desert environment. As a benchmark standard, the 16 m LE90 accuracy specification for SRTM elevation data shall be used.

## MATERIALS AND METHODS

We present case studies from three different desert areas in Eastern Libya (Fig. 1), which provide a representative cross-section of typical morphological features of this landscape: site NC145 (Fig. 2a), Area 124 (Fig. 2b), and site NC32B (Fig. 2c).

Ground control reference data was obtained using Real-Time Kinematic (RTK) Global Positioning System satellite navigation, a technique based on the use of carrier phase measurements of the GPS NAVSTAR signal where a single reference station provides the real-time pseudo-range corrections with high accuracy. In terms of a root mean square error (RMSE), the horizontal and vertical accuracy range of RTK data is 0.10 m. This level of accuracy exceeds that specified for SRTM data by more than an order of magnitude. It is hence justified to treat RTK data in the framework of this study as “true” ground elevation. Both GPS and SRTM data are referenced to the WGS 84 ellipsoid so no datum conversion is necessary.

All ground data used for analysis were collected with a dual frequency Leica System

530 and 1200 GPS receivers along transects with a sampling interval of 10, 15, or 40 m. RTK observations were matched respectively with the corresponding height information of the underlying SRTM or the CGIAR-CSI void-filled DEM value. RTK data lying within a specific DEM pixel were averaged and this average was then used for subsequent comparison with the respective pixel values of the DEM. Where a survey line coincided with both void-free and void-filled data, the survey line was separated accordingly and analysed individually.

The elevation residuals, i.e. the difference between RTK and DEM data, are analysed by calculating a number of statistics (DMA, 1991; Wechsler and Kroll, 2006) which quantify various aspects of elevation accuracy. They are summarised in Table 1.

## RESULTS

Two seismic lines were surveyed in area NC145 (Fig. 2a) in order to obtain adequate cross sections of the topography. Line 1 was approximately 211 km in length, with more than 14,000 RTK observations, recorded at 15 m intervals. The transect traversed over a varied topography with the terrain made up of stone covered plains, relatively low sand dunes, wadis, and dry ephemeral lakes. No large elevation changes were present. Apart from small sand dunes, the topography is made up of relatively hard surface geology. Transect Line 2 has a length of about 81 km with circa 5,400 RTK observations and intersects Line 1 perpendicularly (Fig. 2a). Very similar terrain features were encountered along this transect.

The height observations of both lines coincide with void-free SRTM Level 2 data. The residuals between RTK and SRTM data are small. The RMSE values for Line 1 and 2 are 1.5 m and 1.3 m, respectively. Bias, average relative absolute difference (ARAD), and standard deviation (STD) indicate little systematic error and high precision. A summary of all accuracy estimators is presented in Table 2. With $r > 0.99$, both lines exhibit a very strong positive correlation. The scatter-plots for both lines are presented on Figure 3a, b.

The second study site, Area 124 (Fig. 2b), is a mixture of stony gravel plains, solitary linear dunes on stony plains, and complex sand dunes with sandy intra-dune open

areas. The geomorphology is relatively uniform in north-south direction. Distinct landscape variations occur mainly along an east-west axis. The western part of the area is dominated by a flat, low-lying, gravel-covered plain, with frequent patches of palaeo-lake deposits. To the east, a transition zone is located comprising of distinct lines of simple linear sand dunes with sinuous ridges, oriented in northeast-southwest direction. In this transition zone, the area between dunes is comprised of flat, yet undulating gravel plains, with linear sand dunes becoming more frequent and more condensed towards the east. The eastern edge of Area 124 is characterised by higher and more complex dune systems. The dunes no longer form a mound with a single sinuous ridge but are comprised of sand ridges that are from 1 to 3 km wide. These ridges are characterised with a distinct central crest comprising of a dense network of smaller dune crests on both sides of the main and highest crest line. Approximately two thirds of SRTM voids were encountered in this distinct landscape feature.

Four transect lines have been surveyed in Area 124 (Fig. 2b). Transect Line 1 has a length of 28 km and is aligned in southwest-northeast direction. Line 1 was located in the flat sand/gravel plain with very few undulations in the topography here. Line 1 is the only survey that does not coincide with SRTM data voids. Conversely, Lines 2 to 4 overlap with both original SRTM DEM data and filled data voids. Line 1 can hence serve as site-internal benchmark.

The analysis of Line 1 resulted in a RMSE of 3.8 m. Most of the error appears to be random, as evident from the standard deviation of 3.7 m and the marginal bias of -0.2 m. However, the correlation between RTK and SRTM data is not strong ($r = 0.45$) and the associated scatter plot displays considerable spread (Fig. 3c).

Line 2 has a length of 22 km and is located further eastwards, approximately parallel to Line 1, and traversed a large void of approximately 71 $km^2$ which is heavily populated by a dense field of small linear sand dunes, ranging in height from 10 to 30 m. The southern part of the transect traversed over a flat sand gravel plain with few undulations and no evident voids in the DEM underlay. The non-void part of the DEM data coinciding with the RTK line has an overall accuracy of 4.3 m, with a relative bias of 0.8%. This slight positive bias of the non-void data compares with a

negative relative bias of -1.2% of void-filled elevation. The overall RMSE of the void-filled data is 6.5 m.

Both RMSE are still within the accuracy specifications set by NIMA. Yet, the correlation between field-based RTK data and DEM data is weak, as demonstrated by the scatter plots (Fig. 3d, e). The non-void data has a Pearson's correlation coefficient of r = 0.45. The void-filled DEM data correlates even weaker with a coefficient of r = -0.27 (Table 2).

Transect Line 3 in Area 124 passed through the same large void encountered by Line 2 but at an approximately right angle in east-west direction (Fig. 2b). Additionally, this transect also traversed a long linear sand dune ridge running at a northeast to southwest azimuth. Undulations with a magnitude of 20 to 30 m in height were common near the sand dune ridge. A large number of smaller voids in the SRTM dataset are evident and are directly related to the undulations and complexity of the dunes. In contrast to other lines, the accuracy between non-void and void-filled DEM data for Line 3 is very similar. Both have a slight negative bias, and an RRMSE of approximately 4.3%. The correlation with RTK data is also very similar and with r ~ 0.6 (Table 2) better than in Lines 1 and 2.

Transect Line 4 in Area 124 was surveyed in the south-eastern region of this study site and was approximately 60 km long, commencing from an undulating gravel plain in the western section, then crossing and eventually terminating over large complex sand dune formations in the eastern part of the area (Fig. 2b). These dunes form the southern flank of the Calanscio Sand Sea. The latter section is dominated with large linear sand dune ridges and is represented by large voids in the SRTM data.

Similar to Line 3, the performance of non-void and void-filled DEM data is only marginally different. Non-void data appears to mildly overestimate elevation whereas void-filled areas seem to systematically under-predict height. The RMSE for void-free data is 4.3 m and for void filled data 7.3 m. This, compared to the other transect lines in Area 124, lower accuracy in RMSE terms is contrasted by a higher statistical correlation with the RTK ground data. The void-filled data has a correlation of r = 0.83 and the void-free data r = 0.97 (Table 2). With this, Line 4 has the highest

correlation of all four transects in Area 124.

The third study site is labelled NC32B (Fig. 2c) and located within the southeastern section of the Sirte Basin, approximately 120 km north of Area 124. The region is composed of three distinct types of landscape: soft sand gravel plains in the eastern part, solitary linear dunes on gravel plains in the centre, and large complex sand dunes with sandy intra-dune open areas in the west. The sand dunes range up to a hundred metres in height and are the start of the western flank of the Great Sand Seas, stretching for hundreds of kilometres across the international border into Egypt. The dunes structure becomes increasingly more complex while ridges maintain a general north-south alignment.

The survey in NC32B was conducted in the central-north part of the study area and compiled during the acquisition of a 3D seismic program. The grid design consisted of 240 m line spacing with a station interval of 40 m between each GPS recording.

The RMSE for void-free SRTM DEM pixel is 4.3 m and has no bias. The void-filled DEM data has a large RMSE of 14.4 m, meaning that the absolute vertical accuracy requirement of 16 m (LE90) set by NIMA is significantly exceeded for this transect. The overall accuracy is affected by both significant bias (-5.5 m) and large random error (STD = 13.3 m). Despite the high error, there is still a relatively strong correlation (r = 0.73) between void-filled DEM data and RTK field data. An even stronger correlation is measured for non-void SRTM (r = 0.97) data (Table 2).

## DISCUSSION

Three transect lines coincide with void-free SRTM data and hence can serve as a measure of SRTM accuracy. The other four transect lines overlap with both void-free SRTM data and SRTM-voids. These sections provide also the opportunity to assess the accuracy of the void-filling process undertaken by CGIAR-CSI.

The accuracy of SRTM data assessed by RTK survey data lies within the range of 1.3 – 5.2 m. This is in general agreement with Rodriguez et al. (2006) who specify the SRTM Level 2 LE90 error for the whole African continent with approximately 6 m. It is apparent that the performance of SRTM data varies with landscape type. The

surveys in area NC145 resulted in the smallest RMSE of approximate 1.3 m. The dominant landscapes in NC145 are relatively flat stony plains with interceptions of small dunes. Area 124 and NC32B on the other hand are environments comprised to a large part of extensive undulating sand dune fields. SRTM data in this geomorphological setting have a RMSE of 4–5 m. More striking is the difference in respect to correlation with RTK ground data. NC145 SRTM elevation data reaches $r = 0.99$ whereas in Area 124 the coefficient can be as low as 0.45. This suggests that dune fields do not only due to their morphology and low CDC cause frequent SRTM data voids but also experience decreased accuracy if elevation data is recorded. This confirms earlier findings that dune fields are difficult to image by Radar (Blom, 1987; Abdelsalam et al., 2000).

The performance of the CGIAR-CSI void-filling algorithm in Area 124 appears to be acceptable. In all transects, the NIMA accuracy standard of 16 m (LE90) is met. In transect Line 3, the RMSE and correlation of void-filled data is even better than in existing SRTM data of that survey. In other transects, the accuracy difference between non-void and void-filled data remains in the range of 2–3 m RMSE.

A different picture is painted by the results from the study site NC32B. Here, the void-filled data is failing the 16 m LE90 standard, whereas the existing SRTM data has a RMSE of only 4 m. Site NC32B is mainly composed of extensive dune fields with strongly undulating topography. Figure 4 shows a comparison of a height profile measured in such a dune field and the respective profile created by void-filling interpolation. It can be seen that significant elevation change is taking place over a small distances. This elevation variance is lost in the void-filled DEM, which is based on data points with 1-km spacing. Due to the absence of sufficiently resolved ground data, the interpolation is not able to reproduce characteristic height patterns but instead produces an over-smoothed surface.

The direction of the transect lines appears to be of importance in some of the surveys. In the study site NC145, mainly composed of flat gravel plains, no significant influence in survey direction is apparent, although Line 1 and 2 are aligned in right angle to each other. However, a marked difference appears to exist in Area 124, particularly in the measured correlation of DEM data with RTK ground-

reference elevation. This is the case for both void-free and void-filled DEM data. Lines in N-S alignment have much lower correlation than those in E-W direction. The general N-S alignment of landscape features, including dune fields, apparently has a negative impact on both SRTM performance and void-filling. This is in correspondence with findings of Falorni et al. (2005) suggested that the side-looking geometry of the Shuttle Radar was sensitive to the orientation of landscape features.

Finally, there is an interesting discrepancy in the information provided by different accuracy estimators. Using the RMSE as benchmark, the void-filled part of NC23B survey is performing worst. Despite the large RMSE (14 m), the DEM has a still a relatively strong correlation ($r = 0.73$) with RTK data. This is much better compared to most of the surveys in Area 124. In the worst case (Line 2 void-filled), r is as low as 0.27, resulting in a coefficient of determination of $r^2 = 0.07$. This means that, statistically, only 7% of the variance in the void-filled DEM data is explained by variance in RTK data. Yet, the RMSE of that section is 6.5 m and well within the LE90 accuracy limit. In addition to this, it should be noted that Line 2 of Area 124 exhibits the smallest range in elevation of the study (about 20 m), making a RMSE of 6.5 m much more significant than in areas with ranges of several hundred metres.

All of the correlation coefficients measured are statistically significant ($p < 0.01$), but this can mainly be attributed to the large sample sizes and resulting high degrees of freedom. It also should be noted that many relative RMSE values in Area 124 would lead to significantly higher absolute RMSE and a LE90 error beyond 16 m.

## CONCLUSIONS

Sand dunes appear to have a negative influence on both SRTM data completeness and data accuracy. The void-filling procedure applied by CGIAR-CSI seems to produce acceptable data in arid areas of hard surface geology. However, it is of limited use for areas where extensive dune fields cause large data voids. The high-frequency undulation of these dune fields cannot be reproduced by the interpolation procedure that is utilising input data with 1-km spacing.

Little can be said in this respect about how important is the CGIAR-CSI's underlying algorithm, which stems from a hydrological context and always produces

hydrological sound elevation surface, even in the case of landscape types that are dominantly shaped by aeolean processes as in the Sahara.

Still, it can be concluded that input information with spacing of 1 km, as in the case of CGISAR-CSI interpolation, appears to be not sufficient to reproduce the topography of large sand dunes. It seems hence necessary to explore alternative void-filling methods for such areas, including the use of elevation data derived from alternative sources such as the Advanced Spaceborne Thermal Emission and Reflection Radiometer (ASTER) which has a 30 m spacing (Obrock and Guth, 2005). However, it should be noted that the global coverage of ASTER DEMs is incomplete. In addition to this, ASTER DEMs often exhibit significant horizontal and vertical offsets and require alignment with SRTM data.

## ACKNOWLEDGEMENTS

We are grateful to North African Geophysical Exploration Company and the Libyan National Oil Company for giving access to their survey data. We also would like to thank the two anonymous reviewers for their constructive and helpful comments.

## REFERENCES

Abdelsalam, M.G., Robinson, C., El-Baz, F., and Stern, R.J., 2000, *Applications of Orbital Imaging Radar for Geologic Studies in Arid Regions - The Saharan Testimony*, Photogrammetric Engineering and Remote Sensing, 66, 712-726.

Blom, R., 1987, *Effects of Variation in Incidence Angle and Wavelength in Radar Images of Volcanic and Aeolian Terraces: or, Now See Them, Now You Don't*, International Journal of Remote Sensing, 9, 945-965.

CGIAR-CSI, 2006, *Void-Filled Seamless SRTM Data Version 3*, International Centre for Tropical Agriculture, http://srtm.csi.cgiar.org.

DMA, 1991, *Error Theory as Applied to Mapping, Charting, and Geodesy*, DMA TR 8400.1, U.S. Defence Mapping Agency, 109.

Dowding, S., Kuuskivi, T., and Li, X., 2004, *Void Fill of SRTM Elevation Data - Principles, Processes and Performance*, in Proceedings of the Conference 'ASPRS Images to Decision: Remote Sensing Foundation of GIS Applications', Sept. 12-16 2004, Kansas City, USA. American Society for Photogrammetry and Remote Sensing.

Falorni, G., Teles, V., Vivoni, E.R., Bras, R.L., and Amaratunga, K.S., 2005, *Analysis and Characterization of the Vertical Accuracy of Digital Elevation Models from the Shuttle Radar Topography Mission*, Journal of Geophysical Research, 110, F02005.

Farr, T. and Kobrick, M., 2000, *Shuttle Radar Topography Mission Produces a Wealth of Data*, EOS, 81, 583-585.

Gamache, M., 2004, *Free and Low Cost Datasets for International Mountain Cartography*, in Proceedings of the 4th Mountain Cartography Workshop, 30 Sept.-2 Oct. 2004, Vall de Núria, Spain. Institut Cartogràfic de Catalunya, Barcelona.

Goncalves, J., and Fernandes, J.C., 2005, *Assessment of SRTM-3 DEM in Portugal with Topographic Maps*, in Proceedings of the EARSeL Workshop '3D Remote Sensing - Use of the Third Dimension for Remote Sensing Purposes', June 10-11, 2005, Porto.

Hofton, M., Dubayah, R., Blair, J.B., and Rabine, D., 2006, *Validation of SRTM Elevations Over Vegetated and Non-Vegetated Terrain Using Medium Footprint Lidar*, Photogrammetric Engineering and Remote Sensing, 72, 279-285.

Hutchinson, M., 1989, *A New Procedure for Gridding Elevation and Stream Line Data with Automatic Removal of Spurious Pits*, Journal of Hydrology, 106, 211-233.

Jarvis, A., Rubiano, J., Nelson, A., Farrow, A., and Mulligan, M., 2004, *Practical Use of SRTM Data in the Tropics – Comparisons with Digital Elevation Models Generated from Cartographic Data*, Working Document No. 198. Centro Internacional de Agricultura Tropical (CIAT), Cali.

Krysanova, V., Wechsung, F., Becker, A., Poschenrieder, W., and Graefe, J., 1999, *Mesoscale Ecohydrological Modelling to Analyse Regional Effects of Climate Change*, Environmental Modelling and Assessment, 4, 259-271.

Obrock, K., and Guth, P., 2005, *Filling Holes in SRTM DEMs using ASTER DEMs*, in Proceedings of the 6th International Conference on Military Geology and Geography, 19-22 June 2005, Nottingham, UK.

Rodriguez, E., Morris, C.S., and Belz, J.E., 2006, *A Global Assessment of the SRTM Performance*, Photogrammetric Engineering and Remote Sensing, 72, 249-260.

Rodriguez, E., Morris, C.S., Belz, J.E., Chapin, E.C., Martin, J.M., Daffer, W., and Hensley, S., 2005, *An Assessment of the SRTM Topographic Products*, Technical Report JPL D-31639. Jet Propulsion Laboratory, Pasadena.

Smith, B., and Sandwell, D., 2003, *Accuracy and Resolution of Shuttle Radar Topography Mission Data*, Geophysical Research Letters, 30, 1467.

Tappeiner, U., Tasser, E., and Tappeiner, G., 1998, *Modelling Vegetation Patterns Using Natural and Anthropogenic Influence Factors: Preliminary Experience with a GIS Based Model Applied to an Alpine Area*, Ecological Modelling, 113, 225-237.

U.S. Geological Survey, 1996, *GTOPO30, A 30-arc Seconds Global Digital Elevation Model*. USGS EROS Data Center, Sioux Falls, http://edc.usgs.gov/products/elevation/gtopo30/gtopo30.html.

Van Niel, K.P., and Austin, M.P., 2006, *Predictive Conservation Modelling for Conservation: Impact of Error Propagation for Digital Elevation Data*, Ecological Applications, 17, 266-280.

Wechsler, S.P., and Kroll, C.N., 2006, *Quantifying DEM Uncertainty and Its Effect on Topographic Parameters*, Photogrammetric Engineering and Remote Sensing, 72, 1081-1090.

Table 1. Statistics applied for quantification of DEM accuracy.

| Statistic | Equation |
|---|---|
| Bias | $Bias = \frac{\sum_{i=1}^{N}(\hat{z}_i - z_i)}{N}$ |
| Relative bias (RBias) | $RBias = \frac{\sum_{i=1}^{N}\left[\frac{(\hat{z}_i - z_i)}{z_i}\right]}{N} \times 100$ |
| Average relative absolute difference (ARAD) | $ARAD = \frac{\sum_{i=1}^{N}\left(\frac{\lvert\hat{z}_i - z_i\rvert}{z_i}\right)}{N} \times 100$ |
| Standard deviation (STD) | $STD = \sqrt{\frac{\sum_{i=1}^{N}(\hat{z}_i - \bar{z}_i)^2}{N}}$ |
| Root mean square error (RMSE) | $RMSE = \sqrt{\frac{\sum_{i=1}^{N}(\hat{z}_i - z_i)^2}{N}}$ |
| Relative root mean square error (RRMSE) | $RRMSE = \sqrt{\frac{\sum_{i=1}^{N}\left(\frac{\hat{z}_i - z_i}{z_i}\right)^2}{N}}$ |

$\hat{z}_i$ is the elevation value of the SRTM or void-filled DEM pixel, $z_i$ is the respective RTK elevation, and N is the number of observations.

Table 2. Accuracy statistics of individual transect lines.

| Transect | N | Bias (m) | RBias (%) | ARAD (%) | STD (m) | RMSE (m) | RRMSE (%) | r |
|---|---|---|---|---|---|---|---|---|
| NC145 | | | | | | | | |
| Line 1 non-void | 14125 | -0.7 | 2 | 1.5 | 1.3 | 1.5 | 2 | 0.99 |
| Line 2 non-void | 5411 | -0.7 | 0.9 | 1.3 | 1.1 | 1.3 | 1.7 | 0.99 |
| Area 124 | | | | | | | | |
| Line 1 non-void | 2776 | -0.2 | 0.1 | 2 | 3.7 | 3.8 | 3.2 | 0.45 |
| Line 2 non-void | 1037 | 0.9 | 0.8 | 2.9 | 4.2 | 4.3 | 3.8 | 0.45 |
| Line 2 void-filled | 1182 | -1.5 | -1.2 | 4 | 6.3 | 6.5 | 5.5 | -0.27 |
| Line 3 non-void | 1526 | -0.4 | -0.2 | 3.1 | 5.1 | 5.2 | 4.4 | 0.63 |
| Line 3 void-filled | 666 | -0.9 | -0.7 | 3.3 | 4.8 | 4.9 | 4.2 | 0.61 |
| Line 4 non-void | 3902 | 0.8 | 0.5 | 1.8 | 4.3 | 4.3 | 2.5 | 0.97 |
| Line 4 void-filled | 2016 | -0.3 | 0 | 3.1 | 7.3 | 7.3 | 3.9 | 0.83 |
| NC32B | | | | | | | | |
| Non-void | 6294 | -0.1 | 0 | 2.5 | 4.3 | 4.3 | 3.2 | 0.97 |
| Void-filled | 6006 | -5.5 | -4 | 6.8 | 13.3 | 14.4 | 10 | 0.73 |

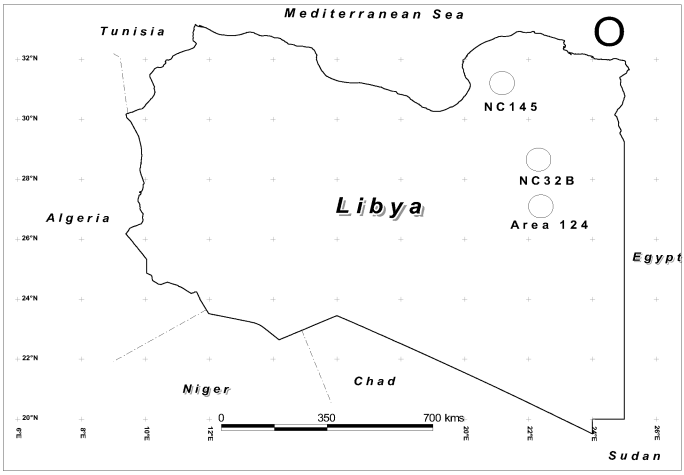


Fig. 1. Overview map showing locations of the study sites.

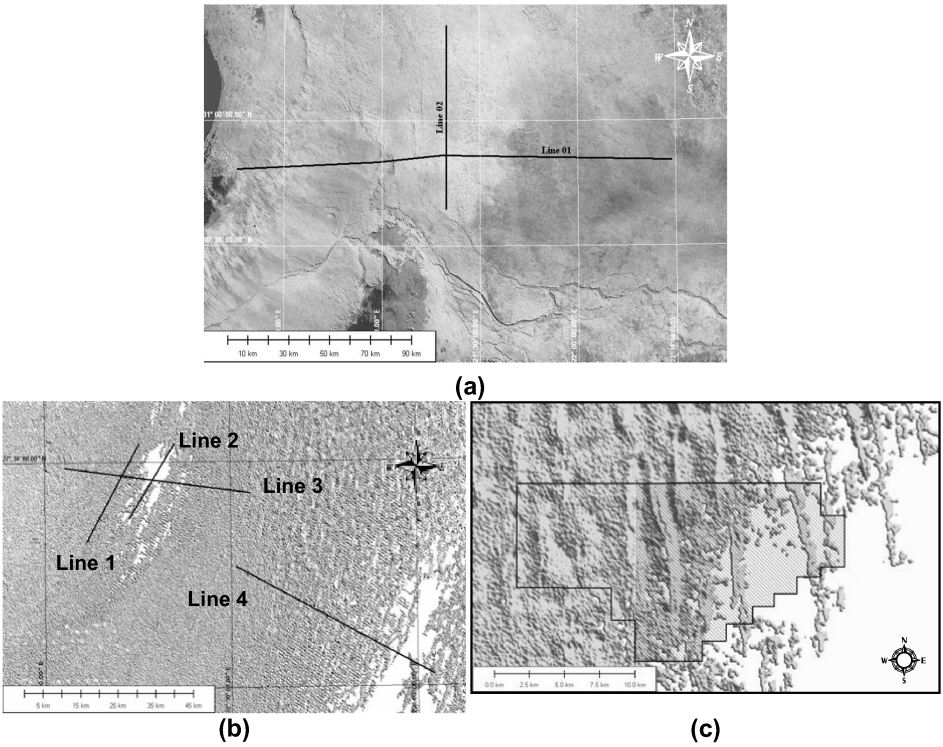


Fig. 2. (a) the site NC145 with RTK survey transect lines; (b) the Area 124 with RTK survey lines. White areas delineate areas with SRTM voids that had to be filled by interpolation; (c) the study area NC32B. The hatched area denotes region where mesh of seismic lines has been surveyed. White areas - SRTM data voids.

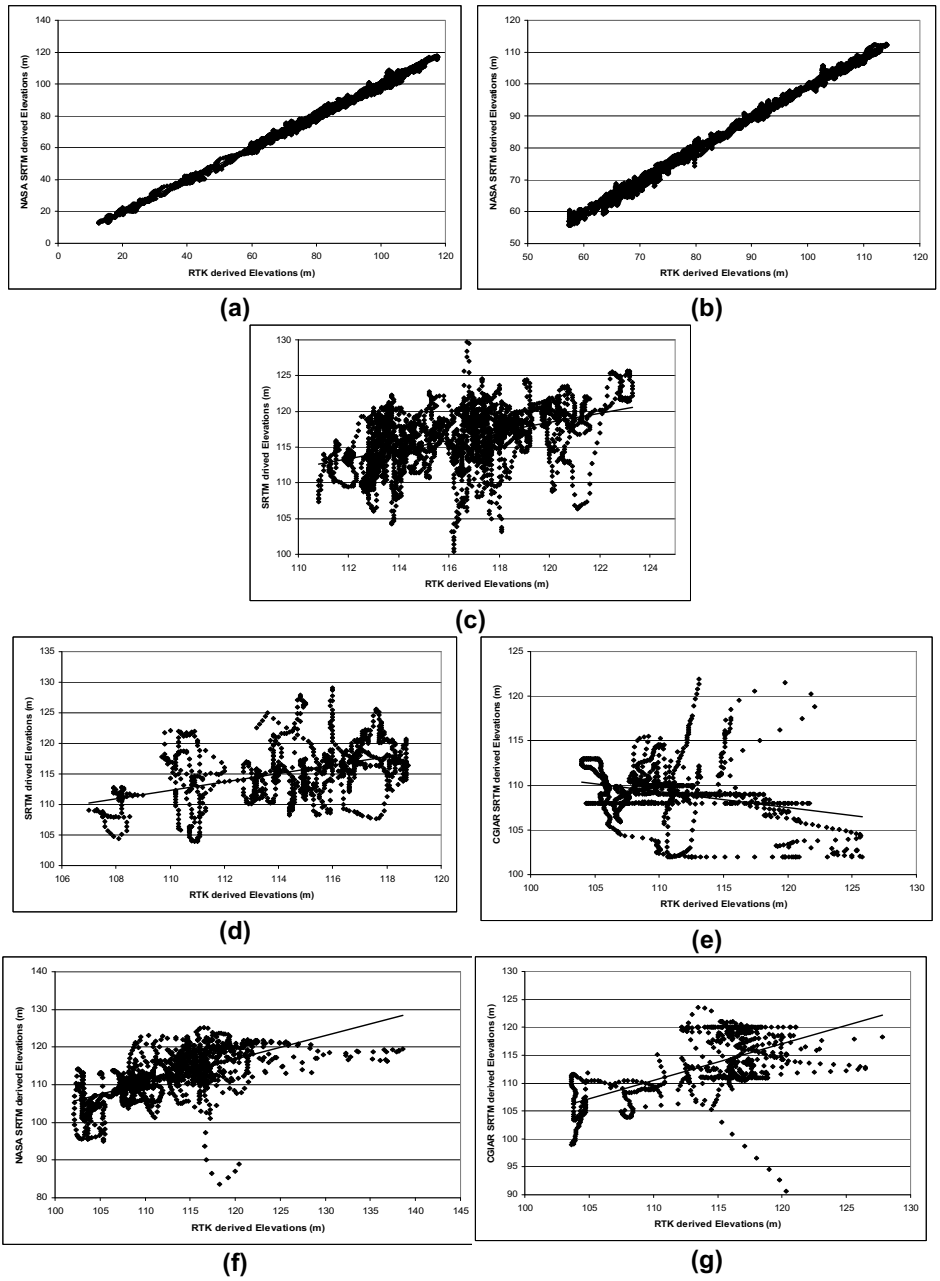


Fig. 3. Scatterplots of RTK measurements: (a) NC 145 Line 1 vs non-void SRTM; (b) NC 145 Line 2 vs non-void SRTM; (c) Area 124 Line 1 vs non-void SRTM; (d) Area 124 Line 2 vs non-void SRTM; (e) Area 124 Line 2 vs void-filled SRTM; (f) Area 124 Line 3 vs non-void SRTM; (g) Area 124 Line 3 vs void-filled SRTM;

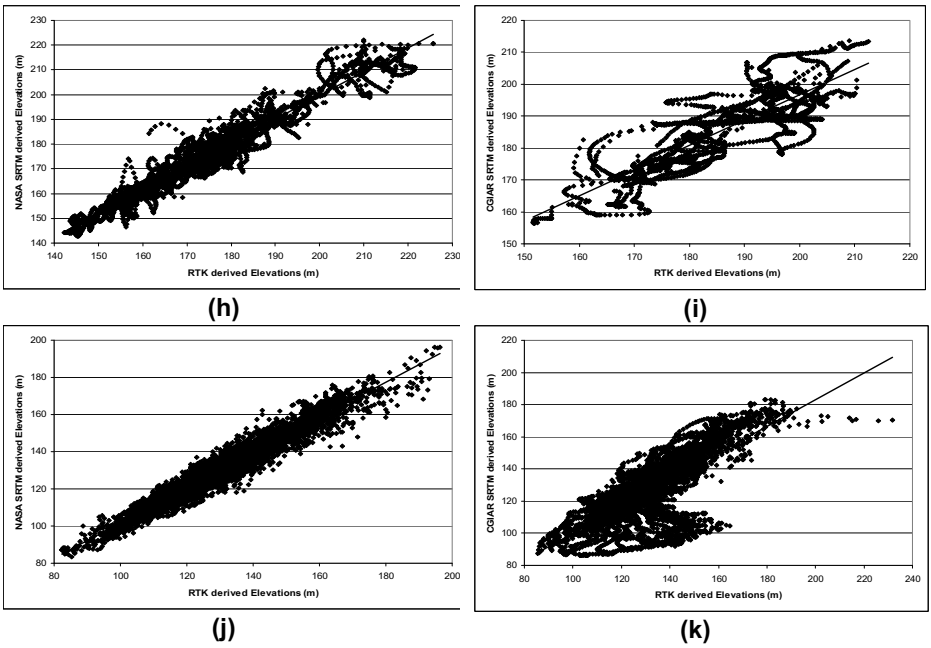


Fig. 3 (cont.): (h) Area 124 Line 4 vs non-void SRTM; (i) Area 124 Line 4 vs void-filled SRTM; (j) NC32B vs non-void SRTM; and (k) NC32B vs void-filled SRTM.

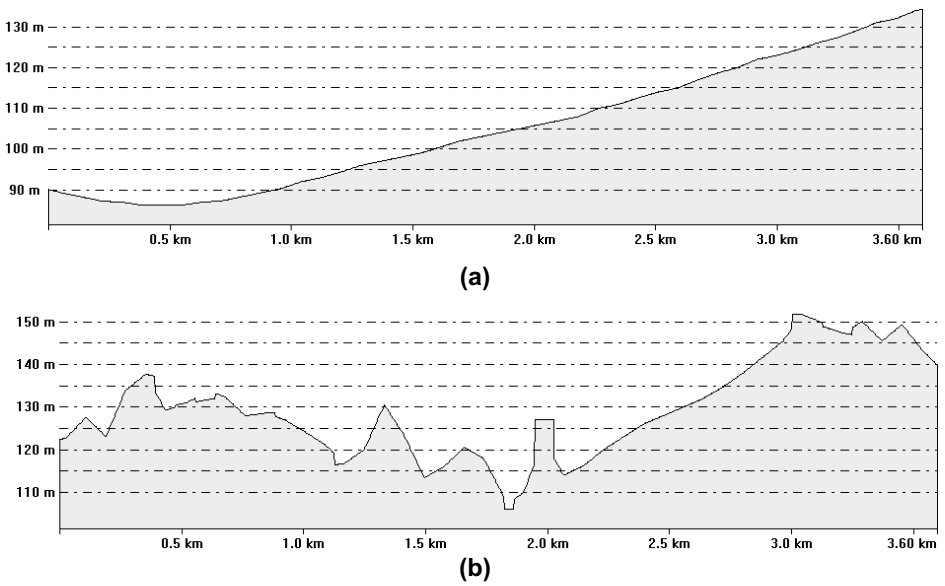


Fig. 4. Comparison of elevations of void-filled DEM data (a), and corresponding average of RTK measurements for respective 90 m cells (b) in the study site NC32B.

*International Journal of Ecology & Development*
*Fall 2007, Vol. 8, No. F07; Int. J. Ecol. Dev.*
*ISSN 0972-9984 ( Print ); ISSN 0973-7308 (Online)*


# Filtering of Digital Terrain Models by Two-Dimensional Singular Spectrum Analysis

**N.E. Golyandina [1], K.D. Usevich [1], I.V. Florinsky [2]**

[1] Department of Statistical Modelling
St.-Petersburg State University
University pr. 28, Petrodvoretz, St.-Petersburg, 198504, Russia

e-mail: nina@gistatgroup.com

[2] Institute of Mathematical Problems of Biology
Russian Academy of Sciences
Pushchino, Moscow Region, 142290, Russia

e-mail: iflor@mail.ru

Received 11 March 2007; accepted 21 May 2007

## ABSTRACT

*Singular Spectrum Analysis (SSA) has been approved as a model-free technique to analyse time series. SSA can solve different problems such as decomposition into a sum of trend, periodicities, and noise, smoothing, and others. In this paper, we validate abilities of 2D-SSA (the extension of SSA to analyse two-dimensional scalar fields) to treat digital terrain models (DTMs). The study is exemplified by a 30-arc-second digital elevation model of a part of South America derived from GTOPO30. Results demonstrate that 2D-SSA is an efficient method to denoise and generalise DTMs. It can be also used to decompose a topographic surface into components of continental, regional, and local scales.*

**Keywords:** Digital Elevation Model, Singular Spectrum Analysis, Image Processing, Filtering, Periodicity, Noise.

**Mathematics Subject Classification:** 62H35, 68U10, 62M15, 93E14, 93E11, 86A30, 86A60

**JEL Classification:** Q19, Q50.

## INTRODUCTION

A surface can be viewed as a sum of surfaces. This triviality forms the basis to solve a variety of problems using digital terrain analysis. The best-known tasks follow: (1) separating topographic components of different scales; (2) denoising digital terrain models (DTMs); and (c) generalising DTMs, that is, removing non-noise high-frequency components from DTMs.

These tasks are usually attacked by multiple regressions (Chorley and Huggett, 1965; Tobler, 1969), weighted moving averages (Tobler, 1969), Fourier analysis (Rudy, 1989), Kalman filtering (Gallant, 2006), and isobase mapping (Grohmann et al., 2007). In this paper, we report the first results of evaluation of two-dimensional Singular Spectrum Analysis (2D-SSA) as a tool to denoise and generalise DTMs and to separate continental, regional, and local components of topography.

SSA was originated as a model-free technique to analyse one-dimensional time series (Elsner and Tsonis, 1996; Danilov and Zhigljavsky, 1997; Golyandina et al., 2001). The SSA can be used to decompose a time series into a sum of trend, oscillations, and noise, to detect periodicities, to smooth and denoise signals, to forecast time series, and to impute missing data (GistaT Group, 1997-2007).

There are multidimensional extensions of SSA. Multichannel SSA (MSSA) is intended to analyse simultaneously a set of time series with common features (Elsner and Tsonis, 1996; Danilov and Zhigljavsky, 1997; Golyandina and Stepanov, 2005). MSSA can be applied to 2D scalar fields if one dimension is considered as time. The 2D-SSA was specially designed to process 2D scalar fields (Danilov and Zhigljavsky, 1997). Unlike MSSA, 2D-SSA is invariant regarding field rotation. 2D-SSA shares common traits with 2D-ESPRIT (Rouquette and Najim, 2001) applied to a specific problem of estimation of frequencies and damping factors.

## 2D-SSA ALGORITHM

Let us consider a 2D discrete field $f : \{1,\ldots,N_r\} \times \{1,\ldots,N_c\} \mapsto \mathbb{R}$ given by a matrix

$$\mathrm{F} = \begin{pmatrix} f(1,1) & f(1,2) & \ldots & f(1,N_c) \\ f(2,1) & f(2,2) & \ldots & f(2,N_c) \\ \vdots & \vdots & \ddots & \vdots \\ f(N_r,1) & f(N_r,2) & \ldots & f(N_r,N_c) \end{pmatrix}. \quad (1)$$

Algorithm parameters are window sizes $(L_r, L_c)$, where $1 \le L_r \le N_r$, $1 \le L_c \le N_c$, $1 < L_r L_c < N_r N_c$. Set $K_r = N_r - L_r + 1$ and $K_c = N_c - L_c + 1$. The algorithm includes two stages, decomposition and reconstruction, each of them consists of two steps (see details on matrix calculus elsewhere – Magnus and Neudecker, 1999, Chapter 1).

## Decomposition

### *Embedding*

The first step consists in the construction of the trajectory matrix of the field F by moving $L_r \times L_c$-windows. In the 1D case, one transforms a 1D object into a 2D matrix (Golyandina et al., 2001). Here, we embed a 2D object into a four-dimensional space. To flatten the 4D object, we transform moving windows

$$\mathrm{F}_{i,j} = \begin{pmatrix} f(i,j) & f(i,j+1) & \dots & f(i,j+L_c-1) \\ f(i+1,j) & f(i+1,j+1) & \dots & f(i+1,j+L_c-1) \\ \vdots & \vdots & \ddots & \vdots \\ f(i+L_r-1,j) & f(i+L_r-1,j+1) & \dots & f(i+L_r-1,j+L_c-1) \end{pmatrix}, \tag{2}$$

where $1 \le i \le K_r$, $1 \le j \le K_c$, to columns of the flattened trajectory matrix $\mathbf{W}$ ($\mathrm{F}_{i,j}$ transfers to the $(i+(j-1)K_r)$th column). For example, if $L_r = L_c = 2$, then the window

$$\begin{pmatrix} f(1,1) & f(1,2) \\ f(2,1) & f(2,2) \end{pmatrix} \tag{3}$$

is transformed into the first column $(f(1,1), f(2,1), f(1,2), f(2,2))^{\mathrm{T}}$.

It is appropriate to use vectorising and matricizing operations: for a $M \times N$-matrix $\mathbf{B}$, $\mathrm{vec}\,\mathbf{B} \in \mathbb{R}^{MN}$ is the vector constructed from stacked columns of $\mathbf{B}$. If we fix matrix sizes $M$ and $N$, then $(M,N)$-matricizing will be opposite to vectorising: $\mathrm{matr}\,\mathrm{vec}\,\mathbf{B} = \mathbf{B}$. Thus, the trajectory matrix $\mathbf{W}$ of the field F consists of $K_r K_c$ columns $\mathrm{vec}\,\mathrm{F}_{i,j}$, $1 \le i \le K_r$, $1 \le j \le K_c$. Furthermore, the matrix $\mathbf{W}$ of the size $L_r L_c \times K_r K_c$ can be presented in a more structured form:

$$\mathbf{W} = \begin{pmatrix} \mathbf{H}_1 & \mathbf{H}_2 & \dots & \mathbf{H}_{K_c} \\ \mathbf{H}_2 & \mathbf{H}_3 & \dots & \mathbf{H}_{K_c+1} \\ \vdots & \vdots & \ddots & \vdots \\ \mathbf{H}_{L_c} & \mathbf{H}_{L_c+1} & \dots & \mathbf{H}_{N_c} \end{pmatrix}, \tag{4}$$

where

$$\mathbf{H}_i = \begin{pmatrix} f(1,i) & f(2,i) & \dots & f(K_r,i) \\ f(2,i) & f(3,i) & \dots & f(K_r+1,i) \\ \vdots & \vdots & \ddots & \vdots \\ f(L_r,i) & f(L_r+1,i) & \dots & f(N_r,i) \end{pmatrix}. \tag{5}$$

The matrix $\mathbf{W}$ has the block-Hankel structure with the same blocks along secondary

diagonals. Each block $\mathbf{H}_i$ is Hankel itself: it is the trajectory matrix of the 1D series $f(\cdot, i)$ (the $i$th column of the initial field F). The matrix $\mathbf{W}$ will be further called the *block-Hankel trajectory matrix* of the field F. Note that there is the one-to-one correspondence between $N_r \times N_c$ fields and block-Hankel matrices with $L_r \times K_r$ Hankel blocks.

*Singular value decomposition*

This step is a singular value decomposition of the block-Hankel trajectory matrix:

$$\mathbf{W} = \sum_{i=1}^{d} \mathbf{W}_i = \sum_{i=1}^{d} \sqrt{\lambda_i} U_i V_i^{\mathrm{T}}, \tag{6}$$

where $\lambda_1, \ldots, \lambda_d$ are non-zero eigenvalues of the matrix $\mathbf{W}\mathbf{W}^{\mathrm{T}}$ arranged in decreasing order of magnitudes ($\lambda_1 \geq \lambda_2 \geq \ldots \geq \lambda_d > 0$), $\{U_1, \ldots, U_d\}, U_i \in \mathbb{R}^{L_r L_c}$, is the corresponding orthonormal system of the *eigenvectors*, and $\{V_1, \ldots, V_d\}, V_i \in \mathbb{R}^{K_r K_c}$, is the orthonormal system of the corresponding *factor vectors*

$$V_i = \mathbf{W}^{\mathrm{T}} U_i / \sqrt{\lambda_i}. \tag{7}$$

By analogue with principal component analysis, the vectors $\sqrt{\lambda_i} V_i$ are called principal component vectors. They are conveniently considered as matrices: the $(L_r, L_c)$-matricizing of an eigenvector is called an *eigenfield*, the $(K_r, K_c)$-matricizing of a factor vector is called a *factor field,* and the $(K_r, K_c)$-matricizing of a vector of principal components is called a *principal component field*. A set of square root of *i*th eigenvalue, *i*th eigenfield, and *i*th factor field is called *i*th *eigentriple* (ET).

## Reconstruction

*Grouping*

This step consists in grouping of addends in the decomposition (Eq. 6), that is, the corresponding eigentriples. Let us divide the set $\{1, \ldots, d\}$ into $m$ disjoint subsets $\mathrm{I}_1, \ldots, \mathrm{I}_m$. Summing $\mathbf{W}_i$, $i \in \mathrm{I}_k$, we come to the expansion

$$\mathbf{W} = \sum_{k=1}^{m} \mathbf{W}_{\mathrm{I}_k}. \tag{8}$$

*Averaging*

Grouped matrices $\mathbf{W}_{\mathrm{I}_k}$ do not necessarily have block-Hankel form. Therefore, one needs an additional step to transfer the decomposition (Eq. 8) of the block-Hankel trajectory matrix $\mathbf{W}$ into a decomposition of the initial field $\mathrm{F}$. This can be done by the orthogonal projection (in Frobenious norm) of the matrices $\mathbf{W}_{\mathrm{I}_k}$ on the set of block-Hankel matrix with Hankel blocks, like Eq. 4. After projection, we obtain

$$\mathbf{W} = \sum_{k=1}^{m} \tilde{\mathbf{W}}_k, \tag{9}$$

where $\tilde{\mathbf{W}}_k$, $k = 1,\ldots,m$, have a form of Eq. 4. Using the one-to-one correspondence between block-Hankel trajectory matrices and 2D fields, we come to the final decomposition of the initial field:

$$\mathrm{F} = \sum_{k=1}^{m} \tilde{\mathrm{F}}_k. \tag{10}$$

Let us discuss the projection algorithm in details. Consider one of components of the decomposition (Eq. 8):

$$\mathbf{W}_{\mathrm{I}} = \begin{pmatrix} \mathrm{W}_{1,1} & \mathrm{W}_{1,2} & \ldots & \mathrm{W}_{1,K_c} \\ \mathrm{W}_{2,1} & \mathrm{W}_{2,2} & \ldots & \mathrm{W}_{2,K_c} \\ \vdots & \vdots & \ddots & \vdots \\ \mathrm{W}_{L_c,1} & \mathrm{W}_{L_c,2} & \ldots & \mathrm{W}_{L_c,K_c} \end{pmatrix}, \tag{11}$$

where $\mathrm{W}_{i,j}$ are $L_r \times K_r$ blocks. The projection is equivalent to two sequential averaging procedures: 'within block' hankelization and 'between blocks' one.

1. 'Within block' hankelization. Averaging $(k,l)$-entries of $\mathrm{W}_{i,j}$ with $k + l = s$, where $1 \le s \le N_r$, we obtain the Hankel matrices. Thus, we have a matrix with Hankel blocks:

$$\mathbf{W}'_{\mathrm{I}} = \begin{pmatrix} \mathrm{W}'_{1,1} & \mathrm{W}'_{1,2} & \ldots & \mathrm{W}'_{1,K_c} \\ \mathrm{W}'_{2,1} & \mathrm{W}'_{2,2} & \ldots & \mathrm{W}'_{2,K_c} \\ \vdots & \vdots & \ddots & \vdots \\ \mathrm{W}'_{L_c,1} & \mathrm{W}'_{L_c,2} & \ldots & \mathrm{W}'_{L_c,K_c} \end{pmatrix}. \tag{12}$$

2. 'Between blocks' hankelization. The matrix $\mathbf{W}'_{\mathrm{I}}$ can be considered as a matrix of

blocks. Therefore, hankelization by blocks lies in averaging of the blocks $W'_{i,j}$, $i+j=s$, where $1 \le s \le N_c$. The final form is block-Hankel with Hankel blocks:

$$\tilde{\mathbf{W}}_{\mathrm{I}} = \begin{pmatrix} \tilde{\mathbf{H}}_1 & \tilde{\mathbf{H}}_2 & \cdots & \tilde{\mathbf{H}}_{K_c} \\ \tilde{\mathbf{H}}_2 & \tilde{\mathbf{H}}_3 & \cdots & \tilde{\mathbf{H}}_{K_c+1} \\ \vdots & \vdots & \ddots & \vdots \\ \tilde{\mathbf{H}}_{L_c} & \tilde{\mathbf{H}}_{L_c+1} & \cdots & \tilde{\mathbf{H}}_{N_c} \end{pmatrix}. \tag{13}$$

Notice that operations 1 and 2 are permutable.

## Comments

The result of the method consists in a decomposition of the initial field into a sum of components. It is expected that if the field F is a sum of a smooth surface, oscillations, and noise, so there exists such a grouping that the resultant decomposition (Eq. 10) is close to the initial field decomposition. This gives an opportunity for smoothing, denoising, removing periodic noise, etc.

Rules to select 2D-SSA parameters are mostly similar to the 1D case (Golyandina et al., 2001). In particular, small window sizes produce adaptive smoothing. The most detailed decomposition and the better separation of the field components can be obtained if window sizes are close to $(N_r/2, N_c/2)$. However, the use of big window sizes can lead to the mixing problem caused by too detailed decomposition of components. Calculation cost can set additional restrictions on parameters, as one should find eigenvectors and eigenvalues of a large matrix $L_r L_c \times L_r L_c$.

At the grouping step, selection of ET in Eq. 6 for the grouping stems from the fact that eigenfields and factor fields are similar to the component of F, which generates them. In particular, smooth surface generates slowly varying factor fields.

## MATERIALS

To validate 2D-SSA, we select a portion of the Northern Andes measuring 4º by 4º, located between 2º S and 2º N, and 78º30' W and 74º30' W (Fig. 1a). The area covers regions of Ecuador, Colombia, and Peru including parts of the coastal plain, the Andean range, and the Upper Amazon basin.

A digital elevation model (DEM) of the study area was extracted from GTOPO30, the 30 arc-seconds gridded global DEM (U.S. Geological Survey, 1996). The DEM measures 480 columns by 481 rows (viz., 230,880 points). It has a grid size of 30" (about 925 m). Elevation ranges from 5 m to 6085 m (Fig. 1b).

We selected this area and GTOPO30 on two counts. First, it is well known that this DEM incorporates a high-frequency noise caused by interpolation errors and inaccurate merging of topographic charts marked by different accuracy. Spatial distribution of noise in these DEMs is uneven and depends on the accuracy of cartographic sources. In particular, the potent noise is typical for forested regions of Africa and South America because reasonably detailed and accurate topographic data were unavailable for such regions. Thus, the interpolation of sparse contours has been used to compile these portions of GTOPO30. Although DEM noise is no obstacle to produce realistic maps of elevation, it leads to derivation of noisy and unreadable maps of secondary topographic variables (e.g., curvatures). This is because their derivation is based on the calculation of the first and second partial derivatives of elevation that increases dramatically the noise (Florinsky, 2002). The study area, consisting of two main zones – high mountains and forested foothills – marked by different signal-to-noise ratio, is ideally suited for validating 2D-SSA as a tool to denoise DEMs. Second, the use of this DEM allows us to test possibilities of 2D-SSA to decompose a topographic surface into components of different scales under complex geomorphic conditions.

## DATA PROCESSING

To reduce the huge range of elevations (6080 m), the initial DEM was transformed by taking the natural logarithm. Logarithmic DEMs were used in the further processing and mapping. We did not interpolate or smooth DTMs.

Using the window size of 30 by 30, the initial DEM was decomposed into 900 eigentriples (Fig. 2). We evaluated various combinations of eigentriples to reconstruct DEMs. Finally, the best variants were selected. To denoise the DEM, a DEM was reconstructed from the ET 1-100. To exemplify DTM generalisation, two DEMs were reconstructed from the ET 1-50 and 1-25. To separate continental,

regional, and local components of topography, six DEMs were reconstructed from the ET 1, 2, 3, 2-3, 4-25, and 51-100. To visualise a noise component of GTOPO30, a DEM was reconstructed from the ET 101-900. DEM processing was done by software 2D-SSA version 1.2 (© K. Usevich and N. Golyandina, 2005-2007).

Horizontal curvature ($k_h$), one of the most important topographic attributes, was derived from the initial and reconstructed DEMs by the method designed for spheroidal trapezoidal grids (Florinsky, 1998). $k_h$ values were also transformed:

$$k_h^{'} = \mathrm{sign}(k_h) \cdot \ln(1 + 10^8 |k_h|). \quad (14)$$

To clarify an effect of denoising and generalisation, we mapped $k_h$ stratifying its values into two levels: $k_h > 0$ and $k_h < 0$ (areas of flow divergence and convergence, correspondingly). For the binary mapping, it does not matter whether $k_h$ was derived from a DEM or logarithmic DEM: map patterns are near-identical.

DTMs produced had a grid size of 30". The plate carrée projection was used for mapping. Calculations and mapping were done with LandLord 4.0 (Florinsky et al., 1995). Statistical characteristics of the initial and reconstructed DTMs were compared with Statgraphics Plus 3.0 (© Statistical Graphics Corp., 1994-1997).

## RESULTS AND DISCUSSION

A visual comparison of elevation maps derived from the initial DEM (Fig. 3a) and two DEMs reconstructed from the ET 1-100 (Fig. 3b) and 1-50 (Fig. 3c) allows one to see nothing but marginal changes in image patterns. A cursory examination may lead to an underestimation of results of the DEM denoising and generalisation. $k_h$ maps give better insight into the results. Indeed, typical manifestation of interpolation errors – 'tracks' of contours (Florinsky, 2002) – can be found on the $k_h$ map derived from the initial DEM (Fig. 3d). These tracks are typical for the Andean foothills covered by dense rain forests. It is hardly probable that this map may be used for any application. However, there are no error tracks on $k_h$ maps derived from DEMs reconstructed from the ET 1-100 (Fig. 3e) and 1-50 (Fig. 3f). One can see so-called flow structures formed by convergence and divergence areas (black and white image patterns, correspondingly). These maps may be used for geomorphic and geological interpretation. A comparison between $k_h$ maps derived from different DEMs (Fig. 3d-

f) shows a pronounced effect of the map generalisation. The less number of the eigentriples used to reconstruct a DEM, the more smooth and simplified image patterns obtained. Reducing the number of ET used for DEM reconstruction leads to the marked reduction of the range of $k_h$ values (Fig. 3d-f) but influences the range of elevation values only slightly (Fig. 3a-c). This is also clearly demonstrated by quantile-quantile plots (they are not presented for reasons of space).

A DEM reconstructed from the ET 1 is marked by the highest level of generalisation. This DEM represents a generalised morphostructure of the continental scale, the Andean Range with foothills (Fig. 4a). Derivation of $k_h$ from this DEM allowes us to reveal a system of near-NW-SE-striking lineaments (Fig. 4b), which may indicate strike-slip faults (Florinsky, 1996). Although there are no structures of this sort in the recent database of Quaternary faults (Eguez et al., 2003), this does not attest that the lineaments are of erosional origin. First, geology of the Upper Amazon basin is poorly known. Second, they may indicate pre-Quaternary structures. Indeed, Chebanenko (1964) has described a system of deep-seated faults with the NW-SE strike situated to the southeast of the study area (Fig. 1a). The lineaments detected may be associated with northwestern extensions of the faults.

A DEM reconstructed from the ET 2-3 (Fig. 4c) represents landforms probably connected with regional tectonic structures. For a DEM reconstructed from the ET 2, patterns agree closely with the direction of the Andean range. A DEM reconstructed from the ET 3 represents features probably related to the $k_h$ lineaments (Fig. 4b). It is conceivable that near-NW-SE-striking structures control spatial distribution of river valleys of the Upper Amazon basin. A DEM reconstructed from the ET 4-25 (Fig. 4d) represents landforms probably associated with geomorphic processes of a regional scale. For example, one can see generalised tributary valleys of Amazon River.

A DEM reconstructed from the ET 51-100 (Fig. 5a) represents high-frequency components, which cannot be considered as noise. However, it is impossible to find familiar patterns of the drainage network on this map. These components might represent topographic manifestation of local geomorphic processes. A DEM reconstructed from the ET 101-900 (Fig. 5b) includes the noise inherent in GTOPO30 (Fig. 3a). This is precisely the noise, which rendered the $k_h$ map derived

from the initial DEM (Fig. 3d) unsuitable for applications. Among 'tracks' of contours, one can see a rectangular feature along the northeastern border of the map (Fig. 5b). This is a trace of the inaccurate merging of adjacent topographic charts marked by different accuracy during the compilation of GTOPO30. This DEM is a residual of the initial DEM (Fig. 3a) after the DEM reconstructed from the ET 1-100 (Fig. 3b).

The DEM reconstructions from the ET 1, 2, 3 and 2-3 may be considered as application of low-pass filters to the initial DEM, while the DEM reconstruction from the ET 101-900 and 51-100 – as application of high-pass filters.

## CONCLUSIONS

The results demonstrate that 2D-SSA is a powerful method to denoise DTMs. The 2D-SSA-based denoising of DEMs leads to extremely fine changes in elevations. These changes cannot be captured except by derivation of secondary terrain attributes. In fact, 2D-SSA can remove the noise without damage to the signal unlike usual smoothing by moving averages. This suggests that 2D-SSA is a method of exceptional importance for preliminary treatment of noisy DEMs including global ones. This opens the way to utilise noisy DEMs for derivation of important topographic variables, such as land surface curvatures.

2D-SSA can be used to decompose a topographic surface into components of continental, regional, and local scales. ET selection to reconstruct topographic components of different scales may be marked by non-uniqueness and ambiguity. The similar problem arises if a multiple regression or spectral filtering is used to extract regional or local components from DEMs. However, the problem is largely associated with the qualitative character of scale notions in geomorphology rather than with mathematical features of a decomposition technique. Moreover, as in the 1D case (Golyandina et al., 2001), 2D-SSA provides techniques to identify ET appropriate for a particular grouping (this was not used in the study). Finally, 2D-SSA is a model-free approach, that is, it does not use *a priori* assumption or statistical hypothesis about DEM structure as contrasted to multiple regressions.

## REFERENCES

Chebanenko, I.I., 1964, *Problems of Fold Belts of the Earth's Crust (In the Context of Block*

*Tectonics)*, Naukova Dumka, Kiev (in Russian).

Chorley, R.J., and Huggett, P., 1965, *Trend-Surface Mapping in Geographical Research*, Transactions of the Institute of British Geographers, 37, 47-67.

Danilov, D.L., and Zhigljavsky, A.A. (Eds.), 1997, *Principal Components of Time Series: The 'Caterpillar' Method*. St. Petersburg University Press, St. Petersburg (in Russian).

Eguez, A., Alvarado, A., Yepes, H., Machette, M.N., Costa, C., and Dart, R.L., 2003, *Database and Map of Quaternary Faults and Folds of Ecuador and Its Offshore Regions*. USGS Open-File Report 03-289.

Elsner, J.B., and Tsonis, A.A., 1996, *Singular Spectrum Analysis: A New Tool in Time Series Analysis*, Plenum Press, New York.

Florinsky, I.V., 1996, *Quantitative Topographic Method of Fault Morphology Recognition*, Geomorphology, 16, 103-119.

Florinsky, I.V., 1998, *Derivation of Topographic Variables from a Digital Elevation Model Given by a Spheroidal Trapezoidal Grid*, International Journal of Geographical Information Science, 12, 829-852.

Florinsky, I.V., 2002, *Errors of Signal Processing in Digital Terrain Modelling*, International Journal of Geographical Information Science, 16, 475-501.

Florinsky, I.V., Grokhlina, T.I., and Mikhailova, N.L., 1995, *LANDLORD 2.0: The Software for Analysis and Mapping of Geometrical Characteristics of Relief*, Geodezia i Cartografia, 5, 46-51 (in Russian).

Gallant, J., 2006, *Multiscale Methods in Terrain Analysis*, in Liu X., Wang Y. (Eds.), Full Papers, Proceedings of International Symposium on Terrain Analysis and Digital Terrain Modelling, 23-25 Nov. 2006, Nanjing, China. Nanjing Normal University, Nanjing (CD-ROM).

GistaT Group, 1997-2007, *'Caterpillar'-SSA: Time Series Analysis and Forecasting*, http://gistatgroup.com/cat/.

Golyandina, N., and Stepanov, D., 2005, *SSA-Based Approaches to Analysis and Forecast of Multidimensional Time Series*, in Ermakov, S.M., Melas, V.B., and Pepelyshev, A.N. (Eds.), Proceedings of the 5th St. Petersburg Workshop on Simulation, June 26 - July 2, 2005. St. Petersburg State University, St. Petersburg.

Golyandina, N.E., Nekrutkin, V.V., and Zhigljavsky, A.A., 2001, *Analysis of Time Series Structure: SSA and Related Techniques*, Chapman and Hall/CRC, London.

Grohmann, C.H., Riccomini, C., and Alves, F.M., 2007, *SRTM-Based Morphotectonic Analysis of the Poços de Caldas Alkaline Massif, Southeastern Brazil*, Computers and Geosciences, 33, 10-19.

Magnus, J.R., and Neudecker H., 1999, *Matrix Differential Calculus with Applications in Statistics and Econometrics, 2nd ed*. Wiley, New York.

Rouquette, S. and Najim, M., 2001, *Estimation of Frequencies and Damping Factors by Two-Dimensional ESPRIT-Type Methods*, IEEE Transactions on Signal Processing, 49, 237-245.

Rudy, R.M., 1989, *On Generalisation of Topography by Convolution*, Geodesia, Aerofotosyemka i Cartografia, 49: 120-126 (in Russian).

Tobler, W.R., 1969, *Geographical Filters and Their Inverses*, Geographical Analysis, 1, 234-253.

U.S. Geological Survey, 1996, *GTOPO30, A 30-arc Seconds Global Digital Elevation Model*. USGS EROS Data Center, Sioux Falls, http://edc.usgs.gov/products/elevation/gtopo30/gtopo30.html.

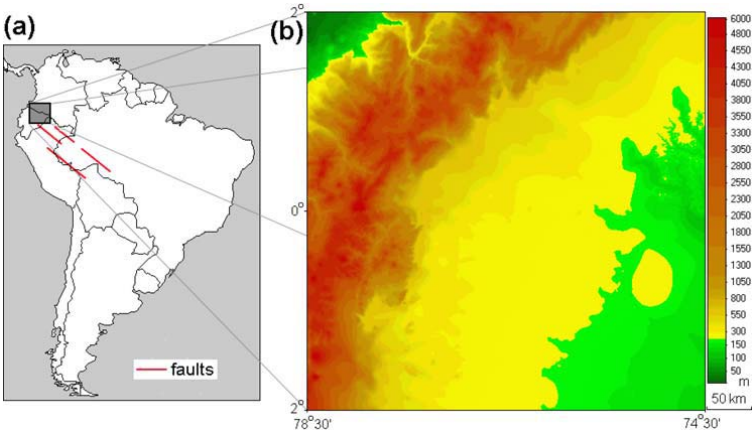


Fig. 1. The study area: (a) geographical location and some deep-seated faults (Chebanenko, 1964); and (b) elevation map.

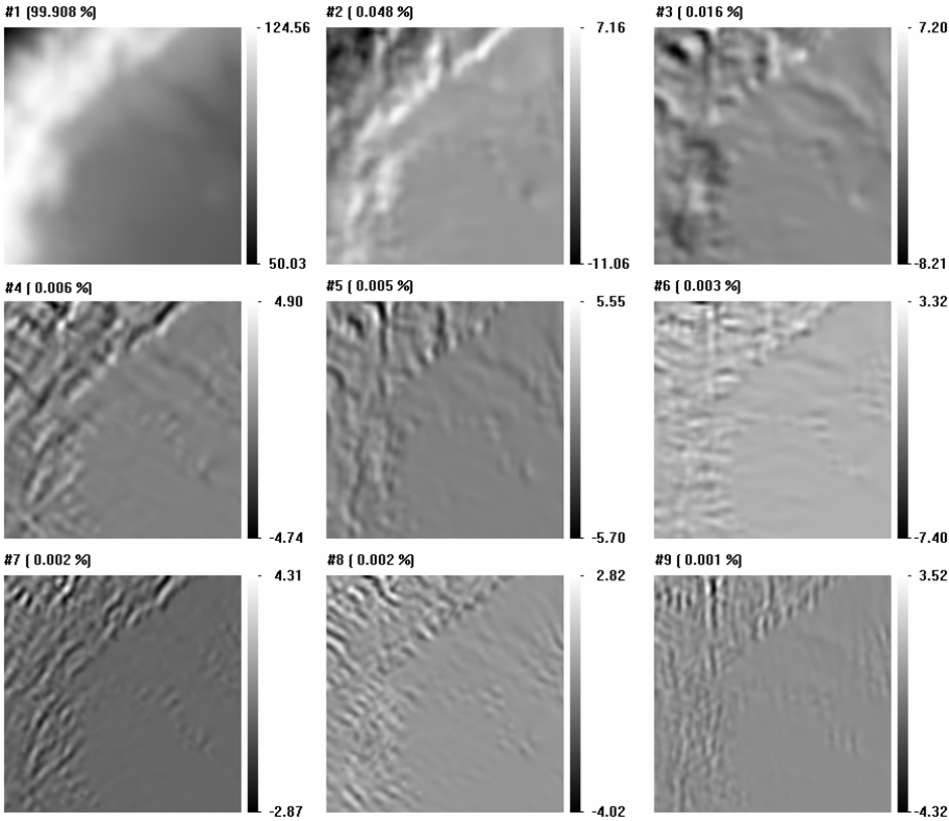


Fig. 2. Principal component fields 1-9 of the DEM decomposition. Percentage reflects shares of the corresponding eigentriples in the singular value decomposition (Eq. 6). Logarithmic scale is used.

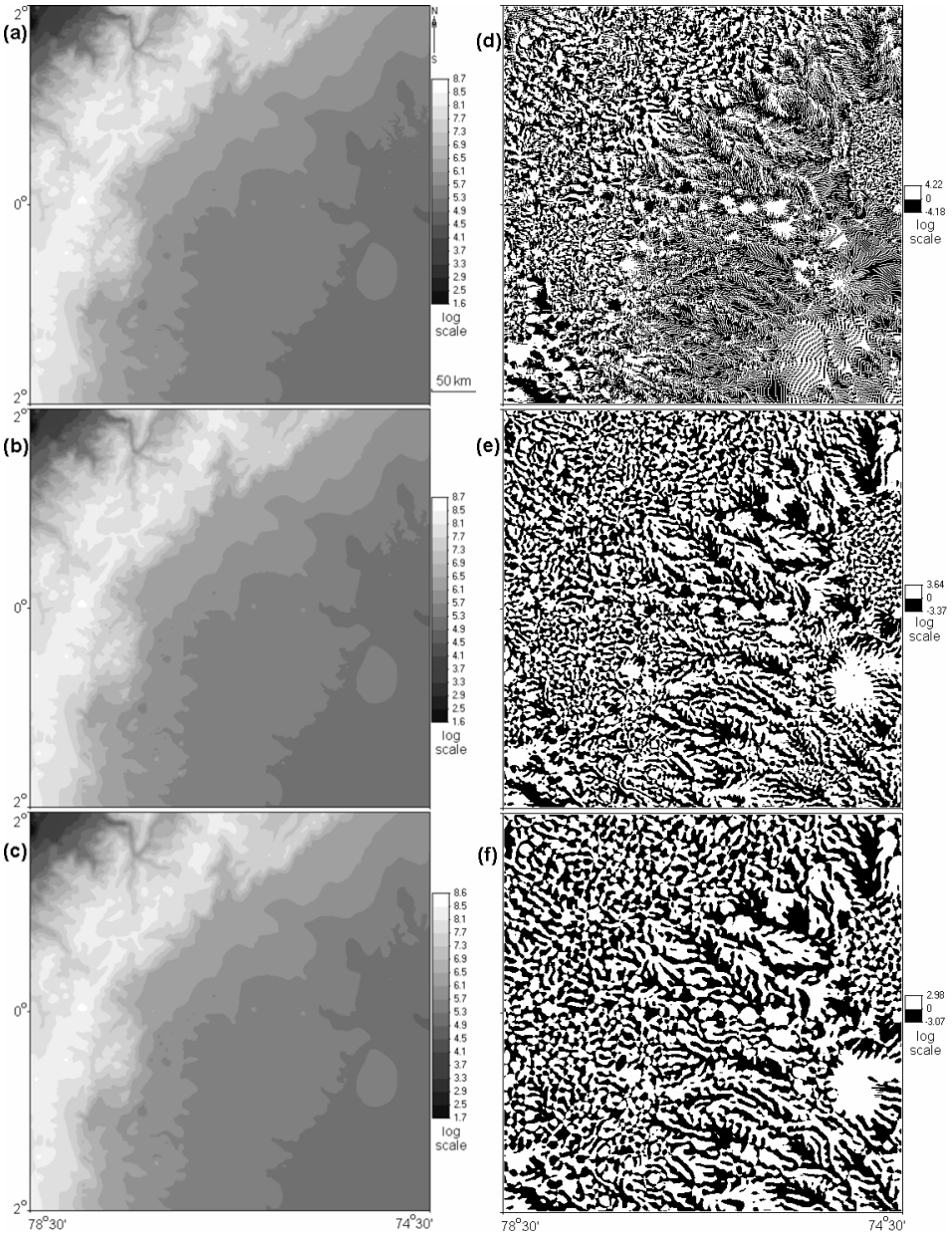


Fig. 3. DTM denoising. Elevation maps derived from the initial DEM (a), reconstructed from the ET 1-100 (b), and 1-50 (c); $k_h$ maps derived from the initial DEM (d), the DEM reconstructed from the ET 1-100 (e), and 1-50 (f).

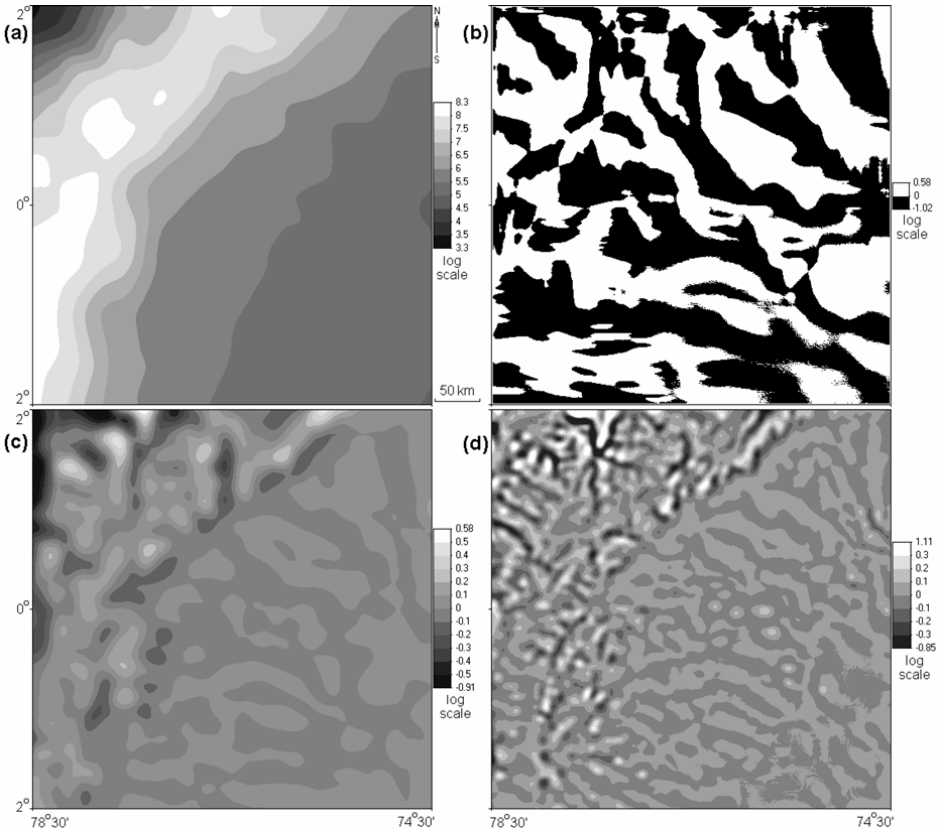


Fig. 4. Low-frequency components. Elevation maps reconstructed from the ET 1 (a), 2-3 (c), and 4-25 (d); (b) $k_h$ map derived from the DEM reconstructed from the ET 1.

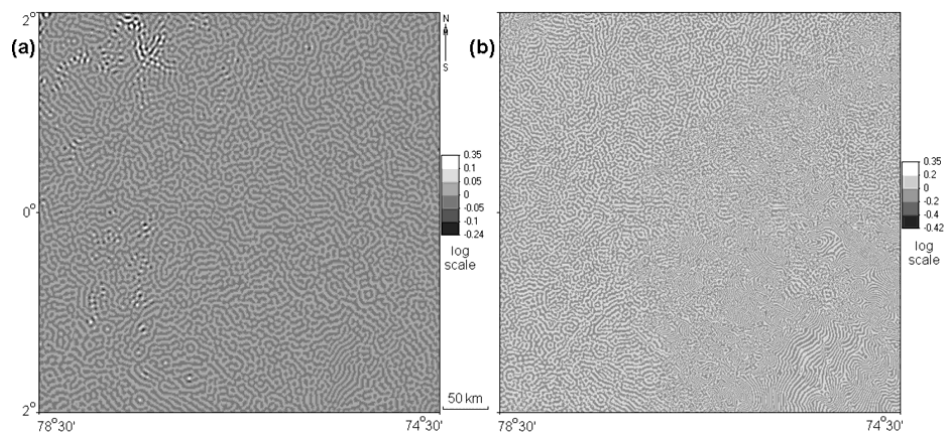


Fig. 5. High-frequency components. Elevation maps reconstructed from the ET 51-100 (a), and 101-900 (b).